CRITICAL BEHAVIOUR OF THE THERMODYNAMIC QUANTITIES FOR THE THERMOTROPIC AND FERROELECTRIC LIQUID CRYSTALS CLOSE TO THE PHASE TRANSITIONS

A THESIS SUBMITTED TO
THE GRADUATE SCHOOL OF NATURAL AND APPLIED SCIENCES
OF
MIDDLE EAST TECHNICAL UNIVERSITY

BY

EMEL KİLİT

IN PARTIAL FULFILLMENT OF THE REQUIREMENTS
FOR
THE DEGREE OF PHILOSOPHY OF DOCTORATE
IN
PHYSICS

FEBRUARY 2011

Approval of the thesis:

CRITICAL BEHAVIOUR OF THE THERMODYNAMIC QUANTITIES FOR THE THERMOTROPIC AND FERROELECTRIC LIQUID CRYSTALS CLOSE TO THE PHASE TRANSITIONS

submitted by **EMEL KİLİT** in partial fulfillment of the requirements for the degree of **Philosophy of Doctorate in Physics Department, Middle East Technical University** by,

Prof. Dr. Canan Özgen _____
Dean, Graduate School of **Natural and Applied Sciences**

Prof. Dr. Sinan Bilikmen _____
Head of Department, **Physics**

Prof. Dr. Hamit Yurtseven _____
Supervisor, **Physics Dept., METU**

Examining Committee Members:

Prof. Dr. Hüsnü Özkan
Physics Dept., METU _____

Prof.Dr. Hamit Yurtseven
Physics Dept., METU _____

Prof. Dr. Fügen Tabak
Physics Engineering, Hacettepe University _____

Prof. Dr. Demet Gülen
Physics Dept., METU _____

Prof. Dr. Mehmet Parlak
Physics Dept., METU _____

Date: _____

I hereby declare that all information in this document has been obtained and presented in accordance with academic rules and ethical conduct. I also declare that, as required by these rules and conduct, I have fully cited and referenced all material and results that are not original to this work.

Name, Last Name: EMEL KİLİT

Signature :

ABSTRACT

CRITICAL BEHAVIOUR OF THE THERMODYNAMIC QUANTITIES FOR THE THERMOTROPIC AND FERROELECTRIC LIQUID CRYSTALS CLOSE TO THE PHASE TRANSITIONS

Kilit, Emel

Ph.D., Department of Physics

Supervisor : Prof. Dr. Hamit Yurtseven

February 2011, 109 pages

The specific heat C_p has been showed at various temperatures in the literature, which shows a sharp increase labeled as the λ-transition at the critical temperature. This transition has been observed previously among the phases of solid-nematic-isotropic liquid in p-azoxyanisole (PAA) and anisaldazine (AAD), and among the phases of solid-smectic-cholesteric-isotropic liquid in cholesteryl myristate (CM). In this thesis work, we analyze the experimental data for the temperature dependence of C_p and the thermal expansion α_p and also pressure dependence of α_p by a power-law formula. From the analysis of pressure dependence of α_p, we calculate the temperature dependencies of specific heat C_p and of the isothermal compressibility κ_T for the phase transitions considered in PAA, AAD and CM. Our calculations for the temperature dependence of the α_p and κ_T can be compared with the experimental data when available in the literature.

Polarization, tilt angle and the dielectric constant have been reported in the literature at various temperatures close to the solid-smectic C*-smectic A-isotropic liquid transition in the ferroelectric liquid crystals of A7 and C7. The mean field model with the free energy ex-

panded in terms of the order parameters (polarization and tilt angle) has been reported in the literature previously. In this thesis work, we apply the mean field model first time by fitting the expressions derived for the temperature dependence of the polarization, tilt angle and the dielectric constant to the experimental data for A7 and C7 from the literature. Since the mean field model studied here describes adequately the observed behaviour of A7 and C7, the expressions for the temperature dependence of the polarization, tilt angle and the dielectric constant which we derive, can also be applied to some other ferroelectric liquid crystals to explain their observed behaviour.

Keywords: Phase Transitions, Liquid Crystals, Thermodynamic Quantities, Polarization, Dielectric Constant

ÖZ

TERMOTROPİK VE FERROELEKTRİK SIVI KRİSTALLERİ İÇİN FAZ GEÇİŞLERİ YAKININDA TERMODİNAMİK NİCELİKLERİN KRİTİK DAVRANIŞI

Kilit, Emel
Doktora, Fizik Bölümü
Tez Yöneticisi : Prof. Dr. Hamit Yurtseven

Şubat 2011, 109 sayfa

Kritik sıcaklıkta λ- geçişi olarakta adlandırılan öz ısının ani artış göstermesi literatürde farklı sıcaklıklar için ölçülmüştür. Bu geçiş daha önce p-azoxyanisole (PAA) ve anisaldazine'nin (AAD) katı-nematik-izotropik sıvı fazları arasında ve cholesteryl myristate'in (CM) katı-smektik-kolesterik-izotropik sıvı fazları arasında gözlenmiştir. Bu tez çalışmasında, sıcaklığa bağlı öz ısı C_p ve ısısal genleşme α_p ile, basınca bağlı α_p deneysel verilerini literatürden alarak güç-yasası formülüyle analiz ediyoruz. Bu analizden PAA, AAD ve CM sıvı kristallerinde göz önüne alınan faz geçişleri için sıcaklığa bağlı α_p ve eşsıcaklıklı sıkıştırılabilirlik κ_T değerlerini hesaplıyoruz. Sıcaklığa bağlı κ_T için değerlerimiz literatürde elde edilebilir deneysel verilerle karşılaştırılabilir.

A7 ve C7 ferroelektrik sıvı kristallerinin katı-smektik C*-smektik A-izotropik sıvı geçişleri yakınında polarizasyon, eğim açısı ve dielektrik sabitinin çeşitli sıcaklıklarda ölçümü literatürde verilmiştir. Düzen parametreleri (polarizasyon ve eğim açısı) terimlerinde serbest enerjinin açılımından elde edilen ortalama alan modeli daha önce literatürde rapor edilmiştir. Bu tez çalışmasında, ortalama alan modelini ilk kez, sıcaklığa bağlı olarak türetilen polarizasyon,

eğim açısı ve dielektrik sabiti bağıntılarını literatürde bulunan A7 ve C7'nin deneysel verilerine fit etmek suretiyle uyguluyoruz. Burada çalışılan ortalama alan modeli A7 ve C7'nin gözlenen davranışlarını yeterince betimlediğinden, türetmiş olduğumuz sıcaklığa bağlı polarizasyan, eğim açısı ve dielektrik sabiti bağıntıları diğer ferroelektrik sıvı kristallere gözlenen davranışlarını açıklamak için uygulanabilir.

Anahtar Kelimeler: Faz Geçişleri, Sıvı Kristaller, Termodinamik Nicelikler, Polarizasyon, Dielektrik Sabiti

To my dear family

ACKNOWLEDGMENTS

I would like to express my deepest gratitude and thanks to my supervisor, Prof. Dr. Hamit Yurtseven, for his excellent supervision, patient guidance, encouragement, friendly attitude, being accessible and continuous support. Without his support I would never have been able to undertake and carry out this work.

I would also like to thank to Prof.Dr. Claudio Zannoni for giving me the opportunity to study with his group also for his encouragement and support during my research period in his laboratory.

A very special thanks goes to Isabella Miglioli for her wonderful friendship, support and encouragement. I would also like to thank Silvia Orlandi, Roberto Berardi, Luca Muccioli and all other friends in the simulation laboratory in Italy who were always patient to my questions and for all their sincere friendship.

I would like to thank to Dilan Kavruk, Mustafa Kurt, Sema Şen and Ali Kiracı for their help, support and encouragement during this thesis work.

Many great thanks are also due to my close friends Özge Amutkan, Rengin Peköz and Vedat Tanrıverdi and my officemate Halil Gamsızkan who as good friends, were always willing to help and give their best suggestions not only in my research but also in my life.

In addition, it is not possible to mention all their names but I wish to thank to all of my friends, who were with me during thesis study.

Finally and the most importantly I would like to thank to my family for their moral support, encouragement and patience during my study and throughout all my life.

TABLE OF CONTENTS

LIST OF TABLES

TABLES

LIST OF FIGURES

FIGURES

CHAPTER 1

INTRODUCTION

In this thesis, the critical behaviour of the thermodynamic quantities such as the specific heat C_p, thermal expansion α_p and the isothermal compressibility κ_T is investigated close to the phase transitions in some liquid crystals. In particular, the λ-type specific heat C_p is studied as a function of temperature for p-azoxyanisole (PAA), anisaldazine (AAD) and cholesteryl myristate (CM) close to the solid-nematic-isotropic (PAA and AAD) and solid-smectic-cholesteric-isotropic (CM) transitions. Additionally, the temperature dependence of the thermal expansion α_p and of the isothermal compressibility κ_T is studied for PAA, and the Pippard relations are applied close to its solid-nematic-isotropic transitions.For calculating the specific heat C_p, thermal expansion α_p and the isothermal compressibility κ_T of PAA, the experimental data from the literature for the pressure dependence of α_p is used. Our calculated α_p values are compared with the results of Maier-Saupe model for the nematic-isotropic (NI) transition of PAA. Also, our calculated C_p values are compared with the experimentally measured values for the NI transition of PAA. For the anisaldazine (AAD) and the cholesteryl myristate (CM), the experimental data for the specific heat C_p is analyzed by a power-law formula. For those analyses, we used the experimental data of Pruzan, Ph., Liebenberg, D.H., and Mills, R.L., J. Phys. Chem. Solids 47, 949-961, (1986) and Barrall, E.M., Porter, R.S., and Johnson, J. F., J. Phys. Chem. 71, 895,(1967) from the literature. There are also some other experimental data of specific heat for p-azoxyanisole (Youngkyu Do, Mu Shik Jhon and Taikyue Ree, Journal of Korean Chemical Society, 20, 118-128, (1976) and P. Tuomikoski, J. Phys. Chem., 99, 16504-16506, (1995)) and thermal expansion data for p-azoxyanisole (Shao-Mu Ma and H. Eyring, Proc. Nat. Acad. Sci. 72, 78-82, (1975)) , specific heat data for cholesteryl myristate (W. L. McMillan, Physics Review A, 6, 936-947, (1971)). For anisaldazine, there is no experimental data of specific heat except that of the Barrall E. M. et

al. We used the experimental data of Barrall, E.M., Porter, R.S., and Johnson, J. F., J. Phys. Chem. 71, 895,(1967) since they measured the specific heat for p-azoxyanisole, anisaldazine and cholesteryl myristate for all the phases included and in the phase transition regions for those thermotropic liquid crystals.

Regarding the ferroelectric liquid crystals of A7, C7 and a binary mixture of 2f+3f which we study here, the temperature dependencies of the polarization P, the tilt angle θ , dielectric constant ε (electric susceptibility χ) are calculated at constant electric fields close to the AC* transition.The experimental data from the literature at zero electric field is used to calculate the polarization and the tilt angle as a function temperature at constant electric fields for A7. Also, the temperature dependence of the dielectric constant at constant electric fields is calculated by using the experimental data for this ferroelectric liquid crystal. Similarly, the temperature dependencies of the polarization and the electric susceptibility are analyzed using the experimental data for C7. Also, by analyzing the experimental data for the electric field dependence of the polarization, the specific heat C_p is predicted in this liquid crystal. Finally, the specific heat data for a binary mixture of 2f+3f is analyzed at various temperatures using a power-law formula close to the AC* phase transition. For the ferroelectric liquid crystals studied here, mean field model with the $P^2\theta^2$ coupling is used to describe the critical behaviour of the thermodynamic quantities considered close to the AC* phase transitions. For those calculations we used the experimental data from the literature especially, Bahr Ch, Heppke G and Sharma NK, Ferroelectrics 76, 151-157, (1987), Bahr, Ch., and Heppke, G., Phys. Rev. A 44, 3669, (1991) and Goates, J. B., Garland, C. W., and Shashidhar, R., Phys. Rev. A 41, 3192, (1990). Again this data includes all the phases and phase transitions that we analyzed.

1.1 Phase Transitions

A phase is a state of material where the physical properties are unique and chemical properties are uniform. A phase transition is the change of the phase from one to another. During a phase transition generally energy is taken by or released from a system. Phase transition occurs as a result of an external condition as temperature, pressure etc. changes. The value of that

external condition at which the transformation occurs is called as the phase transition point.

It is known as there are four phases of matter, that is solid, liquid, gas and plasma. But there are also mesophases (of liquid crystals) such as nematic, smectic etc., which is explained in section 1.2.1.

There are two types of classification of phase transitions. One of them is Ehrenfest classification and the other is modern classification. According to Ehrenfest, phase transitions are classified according to the behavior of the free energy as a function of thermodynamic variables. Ehrenfest divided the phase transitions into two classes. First-order phase transitions exhibit a discontinuity in the first derivative of the free energy with respect to some thermodynamic variable [1]. Second-order phase transitions are continuous in the first derivative but exhibit discontinuity in a second derivative of the free energy [1]. According to modern classification, phase transitions are also divided into two categories, named similarly to the Ehrenfest classes: First-order phase transitions are those that involve a latent heat, second-order phase transitions are continuous phase transitions [2].

Phase transitions can be analyzed by means of critical point exponents, which describe the behaviour of any thermodynamic quantity near the transition point. Close to the transition point, critical exponent dominates and log-log plots of experimental data display straight- line behaviour. From these plots critical exponent values can easily be determined. Thermodynamic quantities sometimes may not be measurable around phase transitions, but critical points are measurable [3].

Types, calculation methods and numerical values according to theoretical models are explained in section 2.1.2. Thus, by knowing the value and type of the critical exponent, one can get information about the relevant thermodynamic quantities and characterization of a phase transition.

1.2 Liquid Crystals

Liquid crystals are materials which do not have a direct phase change from solid to liquid. They show transitions involving new phases between the solid and liquid phases, which is also called mesophase. The symmetry and mechanical properties of these phases are between

liquid and solid phases [4].

In 1888, Friedrich Reinitzer was performing some experiments on substances based on cholesterol, trying to find the value of the melting point, he saw that this substance had two melting points. At 145.5^{o}C the solid crystal melted into a cloudy liquid then at 178.5^{o}C cloudiness suddenly disappeared, turned into a transparent liquid. At first he thought that this might be happened because of impurities in the material. But after purification nothing was changed. The Otto Lehmann started working on this subject and realized that the cloudy liquid was a new state of matter which has the properties of liquid and solid phases. In a normal liquid the properties are isotropic but in a liquid crystal the properties depend on direction even the substance is fluid.

Liquid crystals are partly ordered materials, somewhere between solid and liquid phases. Their molecules are often shaped like rods or plates or some other forms that provide them to align together along a certain direction. The order of liquid crystals can be manipulated with mechanical, magnetic or electric forces.

Between 1910 and 1930 new types of liquid crystalline phases were discovered. Liquid crystals have very variety of application areas. Most known application fields are liquid crystal screens and liquid crystal thermometers [5].

1.2.1 Types of Liquid Crystals

To understand the types of liquid crystals, first we need some definitions. The positional order is the arrangement of the molecules according to the type of the ordered lattice. Orientational order is the direction in which the molecules are mostly ordered. All molecules do not usually point the same direction. Chosen an imaginary direction is called director. The angle between the molecule and the director is called tilt angle . To describe the liquid crystals, the order parameter must be analyzed, which is defined as

$$S = \langle \frac{3\cos^2\theta - 1}{2} \rangle \tag{1.1}$$

Thermotropic Liquid Crystals: Thermotropic liquid crystals are pure substances and un-

dergo phase transitions due to the temperature changes.

Nematic Phases: In the nematic liquid crystal phase, molecules do not have positional order but they tend to head towards in the same direction, so they have orientational order. Thus, the molecules flow like liquids, but differently from liquids, they all point in the same direction.

Smectic Phases: Smectic phase occurs at lower temperatures than nematic phases. In the smectic phases, the arrangement of the molecules form layers (there is a positional order) and those layers can slide over one another. There are many different smectic phases. They have different positional and orientational order. Some of the well known ones are smectic A, B and C. In smectic A, the layer of the phase is perpendicular to the director. In smectic B, again layer is perpendicular to the director but the arrangement of the molecules are like hexagons within the layer. In the smectic C there is an angle (tilt angle) between the layer and the director [6].

Chiral Phases (Cholesteric Phase) : In this phase, there is a twisting of the molecules perpendicular to the director when the molecular axis is parallel to the director. A liquid crystal can have smectic or nematic phase together with chiral phase. As an example, if the liquid crystal is in the smectic C and chiral phase then this phase is shown as smectic C* in the literature [7].

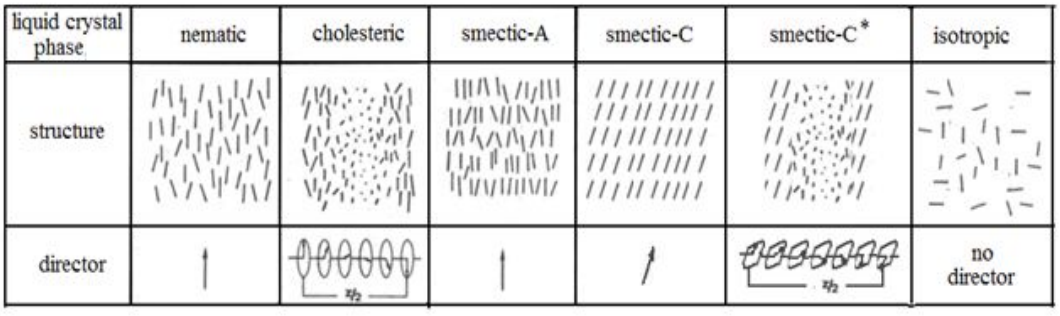

Figure 1.1: Structure and directors of some liquid crystal phases [8].

Blue Phases: Blue phases are liquid crystal phases which take place in the temperature range between a cholesteric nematic phase and an isotropic liquid phase.

Discotic Phases: The molecules of a liquid crystal can be like disk-shaped. The phases formed by these disk-shape molecules are called discotic phases. Discotic phases can be nematic if there is an orientational order but no positional order. And also they can be smectic (columnar) if there is a positional and orientational order.

Lyotropic Liquid Crystal: When two different substances are mixed, the mixture can exhibit a different phase with both the change of the temperature and also the change of the concentration of one compound in this mixture. These liquid crystals are called lyotropic liquid crystals [4, 9].

1.3 Properties of P-Azoxyanisole (PAA), Anisaldazine (AAD) and Cholesteryl Myristate (CM)

P-Azoxyanisole: P-Azoxyanisole (PAA) is one of the first-known liquid crystal. The properties of this liquid crystal have been studied for many years. This is a thermotropic liquid crystal. PAA undergoes phase transitions from the solid phase to the nematic phase and to the isotropic liquid.

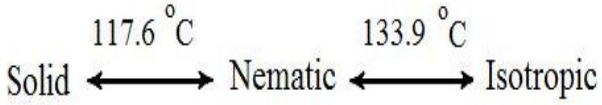

Figure 1.2: Phases and transition temperatures of p-azoxyanisole.

In the nematic mesophase of PAA, the orientation of the molecular axes is nearly parallel, but

the molecular centers are arranged arbitrarily. Because of this arrangement, there is a nearly complete freedom of translational movement of molecules, but rotational movement is only about the long molecular axis.

In the solid phase, PAA has a monoclinic structure with four molecules per unit cell. The cell dimensions are a=15.776 Å , b=8.112 Å, c=11.018 Å, β= 114.570^0.

The molecular weight of PAA is 258.27 g/mol. Its chemical formula $C_{14}H_{14}N_2O_3$. PAA consists of elongated rod-like molecules.

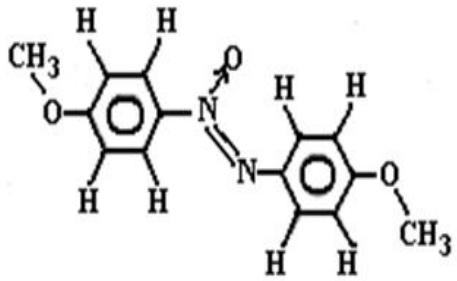

Figure 1.3: Chemical structure of p-azoxyanisole.

The functional groups that exist in chemical structure of the PAA are two benzene rings, two ether gruops and an azoxy group. N-O group which exists in the azoxy group produces a molecular dipole moment [10]. The most important application area of the PAA is liquid crystal displays [11].

Anisaldazine: Anisaldazine is a thermotropic liquid which crystal, undergoes phase transitions as the temperature changes. Anisaldazine changes its phases from the solid phase to the nematic phase and to the isotropic liquid.

Table 1.1: Properties of some thermotropic liquid crystals such as PAA, AAD and CM.

	PAA	AAD	CM
Type of LC	Thermotropic Nematic LC	Thermotropic Nematic LC	Thermotropic Cholesteric LC
Phases	Solid Nematic Isotropic	Solid Nematic Isotropic	Solid Smectic Cholesteric Isotropic
Molecular Structure	Monoclinic	Monoclinic	Monoclinic
Functional Groups	Benzene rings, Ether groups, Azoxy group.	Aniline, Arene, Benzene rings, Amine, Hydrazine, Ether.	Alkene, Carbonyl, Ester.
Phase Transitions	First order (Nematic-Isotropic)	First order (Nematic-Isotropic)	First order (Cholesteric-Isotropic)
Ordering	By an external magnetic field and temperature	By an external magnetic field and temperature	By temperature
Shape of Molecules	Rod-Like	Rod-Like	Rod-Like
λ-Type Specific Heat	X	X	X
Supercooling-Superheating	X	X	X

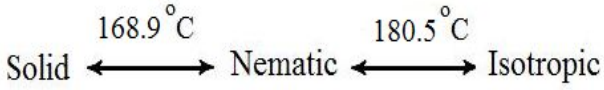

Figure 1.4: Phases and transition temperatures of anisaldazine.

Because of the geometrical non-symmetry of the molecules of anisaldazine, variation of the electrical conductivity occurs when a strong magnetic field is applied. Anisaldazine forms an anisotropic liquid between 168.9^0C and 180.5^0C. In a magnetic field, anisaldazine acts as a strongly doubly refracting crystal, and its optical axis is parallel with the magnetic lines of force. The amount of ionisation as a result of this conductivity of anisaldazine is very small

[12]. The anisaldazine crystals are monoclinic with a= 17.46 Å, b= 10.76 Å, c=8.45 Å, β = $113^0\ 48'$ and there are 4 molecules per unit cell. The molecules are nearly planar and forms chains parallel to *a* [13]. The molecular weight of anisaldazine is 268.31 g/mol.

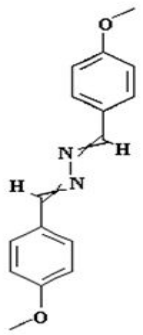

Figure 1.5: Chemical structure of anisaldazine.

The chemical structure of the anisaldazine is $C_{16}H_{16}N_2O_2$. In the chemical structure of the anisaldazine there are aromatics namely aniline, arene and benzene rings and according to CHN containing amine and hydrazine and also according to CHO containing ether as functional groups.

P-Azoxyanisole and anisaldazine are the mesophase systems which are in the same family of molecular organic compounds. These organic compounds undergo the same phases, namely solid, nematic and isotropic phases. Although their molecular structure are similar, the molecular forces are different. Both compounds have benzene rings, and ether in their chemical structure.

Cholesteryl Myristate: Cholesteryl myristate (CM) undergoes phase transitions from isotropic liquid to cholesteric at T_{CI}=85^0C, from cholesteric to smectic at T_{CS} =80^0C, and from smectic to crystal at T_{SC}=72^0C.

Crystals of the cholesteryl myristate are monoclinic with lattice parameters a= 10.260, b= 7.596, c= 101.43 Å, β = 94.41^0 [14]. Molecular weight of cholesteryl myristate is 599.03 g/mol. Cholesteryl myristate has a cholesteric liquid crystal phase.

The chemical formula of the cholesteryl myristate is $C_{41}H_{72}O_2$. The chemical structure of

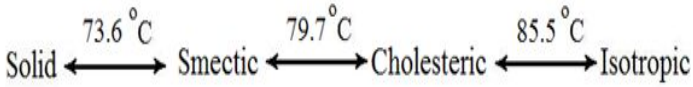

Figure 1.6: Phases and transition temperatures of cholesteryl myristate.

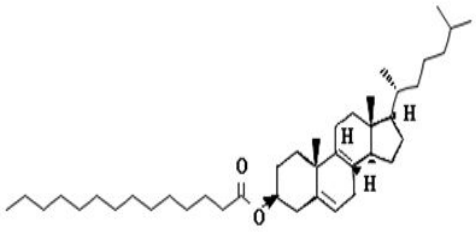

Figure 1.7: Chemical structure of cholesteryl myristate.

cholesteryl myristate consists of some functional groups as alkene (CH only) carbonyl and ester (CHO- containing).

1.4 Properties of 4-(3-methyl-2-chlorobutanoyloxy)-4'-heptyloxybiphenyl (A7), 4-(3-methyl-2-chloropenta- noyloxy)-4'-heptyloxybiphenyl (C7) and a binary mixture of 2f+3f

Ferroelectric Liquid Crystals: Robert Meyer and co-workers discovered ferroelectricity in liquid crystals in 1975. In a certain temperature range, they observed a very large linear electrooptic effect. For a given polarity of the field, the originality uniaxial conical figure tilted as a whole in a plane perpendicular to the direction of the applied field. At large fields, the conical image became biaxial and saturated. At saturation, the tilt of the conical image roughly corresponded to the molecular tilt. By reversing the electric field, the direction of the tilt of the conical image would reverse, which was a direct evidence of a very large, linear electrooptic effect. Meyer's explanation was as follows: In chiral tilted smectic phases, molecules are

arranged in liquid-like smectic layers. Each smectic layer can posses an in-plane spontaneous polarization. By symmetry, the in-plane polarization is allowed in a direction perpendicular to the molecular tilt [15]. In the smectic A and C* phases, the molecules are positioned in layers and their long axes are oriented parallel to the layer normal (Sm A) or they make an angle (tilt angle θ) with the layer normal if the liquid crystal contains optically active molecules (Sm C*). In terms of a one-dimensional density wave describing smectic A and C* phases, its wave vector makes a tilt angle θ with the layer normal and the long axes of the molecules precess around the direction of the one-dimensional density wave in the smectic C* phase. This is a helical structure and the molecules are chiral in the C* phase [6].

For a ferroelectric liquid crystal with high spontaneous polarization, the two order parameters, namely, the tilt angle θ and the polarization P can couple which drives the system to the AC* phase transition. This coupling between θ and P is due to the reduced symmetry of the liquid crystal containing the chiral molecules in the smectic C* phase. There have been suggestions in the literature for this coupling as linear $P\theta$ and biquadratic $P^2\theta^2$ in the free energy expansion in terms of the polarization P and the tilt angle θ using the mean field models [16, 17]. A biquadratic $P^2\theta^2$ coupling has been used in the mean field models and it has been shown that it agrees better with the experimental data for the polarization as functions of temperature [18] and concentration [19].

At zero electric field, a ferroelectric liquid crystal with high spontaneous polarization does not exhibit a quasi-piezoelectrical behaviour [20] since the tilt angle θ is zero in the smectic A phase. As the external electric field increases, the long axes of the molecules become tilted in the smectic A phase so that the electroclinic effect takes place.

By analyzing the temperature dependence of the polarization P and tilt angle θ under an electric field close to the smectic AC* phase transition in the ferroelectric liquid crystal of 4-(3-methyl-2-chlorobutanoyloxy)-4$'$-heptyloxybiphenyl (A7), θ and P were calculated at various temperatures under some other constant electric fields for this ferroelectric liquid crystal [18]. For this calculation, a mean field model was used in the case of nonzero electric field [19] by using data for the tilt angle θ and for the polarization P at zero electric field [18]. The tilt angle and the polarization were calculated as a function of temperature for the AC* phase transition of A7 for constant electric fields at which the measurements of dielectric constant were performed [21].

Phase transitions between smectic A and C* phases in some ferroelectric liquid crystals have been observed experimentally as a second order [22-24]. On the other hand, many ferroelectric liquid crystals have also been obtained experimentally, which exhibit a first order transition between smectic A and chiral C (C*) phases [16, 25-29]. Those liquid crystalline materials exhibit a first order phase transition since their spontaneous polarization is considerably low. Those liquid crystals which exhibit a first order phase transition, have high spontaneous polarization, as observed in A7 [25, 30].

Close to the AC* phase transition in ferroelectric liquid crystals, the dielectric constant increases as the temperature decreases from the smectic A phase to the ferroelectric smectic C (C*) phase, as observed experimentally [21]. It has been indicated that this increase in the dielectric constant is due to a soft mode (phase fluctuations in the amplitude of the tilt angle θ) and also due to a Goldstone mode (phase fluctuations in the azimuthal orientation of the tilt angle θ) [21]. In both smectic A and C* phases, phase fluctuations in the amplitude of the tilt angle θ exist, whereas the phase fluctuations in the azimuthal orientation of the tilt angle θ exist in the smectic C* phase only [21].

The tilted smectic phases possess a spontaneous polarization if the molecules possess a permanent transverse dipole and are chiral [16]. It has been observed experimentally that transitions to the ferroelectric phase occur at higher temperatures by increasing the spontaneous polarization in the chiral systems [16]. It has also been indicated that the ferroelectric transition temperatures are shifted when an external electric field is applied [16]. Here, we calculate the dielectric constant as a function of temperature under some constant electric fields for the AC* phase transition of A7. For the calculation of the dielectric constant we use the mean field model with the $P^2\theta^2$ coupling for nonzero electric field, which has been developed in an earlier study [19]. By using the calculated values of the tilt angle θ and the polarization P at various temperatures for zero electric field (E=0) from a previous study for A7 [19], we calculate in this study the temperature dependence of the dielectric constant at constant electric fields in this liquid crystal.

By examining the critical behaviour of the polarization, tilt angle, electric susceptibility and the specific heat close to the SmA- ferroelectric SmC (SmC*) phase transitions, we also investigate the temperature dependence of the order parameters, namely, polarization P and the tilt angle θ, and that dependence of the electric susceptibility in the presence of the applied

electric field for the ferroelectric liquid crystals close to the AC* phase transitions. This is done by the mean field model with the $P^2\theta^2$ coupling in the expansion of the Landau free energy. With this mean field model, the electric field dependence of the polarization and the temperature dependence of the specific heat C_p are investigated. As an application of our mean field model, in particular we analyze the temperature dependences of the polarization and of the electric susceptibility using the experimental data for C7 (T_C=55.925^{0}C). We also analyze the electric field dependence of the polarization using the experimental data for C7 [31] and we predict the critical behaviour of the specific heat C_p in this crystalline system by means of our mean field model. This model given here is applied to a binary mixture of 2f+3f to describe its critical behaviour close to the AC* phase transition (T_C=393.845 K). By analyzing the experimental data for the specific heat of this mixture [32], we predict the critical behaviour of the susceptibility and the order parameter within the framework of our mean field model.

A7 (4-(3-methyl-2-chlorobutanoyloxy)-4'-heptyloxybiphenyl): A7 is a ferroelectric liquid crystal. A7 has a large spontaneous polarization. Its phase range is ≈8^{0}C that has been found to exhibit a first-order A-C* transition. Spontaneous polarization of A7 is 140nC/cm^2 at 0.2 K below the Sm A-Sm C* transition temperature.

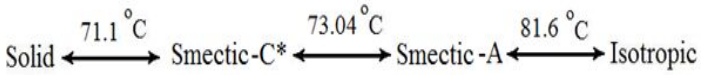

Figure 1.8: Phases and transition temperatures of A7.

Pure optically active A7 undergoes phase transitions from isotropic (I) (81.6^{0}C) to SmA (73.04^{0}C) and from SmA to SmC* (71.1^{0}C). Lastly, it undergoes from SmC* to solid. 50 % optically active A7 has a transition sequence as I (81.9^{0}C)-SmA (72.7^{0}C)-SmC. The transition sequence of racemic mixture is similar, namely, I (82.0^{0}C)-SmA (72.23^{0}C) - SmC (70.2^{0}C)-Solid.

A7 has the transition as a first order in chiral (nonracemic) A7 and while the chiral compound shows a weakly first-order smectic-A-chiral-smectic-C transition (AC*), the racemic

A7 exhibits a continuous smectic-A-smectic-C transition.

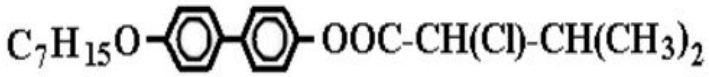

Figure 1.9: Chemical formula of A7.

The functional groups that exist in chemical structure of the A7 are methyl and phenyl groups.

C7 (4-(3-methyl-2-chloropenta- noyloxy)-4'-heptyloxybiphenyl): C7 is a ferroelectric crystal, exhibiting large spontaneous polarization. Spontaneous polarization in the smectic-C* phase of pure chiral C7 changes between 130 and 290 nC/cm^2 with decreasing temperature. The range of the A phase for C7, which exhibits a first-order A-C* transition, is $\approx 7^0$C.

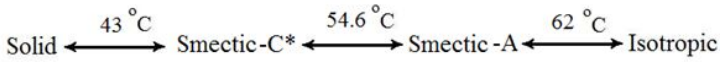

Figure 1.10: Phases and transition temperatures of C7.

The molecules are chiral and thus a ferroelectric spontaneous polarization exists in the smectic C phase [22]. The direction of this polarization is perpendicular to both the tilt direction and the layer normal and by applying a dc electric field along the smectic layers, one can align the tilt direction by the polarization direction and the external field [33].

Chiral 4-(3-methyl-2-chloropenta- noyloxy)-4$'$-heptyloxybiphenyl (C7) possesses the following sequence of liquid-crystalline phases: isotropic (62^0C) smectic-A (54.6^0C) smectic-C*(43^0C)-smectic-G (SmG denotes a more-ordered smectic phase possessing, in contrast to SmA and SmC, a three dimensional long range positional order of the molecules)

The transition of C7 can be examined as a first order or weakly first order due to the amplitude of the spontaneous polarization, or a mixture with another material.

Table 1.2: Properties of some ferroelectric liquid crystals such as A7, C7 and a binary mixture of 2f+3f.

	A7	C7	2f+3f
Type of LC	Thermotropic Smectic LC	Thermotropic Smectic LC	Thermotropic and Lyotropic Smectic LC
Phases	Solid Smectic C* Smectic A Isotropic	Solid Smectic C* Smectic A Isotropic	Solid Smectic C* Smectic A Isotropic
Functional Groups	Methyl, Phenyl	Methyl, Phenyl	Methyl, Phenyl
Phase Transitions	First order (SmA-Isotropic) Weakly first order (SmA-SmC*)	First order (SmA-Isotropic) and (SmA-SmC*)	Second order (SmA-SmC*)
Ordering	By an external electric field and temperature	By an external electric field and temperature	By an external electric field and temperature
Shape of Molecules	Rod-Like	Rod-Like	Rod-Like
Polarization	Large spontaneous Polarization	Large spontaneous Polarization	Large spontaneous Polarization
Tilt Angle	SmC, SmC*	SmC, SmC*	SmC, SmC*

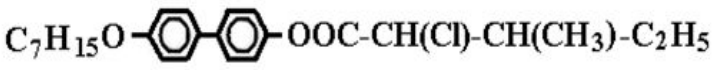

Figure 1.11: Chemical formula of C7.

The functional groups that exist in chemical structure of the C7 are methyl and phenyl groups.

2f+3f: 2f+3f is a two chiral esters of 2.5-diphenyl pyrimidine. 2f is the abbrevation of 2-(p-n-hexyloxyphenyl)5-[p-(2-chloro-4-methylpentanoyloxy)-phenyl] pyrimidine and 3f is the abbrevation of 5-(p-n-hexylphenyl)2-[p-(2-chloro-4-methylpentanoyloxy)-phenyl]pyramidine.

The SmA-SmC* transition in pure 3f is of a second order, while mixtures with compositions (mol % 2f) X_{2f}=58.27 and 60.2 show near-tricritical and strongly first-order behaviour, respectively. Thus, the result for pure 3f indicates that a large spontaneous polarization need

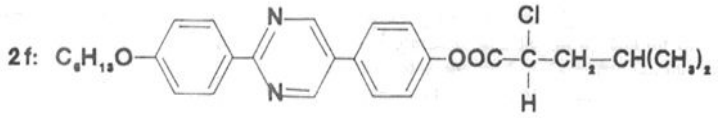

Figure 1.12: Chemical formula of 2f.

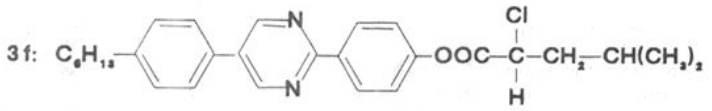

Figure 1.13: Chemical formula of 3f.

not impose a first order character on the SmA-SmC* transition. This fact coupled with the existence of the tricritical point in the mixed system, suggests that there may be a competition between the effects arising from polarization and the SmA temperature range since 3f has a large SmA temperature range (≈40 K) and 2f has no SmA phase [32].

The functional groups that exist in chemical structure of the C7 are methyl and phenyl groups.

CHAPTER 2

THEORY

2.1 Phase Transition Phenomena

Phase transition occurs when one state of matter (phase) changes to another. At the phase transition, there is a singularity on the first or higher order derivatives of the thermodynamic potential. According to Ehrenfest, phase transitions are divided into two groups, namely, first-order and second-order phase transitions [2].

2.1.1 Classification of Phase Transitions

First-Order Phase Transitions: The first derivative of a thermodynamic potential with respect to the thermodynamic variables is discontinuous [34]. So, the phase transitions with the latent heat are first order transitions. Solid-liquid-gas transitions belong to this group.

Second-Order Phase Transitions: The first derivatives of a thermodynamic potential are continuous, but the second derivatives are discontinuous at the transition point [34]. So, the phase transitions without latent heat are second order phase transitions. Ferromagnetic phase transitions belong to this type [2].

Gibbs free energy measures the useful work attainable from a thermodynamic system without increasing its total volume or allowing heat to pass to or from external systems. Gibbs energy is also the chemical potential that is minimized when a system reaches equilibrium at constant pressure and temperature. When a system is identified with the Gibbs free energy (G) as a thermodynamic potential, if the entropy or the specific volume are discontinuous then there is a first order transition since the entropy is equal to S=-$\left(\frac{\partial G}{\partial T}\right)_P$ and specific volume is the first

derivative of Gibbs free energy with respect to the pressure, i.e. V=$\left(\frac{\partial G}{\partial P}\right)_T$.

If the thermodynamic quantities of a system such as the specific heat or isothermal compressibility are discontinuous, then there is a second order phase transition. Since the thermal expansion and isothermal compressibility are obtained from the second derivative of the Gibbs free energy, with respect to the temperature and pressure, respectively, i.e. C_p=-T$\left(\frac{\partial^2 G}{\partial T^2}\right)_P$ and κ_T=-$\frac{1}{V}\left(\frac{\partial^2 G}{\partial P^2}\right)_T$.

Also, when the discontinuity in the specific heat occurs as an infinite peak, this type of second-order transition is called the λ-type phase transitions [35].

2.1.2 Critical Point Exponents

Critical point exponents describe the critical behavior of the transition and of the thermodynamic quantities at the critical (transition) point. Near the transition temperature it is more sufficient to use the reduced temperature, ε=|T-T_c|/T_c, which is a dimensionless variable and it gives the difference of the temperature from the transition temperature. The critical exponent is the limit form of the ratio of any thermodynamic function (f) to the reduced temperature or the temperature difference such as |T-T_c|, which can be expressed as λ=$\lim_{\varepsilon\to 0}\frac{\ln f(\varepsilon)}{\ln \varepsilon}$. Then, the thermodynamic function can be expressed as f(ε)~ε^{λ} [3].

When the specific heat, isothermal compressibility etc. are considered as the thermodynamic function, then the symbol and the value of the critical exponent (α, γ) change correspondingly.

Table 2.1: Summary of definitions of some critical exponents for fluid systems, ε is reduced temperature and defined as ε=|T-T_c|/T_c [3]

Exponent	Definition	Conditions			Quantity
		ε	P-P_c	ρ-ρ_c	
α'	C_v~(-ε)$^{-\alpha'}$	<0	0	0	specific heat
α	C_v~$\varepsilon^{-\alpha}$	>0	0	0	
β	ρ_L-ρ_G~(-ε)$^{\beta}$	<0	0	≠0	liquid-gas density difference
γ'	κ_T~(-ε)$^{-\gamma'}$	<0	0	≠0	isothermal compressibility
γ	κ_T~$\varepsilon^{-\gamma}$	>0	0	0	
δ	P-P_c~$|\rho_L$-$\rho_G|^{\delta}$sgn(ρ_L-ρ_G)	0	≠0	≠0	critical isotherm

Table 2.2: Summary of definitions of some critical exponents for magnetic systems, ε is reduced temperature and defined as ε=|T-T_c|/T_c [3]

Exponent	Definition	Conditions			Quantity
		ε	H	M	
α'	$C_H \sim (-\varepsilon)^{-\alpha'}$	<0	0	0	specific heat at constant magnetic field
α	$C_H \sim \varepsilon^{-\alpha}$	>0	0	0	
β	$M \sim (-\varepsilon)^{\beta}$	<0	0	≠0	zero field magnetization
γ'	$\chi_T \sim (-\varepsilon)^{-\gamma'}$	<0	0	≠0	zero field isothermal susceptibility
γ	$\chi_T \sim \varepsilon^{-\gamma}$	>0	0	0	
δ	$H \sim \lvert M\rvert^{\delta} \mathrm{sgn}(M)$	0	≠0	≠0	critical isotherm

The values of the critical exponents change according to the theoretical models. Some of those values can be seen in the next tables, Tables 2.3 and 2.4.

Table 2.3: Summary of values of some critical exponents.[36]

Exponents	Mean Field	Ising d=2	Ising d=3	Heisenberg d=3, D=3	Spherical d=3, D=∞
α(C,T)	0 (disc)	0 (log)	0.119±0.60	-0.08±0.04	-1
β(M,T)	1/2	1/8=0.125	0.326±0.004	0.38±0.03	1/2
$\gamma(\chi$,T)	1	7/4	1.239±0.003	1.38±0.02	2
δ(B,M)	3	15	4.80±0.05	4.63±0.29	5

Power-Law Formula As can be seen from Tables 2.1 and 2.2, the critical behaviour of the response thermodynamic quantities can be expressed by the critical exponents.

When one takes the logarithm of both sides, then the values of critical exponents can be obtained easily. In this thesis, a power-law formula of the specific heat C_p and dielectric susceptibility χ is used. The analysis of the specific heat C_p as a function of temperature can be performed according to a power-law formula [37-39]

$$C_p = A|T - T_t|^{-\alpha} \tag{2.1}$$

In Eq.2.1, α denotes the critical exponent for the specific heat C_p and A is the amplitude. Here

Table 2.4: Critical exponents of the models.[36]

Exponents	XY Model	Tricritical Model	Classical model
α	0 (log)	1/2	d=∞
β	0.33	1/4	1/2
γ	1.32	1	1

T_t is the phase transition temperature. By taking the logarithm of Eq.2.1, one gets

$$logC_p = logA - \alpha \log|T - T_t| \tag{2.2}$$

(Also, instead of |T-T_t|, one can use the reduced temperature which is defined as ε=|T-T_t|/T_t so that Eq.2.1 is written as

$$C_p = A\varepsilon^{-\alpha} \tag{2.3}$$

After taking the logarithm, we get

$$logC_p = logA - \alpha \log \varepsilon \tag{2.4}$$

and for the dielectric susceptibility [40],

$$\chi = A|T - T_t|^{-\gamma} \tag{2.5}$$

where γ is the critical exponent for the dielectric susceptibility. By taking the logarithm of both sides again we get,

$$log\chi = logA - \gamma \log|T - T_t|. \tag{2.6}$$

Thus, the specific heat C_p (the dielectric susceptibility χ) can be plotted in a log-log scale as a function of temperature (or the reduced temperature ε) according to Eq. 2.2 (Eq. 2.6) from

which the slope α (γ) and the intercept logA can be extracted for phase transitions of a liquid crystal.

2.1.3 Models

Mean Field Model: When a system contains a large number of interacting particles, then it is difficult to solve the system exactly. The difficulty arises from the addition of the interaction terms. Mean field theory reduces many-body system to a one-body system by considering the average of the interaction fields [41].

Ising Model: Ising model deals in ferromagnetic systems with the spins oriented with the spin variables either +1 or -1, which lie on a lattice point on a d-dimensional lattice when they interact only with its nearest neighbors. Ising model is sufficient to analyze the phase transitions as a simplified version of the real systems [42].

The energy of the Ising model is as follows:

$$E = -\sum_{i \neq j} J_{ij} S_i S_j \tag{2.7}$$

where J is the interacting parameter and S_i are the spin variables.

One-dimensional Ising model is can be taken as a one dimensional lattice:

$$E = -\sum_{i} S_i S_{i+1} \tag{2.8}$$

Two dimensional Ising model has been solved exactly by Onsager. He first calculated the partition function for the zero field which allows to calculate the specific heat [3].

Three and more dimensional Ising models have not been solved yet. For an infinite dimensional system, Ising model is considered as a mean field model.

Heisenberg model: Heisenberg model deals with the magnetic moments in the form of quantum mechanical three-dimensional spin operators. Similar to an Ising model, in Heisenberg model the energy is related to the scalar product of these spin operators [43] .

$$E \cong -\sum_{<ij>} \sigma_i \sigma_j \tag{2.9}$$

As Ising model, Heisenberg model does not have an exact solution for a 3-dimensional lattice. Differently from Ising model, Heisenberg model is not capable to solve even two dimensional lattices [43].

Spherical Model: Berlin and Kac [3] solved two and three dimensional lattices, developing and using a nonphysical model, spherical model. In most aspects, the spherical model looks like an Ising model, but around the transition point, exponents of the spherical model agree better with the experimental results. And also the spherical model is sufficient for solving lattice problems in the presence of an external field. In this model, every sites of the lattice system have a spin σ_j interacting with the nearest neighbors and with an external field H. Values of σ_j are not restricted to the values of -1,0,1 but they can take all real values. That is why, the spherical model is not physical [3, 44].

XY Model: In this model the magnetic compasses are attached to the lattice sites. Again, nearest neighbor interactions are considered [43]:

$$E = -J \sum_{<ij>} S_i S_j = \sum_{<ij>} cos(\theta_i - \theta_j) \tag{2.10}$$

where θ_i is the ith spin phase which can be measured in this model .

Tricritical Model: Tricritical model is an approximation in a mean field model, which is used in the three-phase coexistence region or around a triple point [3].

2.2 Pippard Relations

Critical behaviour of the thermal expansivity α_p can be described as [45]

$$\alpha_p = A_1 (P - P_t)^{\gamma} \tag{2.11}$$

where γ is the critical exponent for the thermal expansivity, A_1 is the amplitude and P_t is the

transition pressure.

Close to the transition point, an approximate relation for the slope can be written as

$$\frac{P_t(T) - P}{T - T_t(P)} = \frac{dP_t}{dT} \tag{2.12}$$

By means of Eq. 2.12, the temperature dependence of the thermal expansivity can be obtained as

$$\alpha_p(T) = A_1\left(\frac{dP_t}{dT}\right)^{-\gamma}(T - T_t)^{-\gamma} \tag{2.13}$$

The temperature and pressure dependence of the isothermal compressibility κ_T can be calculated from the thermodynamic relation

$$\frac{\alpha_p}{\kappa_T} = \left(\frac{\partial P}{\partial T}\right)_V = \left(\frac{\partial P}{\partial T}\right)_S \tag{2.14}$$

close to the transition point [45]. Using Eq. 2.11, the pressure dependence of κ_T will become

$$\kappa_T = \frac{1}{(\partial P/\partial T)_S}[A_1(P_1 - P)^{-\gamma}] \tag{2.15}$$

Also, by substituting Eq. 2.13 into Eq. 2.14, the temperature dependence of κ_T can be obtained as

$$\kappa_T = \frac{1}{(\partial P/\partial T)_S}A_1\left(\frac{dP_t}{dT}\right)^{-\gamma}(T - T_t)^{-\gamma} \tag{2.16}$$

Using the definitions of the thermal expansivity $\alpha_p \equiv \frac{1}{V}(\frac{\partial V}{\partial T})_P$ and of the isothermal compressibility $\kappa_T \equiv -\frac{1}{V}(\frac{\partial V}{\partial P})_T$, we can derive the temperature and pressure dependence of volume as

$$V_p(T) = V_t exp\left[\frac{A_1(dP_t/dT)^{-\gamma}(T - T_t)^{1-\gamma}}{1 - \gamma}\right] \tag{2.17}$$

and

$$V_T(P) = V_t exp\Big[\frac{1}{(\partial P/\partial T)_S}\frac{A_1(p_t - p)^{1-\gamma}}{1-\gamma}\Big] \tag{2.18}$$

respectively [46].

Finally, the temperature and pressure dependence of the specific heat C_p can be obtained from the thermodynamic relation

$$C_p = TV\alpha_p\Big(\frac{\partial P}{\partial T}\Big)_S \tag{2.19}$$

Using Eqs. 2.13 and 2.17 in Eq. 2.19, C_p is obtained as a function of temperature [46].

$$C_p = A_1 TV(\partial p_m/\partial T)^{-\gamma+1}(T - T_m)^{-\gamma} \tag{2.20}$$

Similarly, using Eqs. 2.11 and 2.18 in Eq. 2.19, C_p is obtained as a function of pressure [46].

$$C_p = A_1 TV\Big(\frac{\partial p_m}{\partial T}\Big)(p_m - p)^{-\gamma} \tag{2.21}$$

Close to the phase transitions, the specific heat C_p can be related to the thermal expansivity α_p (first Pippard relation) by [35]

$$C_p = TV\Big(\frac{dP}{dT}\Big)_\lambda \alpha_p + T\Big(\frac{dS}{dT}\Big)_\lambda \tag{2.22}$$

where subscript λ denotes the λ-type transition and α_p can be related to the isothermal compressibility κ_T (second Pippard relation) by [35]

$$\alpha_p = \Big(\frac{dP}{dT}\Big)_\lambda \kappa_T + \frac{1}{V}\Big(\frac{dV}{dT}\Big)_\lambda \tag{2.23}$$

Thus, the temperature and pressure dependencies of those thermodynamic quantities, namely, C_p, α_p and κ_T can be related to each other for the phase transitions according to Eqs. 2.22

and 2.23. From a linear variation of C_p with α_p (Eq. 2.22) and also a linear variation of α_p with κ_T (Eq. 2.23), we can deduce the values of the slope dP/dT for the phase transitions. Calculated dP/dT values can then be compared with the experimentally determined values of dP/dT for the phase transitions.

2.3 Stability Limits of Thermal Expansion, Specific Heat and Isothermal Compressibility

Metastable states have a continuous line of stability limits. The locus of that is P_s(T), where the isothermal compressibility κ_T diverges there [47].

The isobaric temperature dependence of several thermodynamic quantities (TQ) have been fitted to equations of the form [48-50]

$$TQ = C_{TQ}(|T - T_s(P)|)^{-\gamma_{TQ}} + TQ_b \tag{2.24}$$

where C_{TQ}, and γ_{TQ} are constants, T_s is the stability temperature and TQ_b is a background correction term.

Thermodynamic reasoning is valid up to a value where $\kappa_T \rightarrow \infty$. When κ_T diverges, then α and C_p also diverge. Because of this reason, the ratios α/κ_T and C_p/κ_T remain finite [47].

α, C_p and κ_T are asymptotically proportional to each other near the line P_s(T)

$$\alpha \sim C_p \sim \kappa_T \tag{2.25}$$

as $P \rightarrow P_s$(T). When Eq. 2.24 is appropriate, then X=α, C_p and κ_T have the same exponent values of γ_{TQ}. The limiting forms of α, C_p, and κ_T along isochores and isobars can be obtained by using Eq. 2.25. At this point some assumptions are necessary:

* At the line of stability limits (the locus of points), measured values of κ_T extrapolate to infinity.

* The Helmholtz potential A(V,T) can be expanded along an isotherm as a Taylor series in V_s(T) - V [47].

$$A(V,T) = \sum_{n=0} C_n(T)[V_s(T) - V]^n \tag{2.26}$$

where

$$C_o(T) = lim_{V \to V_s(T)} A(V,T) \tag{2.27}$$

$$C_n(T) = lim_{V \to V_s(T)} \{-(1/n!)[\partial^n A(V,T)/\partial V^n]\}_T \tag{2.28}$$

where n≥1. (For simplicity, the T dependence of V_s and C_n is not explicitly indicated). The pressure P = -(∂ A/∂ V)$_T$ is obtained by differentiating Eq. 2.26.

$$P = \sum_{n=1} nC_n(V_s - V)^{n-1} \tag{2.29}$$

The term C_1 is determined by $(V_s - V)^o = 1$ so that p → C_1 as V → V_s. Thus, C_1=P_s at V_s.

The reciprocal of the isothermal compressibility $\kappa_T{}^{-1}$ =-V(∂ P/ ∂ V)$_T$ is obtained by differentiating Eq. 2.29

$$\kappa_T^{-1} = V \sum_{n=2} n(n-1)C_n(V_s - V)^{n-2} \tag{2.30}$$

The term C_2 is determined by $(V_s - V)^o = 1$ so that $\kappa_T \to 2VC_2$ as V → V_s. But, by the first assumption, $\kappa_T{}^{-1} \to 0$ as V → V_s, so $C_2 = 0$.

Close to the stability limit lines, merely the first nonzero term in Eq. 2.30 contributes to $\kappa_T{}^{-1}$ so

$$\kappa_T^{-1} = 6VC_3(V_s - V) + ... \tag{2.31}$$

$$\kappa_T = (6VC_3(V_s - V) + ...)^{-1} \tag{2.32}$$

The limiting form is

$$\alpha \sim C_p \sim \kappa_T \sim (V_s - V)^{-1} \tag{2.33}$$

along an isotherm. The limiting form along an isochore is obtained by the line $V_s(T)$ is locally linear, so that for points (V,T) sufficiently close to $V_s(T)$

$$[V_s(T) - V] \propto |T - T_s(V)| \tag{2.34}$$

since (V,T), $V_s(T)$, and $T_s(V)$ are similar [47]. Therefore

$$\alpha \sim C_p \sim \kappa_T \sim (|T - T_s(V)|)^{-1} \tag{2.35}$$

along an isochore. The corresponding isobaric limiting form can be obtained from Eq. 2.29, remembering that $C_2 = 0$

$$P - P_s(T) = 3C_3(V_s - V)^2 + ... \tag{2.36}$$

so that, from Eq. 2.33 and 2.36

$$\alpha \sim C_p \sim \kappa_T \sim (|P - P_s(T)|)^{-1/2} \tag{2.37}$$

along an isotherm. The locus of $P_s(T)$ is locally linear so $|P\text{-}P_s(T)| \propto |T\text{-}T_s(P)|$, and, from Eq. 2.37, along an isobar we get [47],

$$\alpha \sim C_p \sim \kappa_T \sim (|T - T_s(P)|)^{-1/2} \tag{2.38}$$

Thus, the temperature dependence of the specific heat C_p can be expressed as

$$C_p = A|T - T_s|^{-\alpha} \tag{2.39}$$

with α=1/2. In a log-log scale, this gives

$$logC_p = logA - \alpha \log|T - T_s| \tag{2.40}$$

2.4 Mean Field Model

2.4.1 The Landau Energy in the Mean Field Model for the First Order Phase Transitions

The free energy in the mean field model to describe the critical behaviour of the smectic A-smectic C* (AC*) phase transition when the electric field E is applied to the ferroelectric liquid crystals, can be written as

$$g = \frac{1}{2}\alpha\theta^2 + \frac{1}{4}b\theta^4 + \frac{1}{6}c\theta^6 + \frac{1}{2\chi_0\varepsilon_0}P^2 - DP^2\theta^2 + \frac{1}{4}eP^4 - EP \tag{2.41}$$

where θ is the tilt angle of the smectic C* phase and P is the polarization, which have a quadratic coupling $P^2\theta^2$. The temperature-dependent coefficient α is defined as α=a(T-T_0) where T_0 is the transition temperature for the AC* phase transition and a is a constant [51]. The coefficient b is negative since we consider here the AC* transition as a first order. So, we have the additional θ^6 term in our expansion, and the coefficients c, D and e are all positive.

The temperature dependence of the polarization P and the tilt angle θ in the presence of the electric field, can be obtained by minimizing the free energy g (Eq.2.41). We first minimize the free energy with respect to the tilt angle θ, which gives

$$a(T - T_0)\theta + b\theta^3 + c\theta^5 - 2DP^2\theta = 0 \tag{2.42}$$

We then minimize the free energy with respect to the polarization P, expressed as

$$\frac{1}{\chi_0\varepsilon_0}P - 2DP\theta^2 + eP^3 - E = 0 \tag{2.43}$$

We can evaluate the temperature dependence of the tilt angle θ and the polarization P using

the coupled equations 2.42 and 2.43. But, Eqs. 2.42 and 2.43 require to solve the θ^5 and P^3, respectively, which is too complicated for the study given here. Instead, we make an approximation here to calculate the electric field dependence of the polarization by eliminating the tilt angle θ in Eq. 2.43. As performed in an earlier study [18], we follow the same procedure and give the expressions derived previously. By writing Eq. 2.43 as,

$$P^2 = \frac{E}{eP} + \frac{2D}{e}\theta^2 - \frac{1}{e\chi_0\varepsilon_0} \tag{2.44}$$

and setting E=0, we have

$$P^2(E=0) = \frac{2D}{e}\theta^2 - \frac{1}{e\chi_0\varepsilon_0}. \tag{2.45}$$

By substituting Eq. 2.45 into Eq. 2.44, the electric-field dependence of the polarization can be obtained as

$$P^2(E) = P^2(E=0) + \frac{E}{eP(E)} \tag{2.46}$$

Eq. 2.46 can be further approximated to the expression in terms of the polarization at zero electric field only, P(E=0). By writing Eq. 2.46 in the form

$$P(E) = P(E=0)[1 + \frac{E}{eP^2(E=0)P(E)}]^{1/2} \tag{2.47}$$

and expanding the parenthesis in a Taylor series in the case of large e value, P(E) will be approximately equal to

$$P(E) \cong P(E=0)[1 + \frac{1}{2}\frac{E}{eP^2(E=0)P(E)}]. \tag{2.48}$$

Eq. 2.48 can be compared with the expression P(E) expanded in terms of P(E=0), written as

$$P(E) \cong P(E=0)[1 + E(\frac{\partial P}{\partial E})|_{E=0}(\frac{1}{P(E=0)})] \tag{2.49}$$

This comparison gives the susceptibility χ at zero electric field as

$$\chi = \frac{\partial P}{\partial E}|_{E=0} = \frac{1}{2eP(E)P(E=0)} \tag{2.50}$$

Since the susceptibility is calculated at zero electric field according to Eq. 2.50, the polarization P should be independent of the electric field on the right-hand side of this equation [51]. So, by writing approximately , Eq. 2.50 becomes

$$\chi = \frac{\partial P}{\partial E}|_{E=0} \cong \frac{1}{2eP^2(E=0)} \tag{2.51}$$

Thus, with this approximation of P(E), we arrive at the expression written as [51]

$$P^2(E) \cong P^2(E=0) + \frac{E}{eP(E=0)} \tag{2.52}$$

from Eq. 2.46. So, Eq. 2.52 gives the electric field dependence of the polarization P(E) and Eq. 2.51 expresses the polarization dependence of the susceptibility at zero electric field. Eq. 2.50 can be used for the polarization dependence of the susceptibility in the presence of the electric field by using Eq. 2.52.

The transition temperature T_c for constant electric fields E are determined for a first order AC* transition which we consider here according to the relation [51]

$$T_c = T_0 + \frac{3}{16ac}(b - \frac{4D^2}{e})^2 - \frac{2D}{ea\chi_0\varepsilon_0} \tag{2.53}$$

2.4.2 The Landau Energy in the Mean Field Model for the Weakly First Order or Close to Second Order Phase Transitions

For the electric-field induced SmA-SmC* transitions which can be of, a weakly first order or close to second order, the coefficient b in the Landau free energy can be taken as positive and there is no additional θ^6 term [52]. So, we have the expression as follows:

$$g = g_0 + \frac{1}{2}a(T - T_0)\theta^2 + \frac{1}{4}b\theta^4 + \frac{1}{2}\frac{P^2}{\chi} - \frac{1}{2}eP^2\theta^2 - EP \tag{2.54}$$

In this expansion χ=$\chi_0\varepsilon_0$ is the electric susceptibility. Using $\frac{\partial g}{\partial P}$=0, we have

$$\frac{P}{\chi} - eP\theta^2 - E = 0 \tag{2.55}$$

This gives

$$P = \frac{E}{1/\chi - e\theta^2} \tag{2.56}$$

Also, using $\frac{\partial g}{\partial \theta}$=0, we have

$$a(T - T_0) + b\theta^2 - eP^2 = 0 \tag{2.57}$$

This then gives

$$\theta^2 = \frac{eP^2 - a(T - T_0)}{b} \tag{2.58}$$

By substituting Eq. 2.58 into Eq. 2.55, we find

$$(\frac{ea}{b}(T - T_0) + \frac{1}{\chi})P - \frac{e^2}{b}P^3 = E \tag{2.59}$$

This is the electric field dependence of the polarization for the SmA-SmC* phase transitions in liquid crystalline systems [52]. When the electric field is zero (E=0), the Landau free energy can be minimized [52] using $\frac{\partial g}{\partial \theta}$=0, which gives

$$a(T - T_0) + b\theta^2 - eP^2 = 0 \tag{2.60}$$

Also, by using the minimization condition, $\frac{\partial g}{\partial P}$=0 , we then get

$$\theta^2 = \frac{1}{e\chi} \tag{2.61}$$

By substituting Eq. 2.61 into Eq. 2.60, we find

$$P^2 = \frac{a}{e}(T - T_0) + \frac{b}{e^2\chi} \tag{2.62}$$

Eqs. 2.61 and 2.62 represent the temperature dependences of the tilt angle (θ) and of the polarization (P), respectively [52].

The temperature dependence of the nematic susceptibility χ (E=0) can also be obtained from the Landau free energy (Eq. 2.54). By taking the derivative of g-g_0 with respect to θ, we get

$$\frac{\partial}{\partial\theta}(g - g_0) = a(T - T_0)\theta + b\theta^3 - eP^2\theta \tag{2.63}$$

The second derivative gives the inverse nematic susceptibility [52] as

$$\chi^{-1} = \frac{\partial^2}{\partial\theta^2}(g - g_0) = a(T - T_0) + 3b\theta^2 - eP^2 \tag{2.64}$$

Using Eq. 2.58 in Eq. 2.64 gives

$$\chi^{-1} = 2(eP^2 - a(T - T_0)) \tag{2.65}$$

This expresses the temperature dependence of the nematic susceptibility of the liquid crystals which undergo SmA-SmC* phase transitions [52].

Finally, the specific heat C_p can be derived from the Landau free energy (Eq. 2.54) when the electric field is zero (E=0). By substituting Eqs. 2.61 and 2.62 into Eq. 2.54, we obtain the free energy written as

$$g = g_0 + \frac{b}{4e^2\chi^2} + \frac{a}{2e\chi}(T - T_0) \tag{2.66}$$

By means of the temperature dependence of the electric susceptibility χ, the temperature dependence of the specific heat C_p can be derived according to the definition $C_p \equiv T(\partial g^2/\partial T^2)$.

The temperature dependence of the polarization jump $\triangle P_\theta$ can be analyzed using

$$\Delta P_\theta = A(T_c - T)^\beta \tag{2.67}$$

where β is the critical exponent for the order parameter (polarization) and A is the amplitude [52]. The electric susceptibility χ_θ can be analyzed at various temperatures close to the AC* phase transition by means of a power-law

$$(\chi_\theta^{-2} - \chi_{\theta C}^{-2})^{1/2} = A|T - T_c|^\gamma \tag{2.68}$$

where γ is the critical exponent for the susceptibility, A is the amplitude and $\chi_{\theta C}$ is the critical value of the electric susceptibility. The electric field dependence of the polarization can be analyzed according to a power-law

$$|E - E_C| = A(P - P_{\theta C})^\delta \tag{2.69}$$

where δ denotes the critical isotherm, A is the amplitude,$P_{\theta C}$ is the critical value of the polarization and E_c is the critical value of the electric field applied. The temperature dependence of the specific heat C_p can also be investigated according [52] to a power-law

$$\Delta C_p/A* = A(T_k - T)^{-\alpha} \tag{2.70}$$

where the excess heat capacity Δ C_p is scaled with the amplitude A* [24], α is the critical exponent for the specific heat, A is the amplitude and T_k is transition temperature in the metastability limit [52].

2.4.3 The Landau Energy in the Mean Field Model for the Isotropic Liquid Phase

If there is no electric field, then we can write the Landau free energy relation (Eq.2.41) as follows:

$$g = \frac{1}{2}\alpha\theta^2 + \frac{1}{4}b\theta^4 + \frac{1}{6}c\theta^6 + \frac{1}{2\chi_0\varepsilon_0}P^2 - DP^2\theta^2 + \frac{1}{4}eP^4 \tag{2.71}$$

In the isotropic liquid phase, the free energy is zero (F_1=0) since it is assumed that there is no orientational order and no spontaneous polarization in this phase [40]. The free energy g (Eq.2.71) can be minimized with respect to θ and P, which then becomes

$$g = \frac{1}{2}\alpha'\theta^2 + \frac{1}{4}b'\theta^4 + \frac{1}{6}c'\theta^6 \tag{2.72}$$

where

$$\alpha' = \alpha + \frac{2D}{e\chi_o\varepsilon_o}, b' = b - \frac{4D^2}{e}, c' = c \tag{2.73}$$

In terms of these coefficients α', b′ and c′, the condition for a first order transition can be obtained [18]. If we take the experimentally measured transition temperature as T_c, then the coefficient α becomes a constant given by α=a(T_o-T_c) at T=T_c. This gives the temperature difference at the transition point for a first order transition [40] as

$$T_c = T_o + \frac{3}{16}\frac{b'^2}{ac} - \frac{2D}{ea\chi_o\varepsilon_o} \tag{2.74}$$

The inverse susceptibility χ^{-1} can be derived from the free energy g (Eq.2.72) by taking the second derivative of g with respect to θ. We then have

$$\chi^{-1} = \alpha' + 3b'\theta^2 + 5c'\theta^4 \tag{2.75}$$

In Eq. 2.75 α' is the temperature dependent term according to Eq. 2.73 and the other coefficients b′ and c′ are all constants, as stated above [40]. In Eq.2.75, the temperature dependence of the orientational order parameter θ can be calculated from the mean field theory [53] as

$$\theta = [3(1 - \frac{T}{T_c})]^{1/2}, 0 < (T_c - T) << T_c \tag{2.76}$$

Thus, the temperature dependence of the inverse susceptibility χ^{-1} or the dielectric constant ε can be evaluated using Eq. 2.75 by means of Eq. 2.76 [40].

CHAPTER 3

CALCULATIONS AND RESULTS

3.1 Analysis of Some Thermotropic Liquid Crystals

3.1.1 P-Azoxyanisole

3.1.1.1 Pippard Relations for the C-N And N-I Phase Transitions in PAA

To apply the first and second Pippard relations (Eqs. 2.22 and 2.23) in PAA, we analyzed the experimental data for the thermal expansivity α_p [45] as a function of pressure at T=413 K, according to the power-law formula (Eq. 2.11), for the nematic-isotropic (N-I) (T_{NI}=407.1 K) and the solid-nematic (S-N) (T_{SN}=390.6 K) phase transitions. The experimental data which are taken from the literature are given in Figs.3.1 and 3.2 and the data which we analyzed are given in Tables 3.1 and 3.2. For the analysis of the N-I and S-N transitions, we obtained the values of the critical exponent γ and the values of the amplitude A_1, within the pressures between 16 MPa and 54 MPa, are given in Table 3.3 [46].

Using the values of γ and A_1, we then calculated the pressure dependence of the isothermal compressibility κ_T for both transitions of N-I and S-N in PAA, according to Eq. 2.15, where the experimental value of $(\partial P/\partial T)_S$=10 MPa/K [45] was used. By means of Eq. 2.18, the pressure dependence of the volume $V_T(P)$ was also calculated with the same parameters γ, A_1, and $(\partial P/\partial T)_S$ for the N-I and S-N transitions in PAA. The volume value at the transition pressure was taken as V_t=225 cm^3/mol [54] in Eq. 2.18. For those calculations of the isothermal compressibility κ_T (Eq. 2.15) and the volume $V_T(P)$ (Eq. 2.18) at various pressures (T=413 K), we used the values of γ and A_1 for the various pressure ranges in the S-N transition of PAA, as given in Table 3.3.

For the C-N transition, as can be seen from Table 3.3, as the pressure approaches the transition pressure P_{CN} since at phase transition points, some thermodynamic quantities, such as thermal expansion, isothermal compressibility and specific heat,diverge so the γ values increase gradually except for the pressure range of 17 MPa to 51 MPa, where γ has a large value of 1.58. This is due to the fact that within this pressure range our analysis shows that the experimental data points are more scattered compared to our analysis for the other pressure ranges.

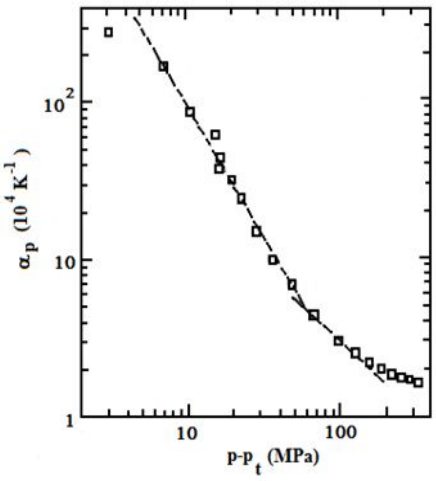

Figure 3.1: Experimental data for the thermal expansivity α_p as a function of pressure along the isotherm 413K in solid PAA and at melting. P_t represents the transition pressure [45].

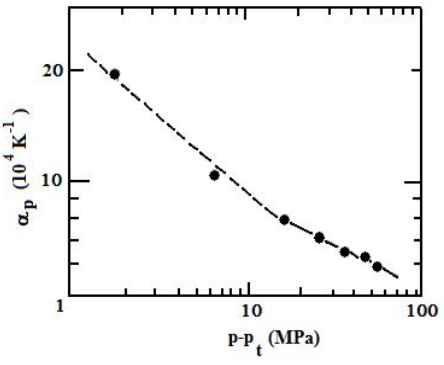

Figure 3.2: Experimental data for the thermal expansivity α_p as a function of pressure along the isotherm 413K in PAA across the nematic isotropic (NI) transition [45].

Table 3.1: Experimental data for the thermal expansivity as a function of pressure along the isotherm 413K in solid PAA and at melting. P_{CN} represents the crystal (C)-nematic (N) transition pressure [45].

P-P_{CN} (MPa)	α_p x 10^4 (K^{-1})
3.13	276.39
7.16	167.10
10.99	84.88
15.72	61.18
17.31	43.12
16.85	38.62
20.16	31.73
22.82	24.93
28.46	15.10
36.48	9.74
48.72	6.87
68.78	4.34
98.48	2.99
128.00	2.46
157.38	2.16
190.80	1.98
222.19	1.77
255.11	1.73
284.74	1.70
335.94	1.66

Finally, by using our calculated values of α_p (Eq. 2.11) and V_T(P) (Eq. 2.18) as a function of pressure (T=413K), we then calculated the specific heat C_p as a function of pressure, according to Eq. 2.19 by using values of γ and A_1 for various pressure ranges given in Table 3.3, for the N-I and S-N transitions.

Once, we calculated values of the thermal expansivity α_p, the volume V and the specific heat C_p, as a function of pressure (T=413K), we then applied the first Pippard relation (Eq. 2.22). Fig. 3.3 gives C_p plotted versus $V\alpha_p$ (Eq. 2.22) for the N-I transition for the pressure range of 16 MPa to 54 MPa in PAA. We plot C_p against $V\alpha_p$ for the S-N transition for all the pressure ranges from 3 MPa to 357 MPa (Table 3.3) in PAA, according to Eq. 2.22, in Fig. 3.5.

We also applied the second Pippard relation (Eq. 2.23) by plotting the thermal expansivity $\alpha_p$against the isothermal compressibility κ_T for the N-I and S-N transitions in PAA, as given in Figs. 3.4 and 3.6, respectively [46]. Both figures give α_p and κ_T values at various pressures

Table 3.2: Experimental data for the thermal expansivity α_p as a function of pressure along the isotherm 413K in PAA across the nematic isotropic (NI) transition. P_{NI} denotes the nematic (N)-isotropic liquid (I) transition pressure [45].

P-P_{NI} (MPa)	α_p x 10^4 (K^{-1})
1.856	19.42
6.70	10.91
16.18	4.52
25.78	3.16
35.96	2.41
46.17	2.15
54.50	1.76

Table 3.3: Values of the critical exponent γ and the amplitude A_1 for the pressure ranges indicated for the nematic-isotropic liquid (N-I) and for the crystal-nematic (C-N) phase transitions in PAA from the analysis of the experimental data for the thermal expansivity α_p according to Eq. 2.11

Pressure range (MPa)	γ	A_1 (MPa/K)
16<P-P_{NI}<54	0.85±0.06	$8.99x10^2$±0.21
3<P-P_{CN}<17	0.96±0.14	$4.34x10^4$±2.28
17<P-P_{CN}<51	1.58±0.09	$1.00x10^9$±1.58
72<P-P_{CN}<201	0.75±0.08	$2.93x10^2$±1.46
239<P-P_{CN}<357	0.36±0.03	0.20±0.58

(Table 3.3) for T=413K in PAA. From our plots (Figs.3.3-3.6), we deduced the values of the slope dP/dT and of the intercept T(dS/dT) (Figs. 3.3 and 3.5) and $\frac{1}{V}$ ($\frac{dV}{dT}$) (Figs. 3.4 and 3.6). Our values of dP/dT calculated from Eqs. 2.22 and 2.23 are given in Table 3.4. Our intercept values are tabulated in Table 3.5 [46].

Table 3.4: Values of the slope $(dP/dT)_\lambda$ calculated from Eqs. 2.22 and 2.23 for the nematic-isotropic (N-I) and crystal-nematic (C-N) phase transitions in PAA.

Transition	T(K)	Calculated (Eq. 2.22) $(dP/dT)_\lambda$ (MPa/K)	Calculated (Eq. 2.23) $(dP/dT)_\lambda$ (MPa/K)
N-I	407.1	10.39	9.38
C-N	390.6	10.35	9.46

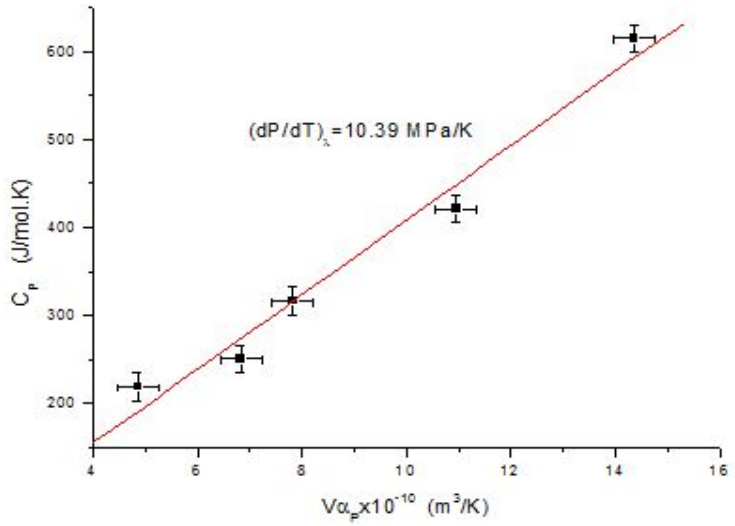

Figure 3.3: Specific heat C_p versus $V\alpha_p(=\partial V/\partial T)$ for the nematic-isotropic liquid (NI) phase transition for the pressure range P_{NI} given in Table 3.3 at T= 413 K in PAA (T_{NI}=407.1 K) according to the first Pippard relation (Eq. 2.22)

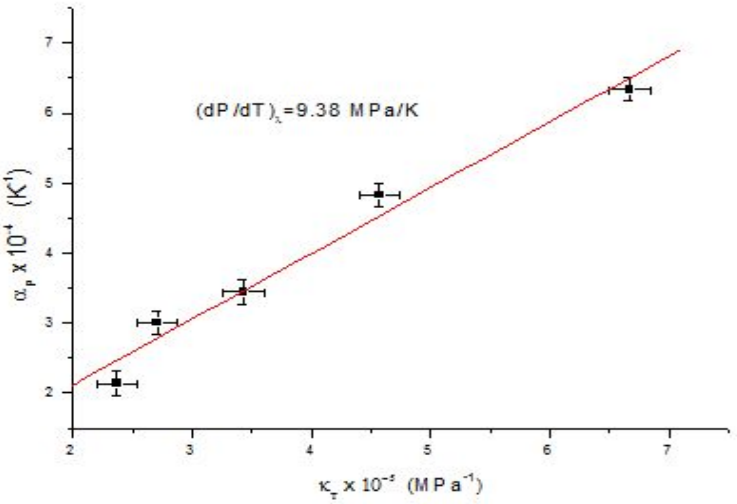

Figure 3.4: Thermal expansivity α_p versus the isothermal compressibility κ_T for the nematic-isotropic liquid (NI) phase transition for the pressure range P_{NI} given in Table 3.3 at T=413 K in PAA (T_{NI}= 407.1 K) according to the second Pippard relation (Eq. 2.23).

Using our linear plots, the values of the slope dP/dT, which we deduced are very close to each other for N-I and C-N transitions in PAA. As can be seen from Table 3.4, those slope values are very close to the experimental value of slope which is equal to 10 MPa/K.

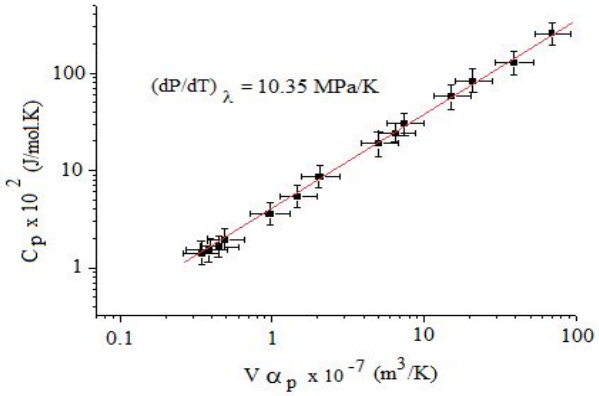

Figure 3.5: Specific heat C_p versus $V\alpha_p$ (=$\partial V/\partial T$) for the crystal-nematic (CN) phase transition for the pressure ranges P_{CN} given in Table 3.3 at T=413 K in PAA (T_{CN}= 390.6 K) according to the first Pippard relation (Eq. 2.22).

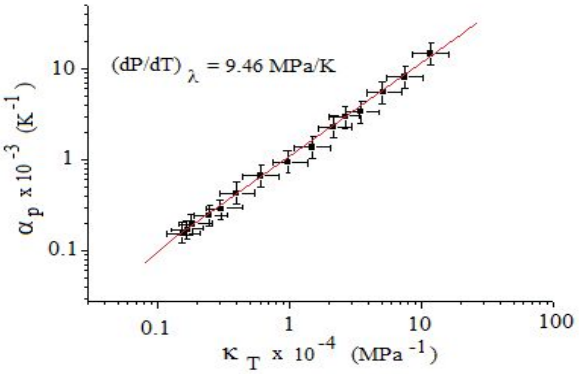

Figure 3.6: Thermal expansivity α_p versus the isothermal compressibility κ_T for the crystal-nematic (CN) phase transition for the pressure ranges P_{CN} given in Table 3.3 at T=413 K in PAA (T_{CN}=390.6 K) according to the second Pippard relation (Eq. 2.23).

Table 3.5: Values of the intercept $T(\frac{dS}{dT})_\lambda$ (Eq. 2.22) and $\frac{1}{V}\left(\frac{dV}{dT}\right)_\lambda$ (Eq. 2.23) for the nematic-isotropic (N-I) and crystal-nematic (C-N) phase transitions in PAA

Transition	T(K)	$-T(\frac{dS}{dT})_\lambda$ (J/mol.K)	$\frac{1}{V}\left(\frac{dV}{dT}\right)_\lambda$ x 10^{-4} (K^{-1})
N-I	407.1	14.77	0.25
C-N	390.6	89.89	1.56

3.1.1.2 Temperature Dependence of the Thermal Expansivity and the Specific Heat Near the Nematic-Isotropic (NI) Phase Transition in PAA

While applying the Pippard relations we analyzed the thermal expansivity and specific heat as a function of pressure. For this study we calculated the thermal expansivity α_p as a function of temperature for the nematic-isotropic (NI) phase transition in PAA, according to Eq. 2.13. For the calculation of the thermal expansivity α_p, we used the values of γ and A_1 from our previous analysis, as given in Table 3.3. We plot our calculated α_p as a function of temperature in Fig. 3.7. The experimental data for the thermal expansion α_p and the specific heat C_p which are taken from the literature for this analysis, are given in Table 3.6. The values of α_p calculated by Maier and Saupe [54] are also given in Fig. 3.7 for comparison [55]. Our calculated α_p values were normalized to compare with the values of Maier and Saupe [54]. So, the background thermal expansivity α_0 (α_0=6.3651x10^{-4} ^{o}C^{-1}) was introduced in Eq. 2.13 as follows [55].

$$\alpha_p(T) = \alpha_0 + A_1(\frac{dP_t}{dT})^{-\gamma}(T_t - T)^{-\gamma} \tag{3.1}$$

Also, since the transition temperature was T_c=408.2 K or 135.05^{o}C for the thermal expansivity data [54], we shifted our calculated α_p by ΔT=1.15^{o}C according to the T_{NI} value of 133.9^{o}C for the specific heat C_p data [56].

We also calculated the specific heat C_p as a function of temperature for the nematic- isotropic (N-I) phase transition in PAA, according to Eq. 2.20, as shown in Fig. 3.8. For this calculation, in Eq.2.20 we used the values of the critical exponent γ and the amplitude A_1 (Table 3.3) which we deduced from our analysis of the experimental data for the thermal expansivity α_p [45] in the pressure range of 16<P-P_{NI}<54 MPa, according to Eq. 2.11, as before. The experimental data for C_p using differential scanning calorimetry [57] are also shown in Fig. 3.8. We normalized our calculated specific heat C_p with the experimental C_p at 150^{o}C and compared with the experimental data. So, in Eq. 2.20 the background specific heat C_0 (C_0=0.3867 cal/g.deg) was introduced, as follows [55]

$$C_p = C_0 + A_1 TV(dP_m/dT)^{1-\gamma}(T - T_m)^{-\gamma} \tag{3.2}$$

As can be seen from Fig. 3.8, at the transition point C_p diverges, since C_p and α_p have the same divergence property close to the transition points (Eq. 2.25), one can expect, α_p, to

Table 3.6: Experimental data for the thermal expansivity α_p and the specific heat C_p as a function of temperature for the nematic-isotropic (NI) phase transition in PAA [54, 56].

T(^{o}C)	α_p x 10^{-4} (^{o}C^{-1})	T (^{o}C)	C_p (cal/g.deg)
106.12	7.305	118.2	0.460
108.58	7.345	120	0.462
111.15	7.359	125.5	0.474
113.5	7.399	127	0.480
116.17	7.522	128	0.484
118.63	7.617	129	0.493
121.29	7.823	130	0.497
123.31	7.970	131	0.512
126.6	8.343	131.47	0.524
128.51	8.653	132.390	0.541
131.55	9.353	132.4	0.544
132.08	9.492	133.17	0.533
133.53	10.019	133.3	0.628
134.56	10.543	133.82	0.674
135.26	11.094	135.34	0.858
135.75	11.643	135.49	0.731
136.02	12.245	135.5	0.585
136.27	13.066	136.4	–
136.39	14.187	136.54	–
136.44	14.843	137	0.485
136.99	9.682	137.4	–
137.25	9.164	138	0.468
137.73	8.539	138.5	–
138.29	8.241	139.3	–
138.52	8.160	140	0.465
139.06	8.026	142	0.466
139.94	7.813	144	0.466
140.26	7.787	146	0.466
140.8	7.708	148	0.466
141.24	7.655	150	0.467
142.1	7.605	–	–
142.64	7.581	–	–
143.18	7.529	–	–
143.5	7.5580	–	–
143.82	7.533	–	–
144.250	7.508	–	–
144.79	7.510	–	–

diverge to infinity at the transition temperature. Fig. 3.7 shows that α_p diverges to infinity at the transition point as expected. Also Figs.3.7 and 3.8 show, both calculated values of α_p and

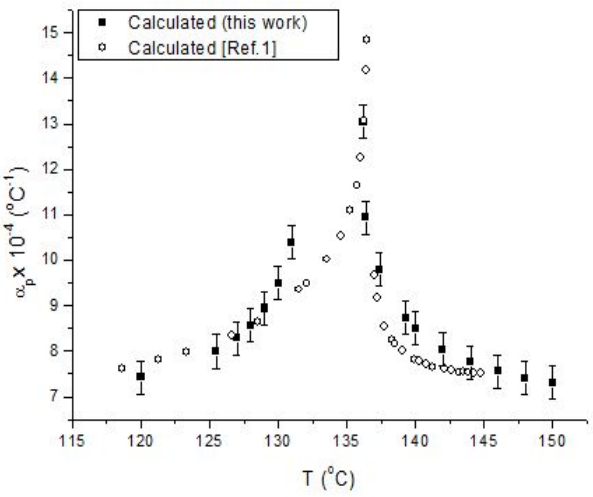

Figure 3.7: Our calculated thermal expansivity α_p as a function of temperature for the nematic-isotropic (NI) phase transition in PAA according to Eq. 2.13. Calculated α_p values (T_{NI}=135.1^{o}C) due to Maier and Saupe [54] are also shown here for comparison.

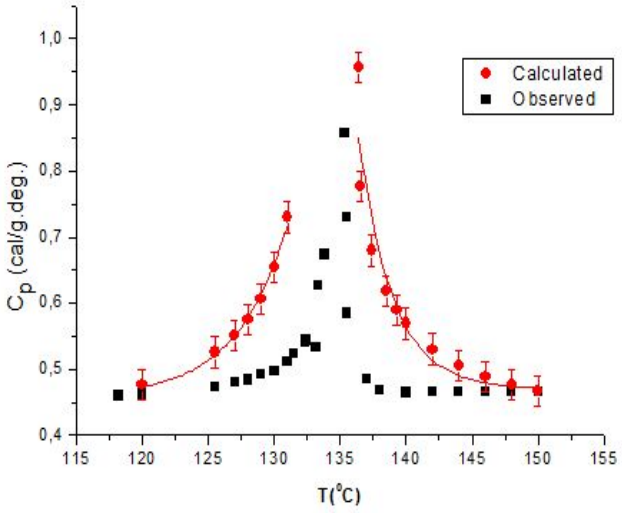

Figure 3.8: Our calculated specific heat C_p represented by solid lines as a function of temperature for the nematic-isotropic (NI) phase transition in PAA (T_{NI}=133.9^{o}C) according to Eq. 2.20. Experimental data [56] are also shown here for comparison.

C_p are in a good agreement with the experimental data of α_p [54] and C_p [56].

Some discrepancy occurs between our calculated thermal expansivity α_p with the α_p calcu-

lated previously [54]. In particular, below T_{NI} from the melting temperature the discrepancy occurs for the N-I transition in PAA. Above T_{NI} both calculated values of the thermal expansivity are in better agreement (Fig.3.7).

As can be seen from Fig. 3.8, as the temperature increases from the nematic phase, our calculated C_p values get larger up to the transition temperature where both the calculated and experimental C_p values diverge. Above T_{NI}, there is a sharp decrease in the observed C_p values in comparison with our calculated C_p values which decrease gradually up to nearly 150^oC, where the background specific heat C_0 was determined using both observed and calculated C_p values.

The discrepancy between our calculated and the observed C_p may be due to the lack of experimental data for the isobaric expansivity α_p which we used for the nematic-isotropic (N-I) transition in PAA to calculate the specific heat C_p as a function of temperature. Also, the approximations used for the slopes according to our analysis of the experimental thermal expansivity α_p within the pressure range of 15<P-PL<54 MPa, may not be fully satisfied to calculate the specific heat C_p in PAA close to the melting point. Around the melting point, orientational disorder increases. Our calculations of the thermal expansivity α_p and the specific heat C_p exhibit an anomalous behaviour in PAA, which can be considered as a second order phase transition with a particular type of orientational disorder.

3.1.1.3 Analysis of the Specific Heat of P-Azoxyanisole (PAA) Near the Phase Transitions

After analyzing the specific heat C_p using the power-law formula for the nematic-isotropic liquid (NI) and the crystal-nematic (CN) phase transitions in PAA, in this study we also used a renormalization-group expression with a corrections to scaling term [39]. From the analysis of the specific heat C_p, we then calculated the enthalpy H and the entropy S as a function of temperature in the nematic phase for $T<T_{NI}$ and for $T>T_{CN}$ in PAA. The experimental data for the specific heat taken from the literature is given in Fig. 3.9 and in Tables 3.7 and 3.8.

Analysis of the specific heat C_p

We analyzed the specific heat C_p using a power-law formula, with the reduced temperatures in Eq. 2.3 for the isotropic liquid-nematic (T_{NI}=133.9^{o}C) and solid-nematic (T_{SN}=117.6^{o}C)

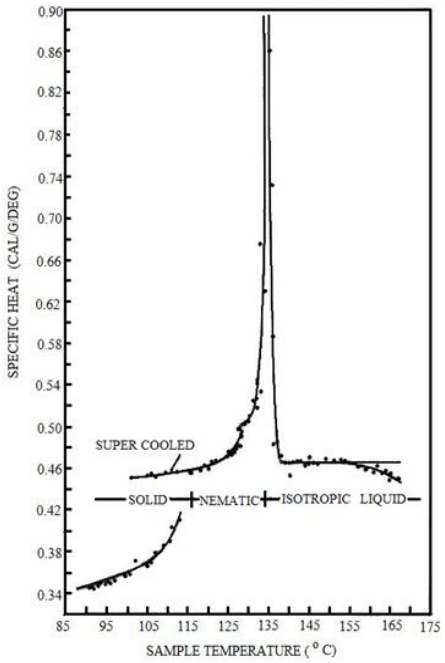

Figure 3.9: Experimental data for the specific heat C_p as a function of temperature above and below the transition temperature of the nematic-isotropic phase transition in PAA [56].

Table 3.7: Experimental data for the specific heat C_p as a function of temperature above and below the transition temperature of the nematic-isotropic phase transition in PAA [56].

T (^{o}C)	C_p (cal/g.deg)	T (^{o}C)	C_p (cal/g.deg)
T>T_{NI}		T<T_{NI}	
154.93	0.863	133.72	0.562
158.27	0.733	133.71	0.557
164.72	0.586	133.54	0.555
175.18	0.484	133.53	0.554
–	–	133.52	0.548
–	–	133.35	0.546
–	–	133.34	0.541
–	–	133.33	0.538
–	–	133.15	0.533
–	–	133.14	0.528

phase transitions in PAA. The experimental C_p data [56] was used for our analysis. Table 3.9 gives the values of α and A within the interval of the reduced temperature ε above and below T_{NI} (T_{SN}) for PAA. We plot in a log-log scale C_p against ε according to the Eq. 2.3 for both N-I and S-N transitions. Figs. 3.10 and 3.11 give our plots above and below T_{NI}, respectively.

Table 3.8: Experimental data for the specific heat C_p as a function of temperature above and below the transition temperature of the nematic-solid (SN) phase transition in PAA [56].

T (^{o}C)	C_p (cal/g.deg)	T (^{o}C)	C_p (cal/g.deg)
T>T_{SN}		T<T_{SN}	
128.68	0.482	113.87	0.410
128.16	0.479	111.41	0.391
127.64	0.475	109.85	0.385
126.77	0.474	107.93	0.379
125.90	0.472	107.06	0.373
–	–	104.80	0.368
–	–	101.15	0.358
–	–	95.26	0.350
–	–	91.44	0.346
–	–	88.32	0.344

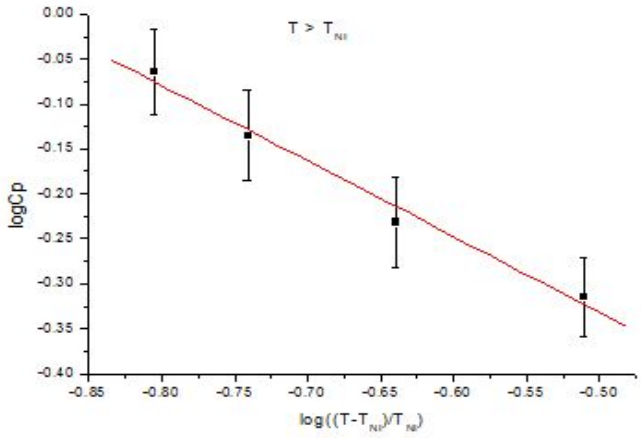

Figure 3.10: The specific heat C_p in a log-log scale as a function of the reduced temperature, $\varepsilon=\left|T\text{-}T_{NI}\right|/T_{NI}$,above T_{NI} for the nematic-isotropic liquid phase transition in PAA according to Eq. 2.4. Uncertainties in C_p calculated from the uncertainties in α and logA (Table 3.9), are shown as vertical lines.

logC_p is plotted against logε in Figs. 3.12 and 3.13 above and below T_{SN}, respectively for PAA [39].

In Figs. (3.10-3.13) we represent with vertical lines the uncertainties in the specific heat C_p, which we determined when Eq. 2.4 was fitted to the experimental data [56]. Uncertainties in the critical exponent α and in logA, as given in Table 3.9, which is also given in Table

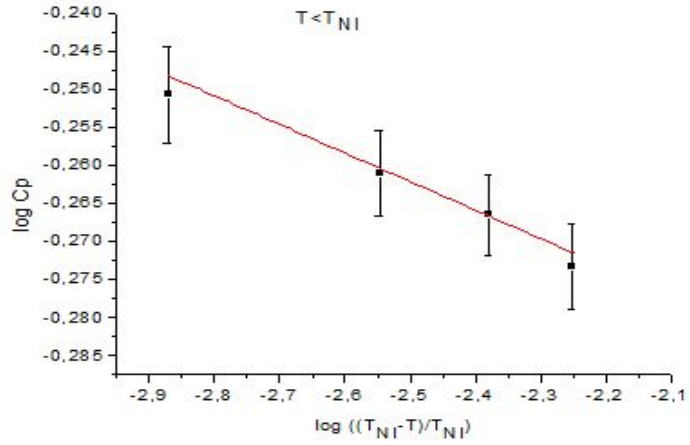

Figure 3.11: The specific heat C_p in a log-log scale as a function of the reduced temperature, $\varepsilon=|T-T_{NI}|/T_{NI}$, below T_{NI} for the nematic-isotropic liquid phase transition in PAA according to Eq. 2.4. Uncertainties in C_p calculated from the uncertainties in α and logA (Table 3.9), are shown as vertical lines.

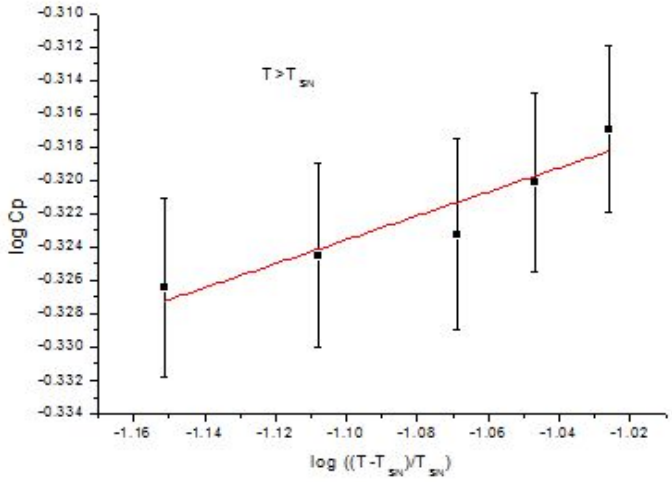

Figure 3.12: The specific heat C_p in a log-log scale as a function of the reduced temperature, $\varepsilon=|T-T_{SN}|/T_{SN}$, above T_{SN} for the solid-nematic phase transition in PAA according to Eq.2.4. Uncertainties in C_p calculated from the uncertainties in α and logA (Table 3.9), are shown as vertical lines.

3.15 were used to determine the uncertainties in the specific heat values (Figs. 3.10-3.13). In particular in Figs. 3.11 and 3.12, because of the data dispersion, the uncertainties in the specific heat C_p are much larger and the solid lines represent the best fits to the experimental

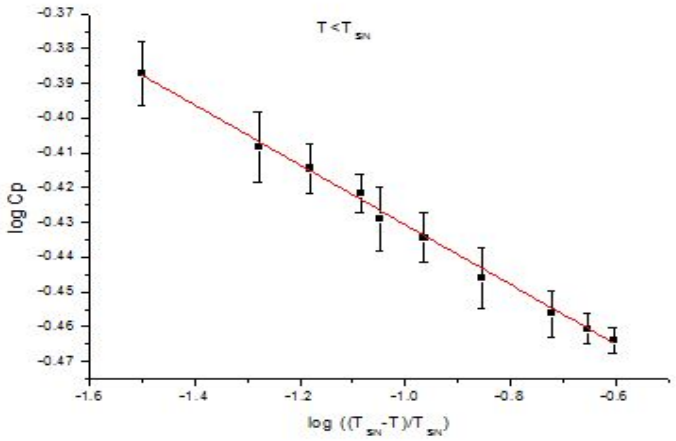

Figure 3.13: The specific heat C_p in a log-log scale as a function of the reduced temperature, ε=$\left|\text{T-T}_{SN}\right|$/$T_{SN}$, below T_{SN} for the solid-nematic phase transition in PAA according to Eq.2.4. Uncertainties in C_p calculated from the uncertainties in α and logA (Table 3.9), are shown as vertical lines.

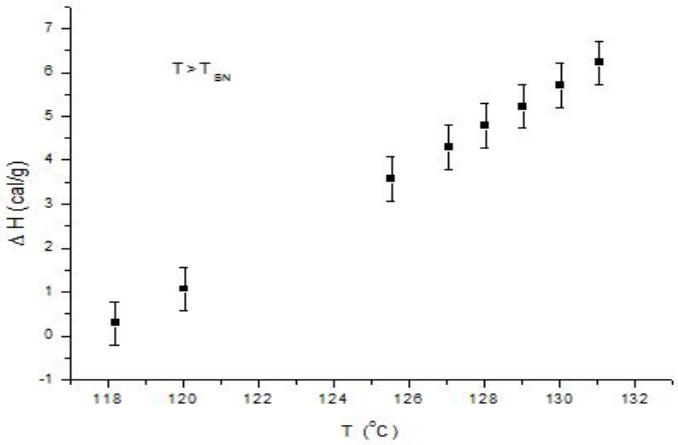

Figure 3.14: The enthalpy difference (ΔH=H-Ho) calculated from Eq. 3.5 as a function of temperature in the nematic phase ($T>T_{SN}$) of PAA (T_{SN}=117.6^{o}C).

data [56]. The critical specific heat associated with the nematic-isotropic liquid (N-I) and solid-nematic (S-N) phase transitions can also be described by the expression [58]

$$C_p = \begin{cases} A\varepsilon^{-\alpha}(1 + D\varepsilon^{\Delta}) + B, for T > T_c \\ A'\varepsilon^{-\alpha'}(1 + D'\varepsilon^{\Delta}) + B', for T < T_c \end{cases} \tag{3.3}$$

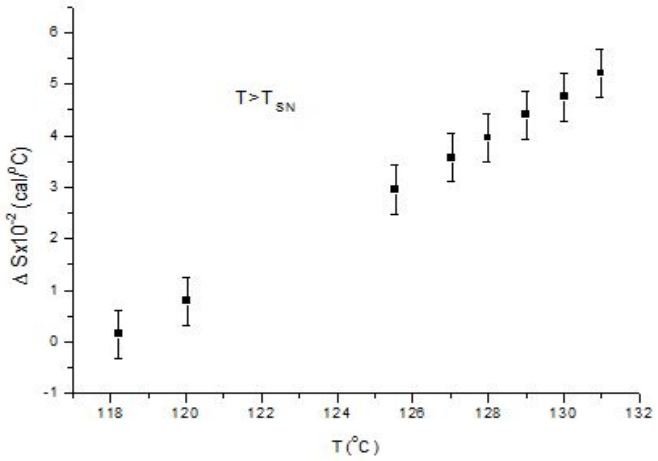

Figure 3.15: The entropy difference (ΔS=S-S_o) calculated from Eq. 3.7 in the nematic phase (T>T_{SN}) of PAA (T_{SN}=117.6^{o}C).

Table 3.9: Values of the critical exponent α for the specific heat C_p and the amplitude A within the interval of the reduced temperature ε according to the power-law formula (Eq. 2.3) for the nematic-isotropic (T_{NI}=133.9^{o}C) and nematic-solid (T_{SN}=117.6^{o}C) phase transitions in PAA. Uncertainties in α and logA are given from fitting Eq. 2.3 to the experimental C_p data [56].

Phase Transitions	T(K)	α	LogA	ε=| T-T_c |/T_c (T_c=T_{NI},T_{SN})
Nematic-Isotropic Liquid (NI)	T>T_{NI}	0.85 ± 0.07	-1.604 ± 0.12	$1.57\text{x}10^{-2} < \varepsilon < 3.08\text{x}10^{-2}$
	T<T_{NI}	0.04 ± 0.005	-0.354 ± 0.014	$1.34\text{x}10^{-3} < \varepsilon < 5.68\text{x}10^{-3}$
Nematic-Solid (SN)	T>T_{SN}	-0.07 ± 0.01	-0.246 ± 0.016	$7.06\text{x}10^{-2} < \varepsilon < 9.42\text{x}10^{-2}$
	T<T_{SN}	0.09 ± 0.002	-0.518 ± 0.002	$3.17\text{x}10^{-2} < \varepsilon < 2.48\text{x}10^{-1}$

where $D\varepsilon^{\Delta}$ is a corrections-to-scaling term in which $\Delta\approx0.5$ and B is a nonsingular critical contribution [59]. When D=0, which was the constraint to analyze the C_p data [59], the above relation reduces to Eq. 2.3 with the coefficient B [39].

For this analysis again we examined the specific heat C_p, using the experimental data [56] at various temperatures for the NI and S-N transitions of PAA . From this nonlinear fitting the values of the critical exponent α for C_p and, the parameters A, B and D are given within the temperature intervals ε in Table 3.10. Some parameters are given in the table with their uncertainties. Those without uncertainties were held constant and the remaining parameters

were varied in Eq. 3.3 during the fitting procedure [39].

The exponent values of α=0.04 (T<T_{NI}), -0.07 (T>T_{SN}) and 0.09 (T<T_{SN}), are all nearly equal to 0.1 which is not expected from the mean field theory (α=α'=0). Those exponent values can be compared with the value of α=1/8 predicted from a three-dimensional Ising model. The negative exponent value of -0.07 is in agreement with the helium analogy and the inverted XY model for liquid crystals which can be renormalized according to the Fisher's renormalization formula,α_R=-α/(1-α), which gives the value of α=0.06. This value is also close to the value of the three-dimensional Ising model.

Our exponent value of α=0.85 (T>T_{NI}) is too large to compare with the predictions of the models considered above. This may be due to the fact that the observed C_p drops rapidly just above T_{NI}=133.9^{0}C and it does not vary considerably with the temperature in the isotropic liquid phase from 137 to 150^{0}C. This large value of the critical exponent led us to investigate the mechanism of the nematic-isotropic liquid (NI) phase transition in PAA. We used the renormalization- group expression and adopted it to analyze the observed C_p data for the NI and SN transitions in PAA. From our analysis, we obtained α=0.5 for T<T_{NI} and T<T_{SN}, as the mean-field-tricritical value. Unexpected behaviour occurs above T_{SN} in the nematic phase with a large negative value of α=-0.85 according to the renormalization- group-analysis. This is also associated with the mean field tricritical behaviour (α=0.5) below T_{SN} . On the other hand, the renormalization-group-analysis does not give the expected critical behaviour above T_{SN} with the exponent value of -0.85 if one assumes a mean field tricritical transition below T_{SN}. So, the simple power-law formula describes adequately the solid-nematic transition with the α values.

Calculation of the enthalpy H

We calculated the temperature dependence of the enthalpy H in the nematic phase from the specific heat C_p for the solid-nematic (S-N) phase transition in PAA. By defining C_p=∂H/∂T and using the power-law formula for the specific heat (Eq. 2.3), the temperature dependence of the enthalpy H can be calculated from the integral expression:

$$H = \int_{T}^{T_c} A\left|\frac{T - T_c}{T_c}\right|^{-\alpha} dT + H_0 \tag{3.4}$$

where T_C=T_{SN}. From Eq. 3.4, the temperature dependence of the enthalpy in the nematic

phase of PAA for T>T_{SN} can be calculated as

$$H = H_0 + \frac{AT_{SN}}{1-\alpha}\left(\frac{T-T_{SN}}{T_{SN}}\right)^{1-\alpha} \tag{3.5}$$

where H_0 denotes the enthalpy at the transition temperature T_{SN} when α<1. We calculated the temperature dependence of the enthalphy difference, $\Delta H = H - H_0$, in the nematic phase for T>T_{SN} using our values of α, A (Table 3.9), T_{SN}=117.6^{0}C and H_0=28.1 cal.g^{-1} [56] according to Eq. 3.4. Our calculated ΔH values are plotted as a function of temperature (T>T_{SN}) in Figure 3.14 [39].

Calculation of the entropy S

We also calculated the temperature dependence of the entropy S in the nematic phase above the solid-nematic (S-N) phase transition in PAA. By defining $C_p = T(\partial S/\partial T)_P$, the entropy S can be calculated from the specific heat C_p at T=T_C using the power-law formula (Eq. 2.3) according to the integral expression:

$$S = \int \frac{A}{T_c}\left(\frac{T-T_c}{T_c}\right)^{-\alpha} dT + S_0 \tag{3.6}$$

where T_C=T_{SN}. The entropy expression can be obtained above the solid-nematic transition (T>T_{SN}) from Eq. 3.6, which gives:

$$S = S_0 + \frac{A}{1-\alpha}\left(\frac{T-T_{SN}}{T_{SN}}\right)^{1-\alpha} \tag{3.7}$$

where S_0 denotes the entropy at T=T_{SN} when α<1. As we performed for the calculation of the enthalpy H, we calculated the entropy difference $\Delta S = S - S_0$, as a function of temperature by using the values of the critical exponent α and the amplitude A for T>T_{SN} (Table 3.9) according to Eq. 3.7. Fig. (3.15) gives the entropy difference ΔS (entropy S with respect to the entropy value S_0 at the transition temperature) as a function of temperature in the nematic phase for T>T_{SN} in PAA [39].

Figs. 3.14 and 3.15 show that the enthalpy difference ΔH and the entropy difference ΔS increase with increasing temperature.

Table 3.10: Values of the critical exponent α for the specific heat C_p and the parameters A, B and D within the interval of the reduced temperature ε according to Eq. 3.3 for the nematic-isotropic liquid (N-I) and nematic-solid (S-N) phase transitions, respectively, in PAA.

T(K)	α	A ($cal.g^{-1}{}^{o}C^{-1}$)	B ($cal.g^{-1}{}^{o}C^{-1}$)	D	$\varepsilon=\lvert T-T_c\rvert/T_c$ ($T_c=T_{NI},T_{SN}$)
$T>T_{NI}$	0.006	(1.69±0.22) x10^2	(-1.74±0.23) x10^2	0.067±0.003	$9.0\text{x}10^{-3}<\varepsilon<4.6\text{x}10^{-2}$
$T<T_{NI}$	0.5	0.025±0.013	-7.4x10^4	2.9x10^6	$2.2\text{x}10^{-3}<\varepsilon<4.4\text{x}10^{-2}$
$T>T_{SN}$	-8.05	-0.85x10^7	8.05x10^7	-1.13±0.02	$5.1\text{x}10^{-3}<\varepsilon<9.4\text{x}10^{-2}$
$T<T_{SN}$	0.5	-1.32x10^6	1.32x10^6	-1.02±0.01	$2.2\text{x}10^{-2}<\varepsilon<2.5\text{x}10^{-1}$

3.1.1.4 Analysis of the Specific Heat of PAA in the Supercooled Solid Phase of Liquid Crystals

The specific heat was analyzed in the supercooled and solid regions for PAA by a power-law formula using the experimental data [56] for the specific heat taken from the literature, which is given in Table 3.11. For PAA, we were in particular interested in the stability limit for the supercooled solid. Using Eq. 2.1 and taking T_s instead of the transition temperature T_t, the

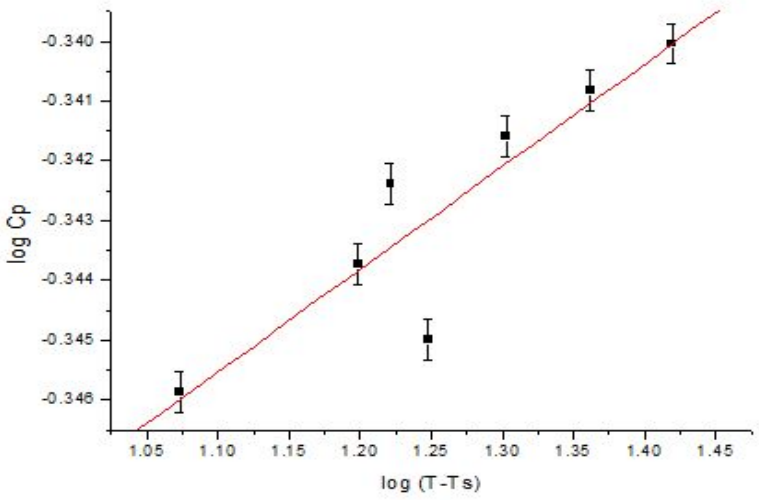

Figure 3.16: The specific heat C_p in a log-log scale as a function of the temperature with respect to the stability temperature T_s for the supercooled solid phase of PAA using the experimental data [56] analyzed according to Eq. 2.39 (see Table 3.18).

C_p data [56] was analyzed with the stability temperature of T_s=90^{o}C for PAA in the solid phase.Then, the fitted parameters were determined, as given in Table 3.18. Fig. 3.16 gives a plot of C_p against T-T_s in the log-log scale according to Eq.2.2 for the supercooled region of PAA. We also analyzed the C_p data for the solid phase of PAA through Eq.2.1 with the T_s=90^{o}C. The fitted parameters α and A in the temperature interval studied, are given in Table 3.18 for the solid phase of PAA. Finally, Fig. 3.17 gives our plot of logC_p against log(T-T_s) for the solid phase of this liquid crystal [56].

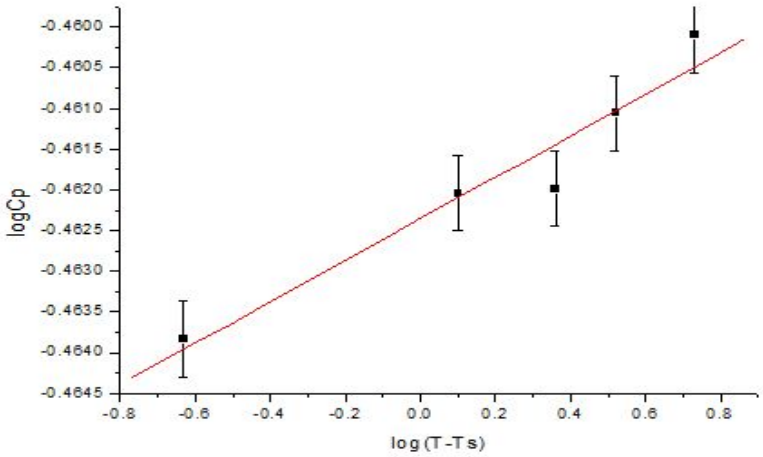

Figure 3.17: The specific heat C_p in a log-log scale as a function of the temperature with respect to the stability temperature T_s for the solid phase of PAA using the experimental data [56] analyzed according to Eq. 2.39 (see Table 3.18).

Our analysis gave us the values of -0.02 (supercooled solid phase) and ~0 (solid phase). The power-law formula for the stability limit was not satisfactory for the supercooled solid phase of PAA.

Table 3.11: Experimental data for the specific heat C_p as a function of temperature for the supercooled solid phase and solid phase of PAA[56].

Supercooled Solid Phase of PAA		Solid Phase of PAA	
T (^{o}C)	C_p (cal/g.deg)	T (^{o}C)	C_p (cal/g.deg)
101.84	0.451	90.23	0.344
105.79	0.453	91.26	0.345
106.65	0.455	92.29	0.345
107.68	0.452	93.32	0.346
110.08	0.455	95.38	0.347
113.00	0.456	–	–
116.26	0.457	–	–

3.1.2 Anisaldazine

3.1.2.1 Temperature Dependence of the Specific Heat of Anisaldazine Close to Phase Transitions

The analysis of the specific heat C_p measured as a function of temperature for the nematic-isotropic liquid (T_{NI}=180.5^{o}C) and the solid-nematic (T_{SN}=168.9^{o}C) transitions in anisaldazine, was performed here according to a power-law formula [37].

In this study we analyzed the experimental data for the specific heat C_p taken from the literature, which is given in Fig. 3.18 and Table 3.12. For this analysis, we used the linear relation (Eq. 2.4) above and below the transition temperature for the nematic-isotropic and solid- nematic transitions in anisaldazine. Table 3.15 gives the values of the critical exponent α and the amplitude A above (T>T_{NI}) and below (T<T_{NI}) the transition temperature T_{NI} and also above (T>T_{SN}) and below (T<T_{SN}) the transition temperature T_{SN} in anisaldazine [37].

Since the experimental data for C_p was scattered above T_{NI} [56], it was analyzed in two temperature intervals and, the values of α and A were extracted according to Eq. 2.4, as tabulated in Table 3.15. Fig. 3.19 gives our plot of the specific heat C_p against the temperature in a log-log scale according to Eq. 2.4 in the temperature interval considered here (T>T_{NI}) for the nematic-isotropic liquid transition in anisaldazine. We have given here Fig. 3.19 only as the representative plot for the nematic-isotropic liquid transition of anisaldazine. As we extracted the values of α and A from Fig. 3.19, those α and A values were also extracted from our plots of C_p against the temperature for the nematic-isotropic liquid transition in the

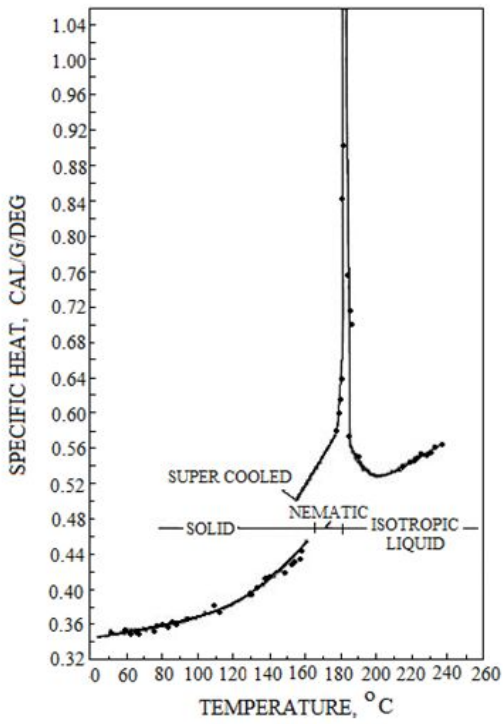

Figure 3.18: Specific heat C_p of anisaldazine from 47 to 237^o [56].

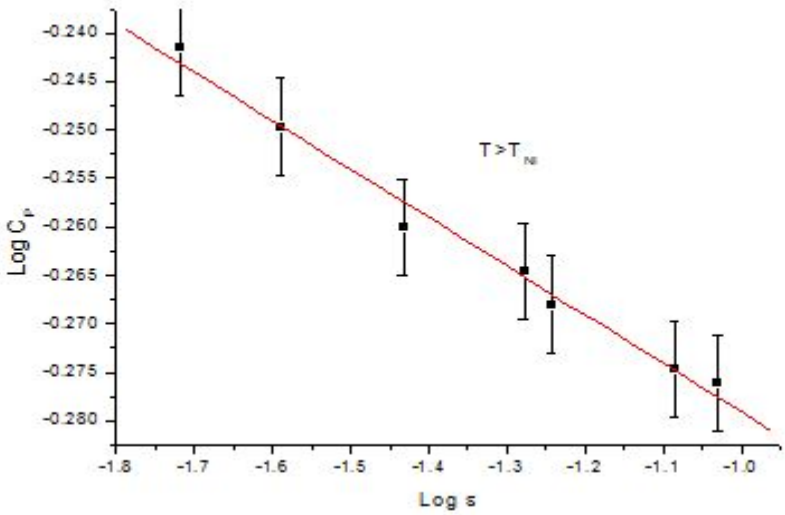

Figure 3.19: The specific heat C_p in a log-log scale as a function of reduced temperature (T_{NI}=180.5^{o}C) in the temperature interval for T>T_{NI} in anisaldazine according to a power-law formula (Eq. 2.4).

Table 3.12: Experimental data for the specific heat C_p as a function of temperature above T_{NI} and below T_{SN} in anisaldazine [56].

$T>T_{NI}$		$T<T_{SN}$	
T (^{o}C)	C_p (cal/g.deg)	T (^{o}C)	C_p (cal/g.deg)
181.03	16.85	168.31	0.654
181.03	14.81	168.32	0.882
181.04	10.32	168.34	1.189
181.04	9.51	168.36	1.604
181.05	6.66	168.37	2.164
181.06	4.65	168.39	2.919
181.07	3.46	168.41	3.937
–	–	168.42	5.311
–	–	168.43	7.163
–	–	168.45	9.662
–	–	168.46	13.032
–	–	168.48	17.578
–	–	168.49	23.710
–	–	168.50	31.982
–	–	168.51	43.138
–	–	168.52	58.186
–	–	168.54	78.484
–	–	168.55	105.862
–	–	168.56	142.791
–	–	168.57	192.602

temperature intervals indicated in Table 3.15 according to Eq. 2.4. In Fig. 3.20 we plot C_p in a log-log scale as a function of temperature for $T<T_{SN}$ in the temperature interval studied here. Again, as for the nematic-isotropic liquid transition, Fig. 3.20 is a representative plot of the specific heat at various temperatures for the solid-nematic transition in a given temperature interval for anisaldazine [37].

Values of the critical exponent α are nearly equal to 0.1 for $T>T_{NI}$ and $T<T_{SN}$. Below the nematic-isotropic liquid transition, our exponent value gets larger and it becomes α=0.2. Our values of $\alpha\sim$0.1 and α=0.2 are not equal to the value expected from the mean field theory ($\alpha=\alpha'=0$). On the other hand, the value of α=-0.02 which we extracted for the solid-nematic transition within the temperature interval studied ($T>T_{SN}$), agrees with the value expected from the helium analogy and the inverted XY model for liquid crystals. Our exponent value of -0.02 ($T>T_{SN}$) changes to 0.2 ($T<T_{NI}$) from the solid phase to the nematic phase as the temperature increases in anisaldazine. This rapid change in the values of the critical exponent

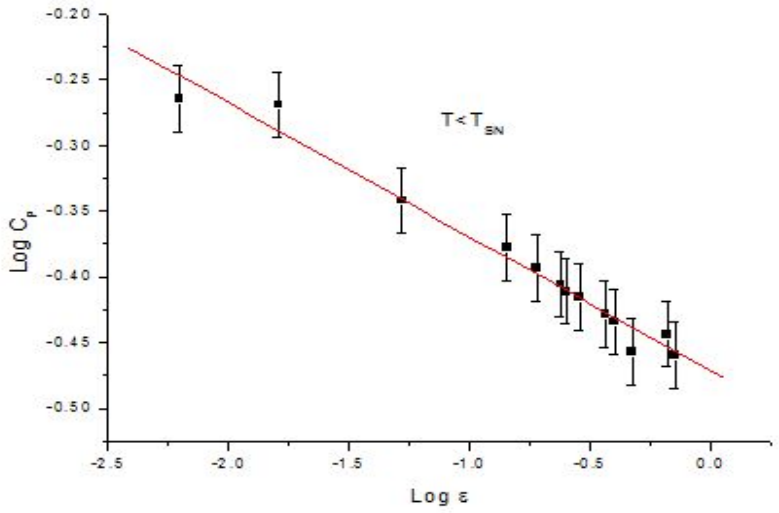

Figure 3.20: The specific heat C_p in a log-log scale as a function of reduced temperature (T_{SN}=168.9^{o}C) in the temperature interval for T<T_{SN} in anisaldazine according to a power-law formula (Eq. 2.4).

α within the temperature intervals, is due to the fact that there is a jump discontinuity in the specific heat C_p data as the solid phase is transformed into the nematic phase, in particular in the supercooled region. At low temperatures in the solid phase and at high temperatures in the isotropic liquid, similar critical behaviour of the specific heat C_p occurs within the temperature intervals studied.

3.1.3 Cholesteryl Myristate

3.1.3.1 Temperature Dependence of the Specific Heat of Cholesteryl Myristate Close to Phase Transitions

The temperature dependence of the specific heat of cholesteryl myristate was analyzed according to a power-law formula above and below the transition temperatures (T_{CI} and T_{SC}) and the values of the critical exponent α were extracted by using the experimental data [56] for the specific heat. This data was taken from the literature, which is given in Fig. 3.21 and in Tables 3.13 and 3.14. Figs. 3.22 and 3.23 give C_p as a function of |T-T_{CI}| above and below the transition temperature (T_{CI}=85.5^{o}C), respectively. For the transition between the smectic and cholesteric phases (T_C=79.7^oC) in cholesteryl myristate, we also plot the specific heat as

a function of |T-T_{SC}| in a log-log scale, as given in Figs. 3.24 and 3.25 (T>T_{SC}) and Fig. 3.26 (T<T_{SC}). We had two plots of C_p against T-T_{SC} because of the two different temperature intervals according to Eq. 2.2. This gave us the two different α values, as given in Table 3.15 [38].

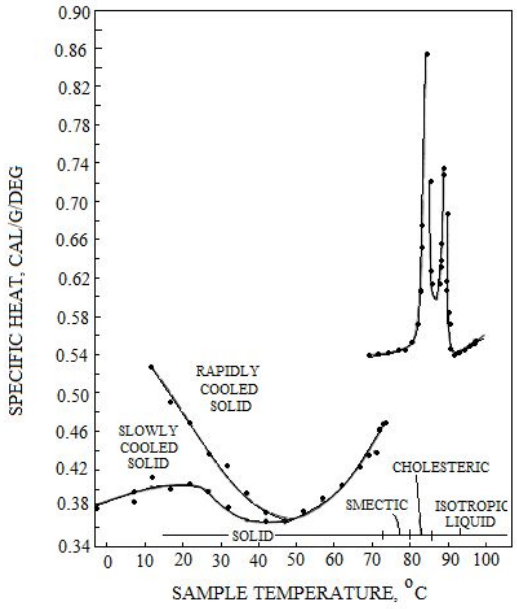

Figure 3.21: Specific heat of cholesteryl myristate from -3 to 97^o [56].

The values of the critical exponent α for the specific heat C_p, which we extracted vary from 0.03 to 0.50 for the CI and SC transitions in different temperature intervals. Above T_{CI} and below T_{SC}, the exponent values of 0.03 and 0.05, respectively, are close to the mean field value of α=α'=0.In between below T_{CI} and above T_{SC} the exponent values which vary from 0.1 to 0.5, are not in agreement with the mean field value. This means that below T_{CI} and above T_{SC}, the critical behaviour of the specific heat C_p changes from a second order transition (α=α'=0 from the mean field theory) toward a first order through a tricritical transition (α=0.5 tricritical mean field theory). In particular, our exponent value of α=0.5 just above the smectic-cholesteric (SC) transition (T_{SC}=79.7^{0}C) within the temperature interval (80.43 < T(^{0}C) < 80.99), is the tricritical mean field value.

Table 3.13: Experimental data for the specific heat C_p as a function of temperature above and below the transition temperature of cholesteric-isotropic liquid phase transition in Cholesteryl Myristate. T_{CI} denotes the cholesteric-isotropic liquid transition temperature [56].

$T>T_{CI}$		$T<T_{CI}$	
T (^{o}C)	C_p (cal/g.deg)	T (^{o}C)	C_p (cal/g.deg)
86.061	3.320	84.842	1.049
86.063	2.880	84.851	1.093
86.068	2.410	84.866	1.050
86.074	1.760	84.883	1.570
86.075	0.890	84.894	2.000
86.088	1.150	84.895	2.520
86.0958	0.850	–	–
86.103	0.380	–	–

Table 3.14: Experimental data for the specific heat C_p as a function of temperature above and below the transition temperature of cholesteric-solid phase transition in Cholesteryl Myristate. T_{SC} represents the cholesteric-solid transition temperature [56].

$T>T_{SC}$		$T<T_{SC}$	
T (^{o}C)	C_p (cal/g.deg)	T (^{o}C)	C_p (cal/g.deg)
80.381	1.290	78.969	0.010
80.417	1.210	79.092	0.650
80.503	0.910	79.113	1.000
80.555	0.820	79.129	1.640
80.626	0.730	79.144	2.640
80.306	2.760	79.155	4.670
80.315	2.330	79.161	5.750
80.345	1.810	–	–
80.382	1.290	–	–
80.417	1.210	–	–

Our values of the critical exponent α for the specific heat C_p indicate that the cholesteric-isotropic liquid ($T>T_{CI}$) and the smectic-cholesteric ($T<T_{SC}$) transitions can be of a second order type. Our exponent values also indicate that below T_{CI} and above T_{SC}, the transition tends to change toward a first order in cholesteryl myristate.

Table 3.15: Values of the critical exponent α for the specific heat C_p and the amplitude A within the interval of the reduced temperature ε according to a power-law formula (Eq. 2.4) for the all phase transitions of Cholesteryl Myristate (CM), Anisaldazine (AAD) and P-Azoxyanisole (PAA).

Liquid Crystal	Phase Transition	Temperature Region (^{o}C)	α	A [cal/g.^{o}C]	$\varepsilon=\lvert T-T_c\rvert/T_c$
CM	Cholesteric-Isotropic Liquid	$T>T_{CI}$	0.03±0.01	0.585±0.002	$4.4\text{x}10^{-3}<\varepsilon<3.0\text{x}10^{-2}$
		$T<T_{CI}$	0.09±0.02	0.649±0.004	$3.0\text{x}10^{-2}<\varepsilon<1.2\text{x}10^{-2}$
	Smectic-Cholesteric-SC	$T>T_{SC}$	0.50±0.03	0.779±0.003	$9.1\text{x}10^{-3}<\varepsilon<1.6\text{x}10^{-2}$
			0.19±0.02	0.728±0.007	$1.5\text{x}10^{-2}<\varepsilon<3.4\text{x}10^{-2}$
		$T<T_{SC}$	0.050±0.001	0.587±0.001	$7.2\text{x}10^{-2}<\varepsilon<1.3\text{x}10^{-4}$
	Smectic-Solid	$T<T_{SS}$	0.06	0.368	$1.2\text{x}10^{-2}<\varepsilon<2.0\text{x}10^{-1}$
			0.10	0.336	$6.5\text{x}10^{-2}<\varepsilon<3.0\text{x}10^{-1}$
AAD	Nematic-Isotropic Liquid	$T>T_{NI}$	0.050±0.003	0.608±0.004	$1.9\text{x}10^{-2}<\varepsilon<9.3\text{x}10^{-2}$
			0.09±0.02	0.809±0.03	$1.1\text{x}10^{-2}<\varepsilon<2.4\text{x}10^{-2}$
		$T<T_{NI}$	0.19±0.01	0.732±0.03	$1.9\text{x}10^{-3}<\varepsilon<2.2\text{x}10^{-2}$
	Solid-Nematic	$T>T_{SN}$	-0.020±0.003	0.549±0.010	$8.6\text{x}10^{-3}<\varepsilon<4.3\text{x}10^{-2}$
		$T<T_{SN}$	0.10±0.01	0.569±0.01	$0.14<\varepsilon<0.71$
PAA	Nematic-Isotropic Liquid	$T>T_{NI}$	0.85±0.07	-1.604±0.12	$1.57\text{x}10^{-2}<\varepsilon<3.08\text{x}10^{-2}$
		$T<T_{NI}$	0.04±0.005	-0.354±0.014	$1.34\text{x}10^{-3}<\varepsilon<5.68\text{x}10^{-3}$
	Nematic-Solid	$T>T_{SN}$	-0.07±0.01	-2.246±0.016	$7.06\text{x}10^{-2}<\varepsilon<9.42\text{x}10^{-2}$
		$T<T_{SN}$	0.09±0.002	-0.518±0.002	$3.17\text{x}10^{-2}<\varepsilon<2.48\text{x}10^{-1}$

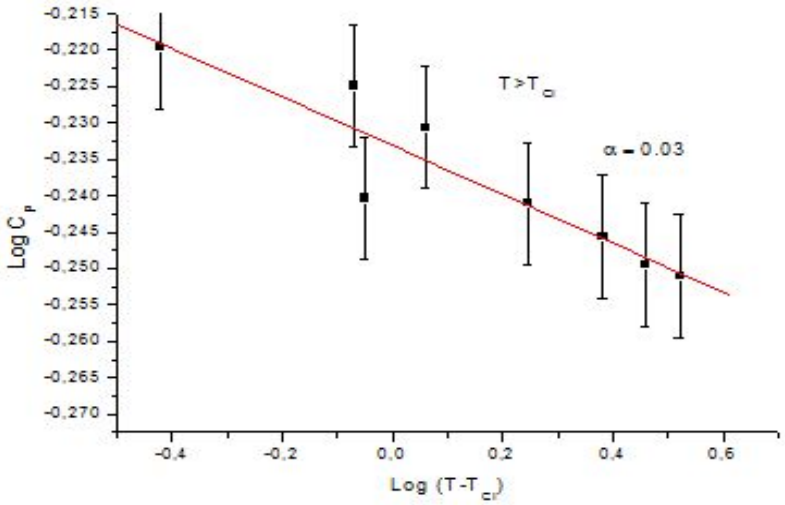

Figure 3.22: The specific heat C_p in a log-log scale as a function of the temperature according to Eq. 2.1 above the cholesteric-isotropic liquid (CI) phase transition (T_{CI}=85.5^{o}C) for cholesteryl myristate.

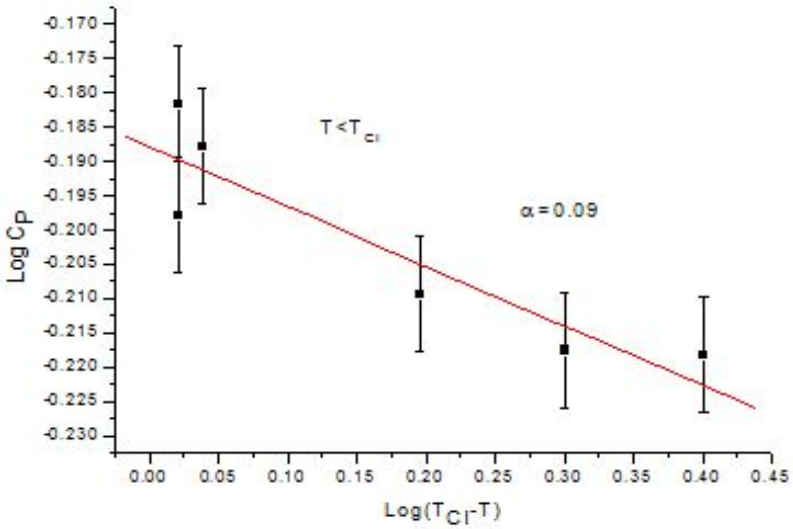

Figure 3.23: The specific heat C_p in a log-log scale as a function of the temperature according to Eq. 2.1 below the cholesteric-isotropic liquid (CI) phase transition (T_{CI}=85.5^{o}C) for cholesteryl myristate.

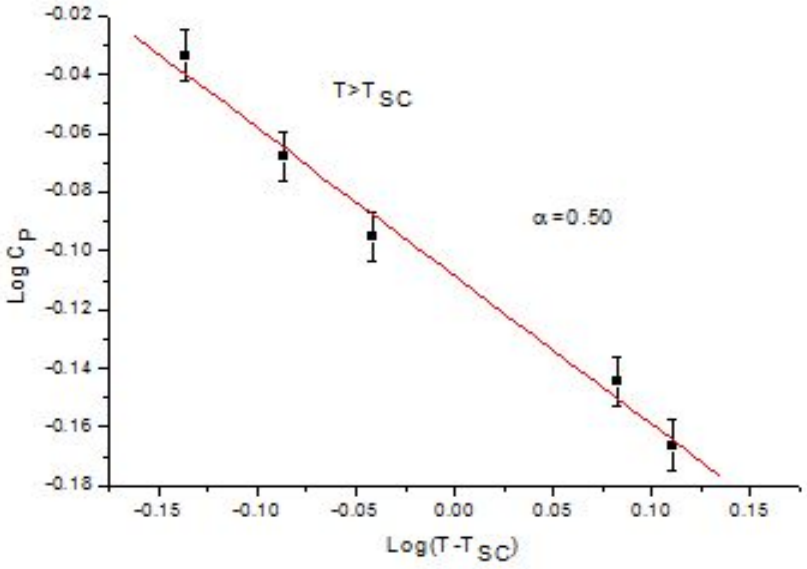

Figure 3.24: The specific heat C_p in a log-log scale as a function of the temperature according to Eq. 2.1 above the smectic-cholesteric (SC) phase transition (T_{SC}=79.7^{o}C) for cholesteryl myristate.

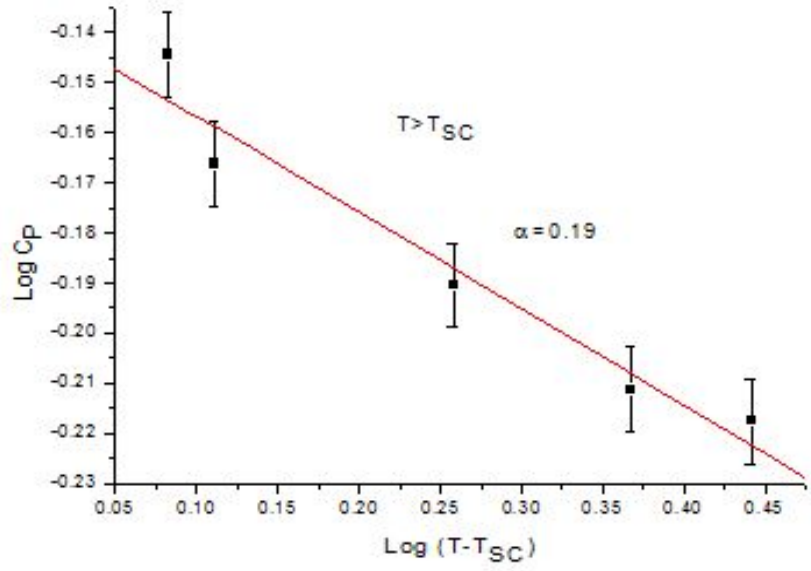

Figure 3.25: The specific heat C_p in a log-log scale as a function of the temperature according to Eq. 2.1 above the smectic-cholesteric (SC) phase transition (T_{SC}=79.7^{o}C) for cholesteryl myristate.

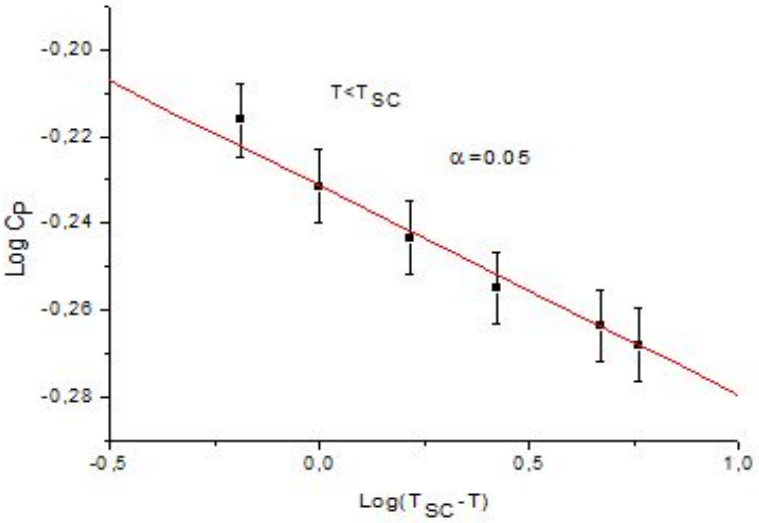

Figure 3.26: The specific heat C_p in a log-log scale as a function of the temperature according to Eq. 2.1 below the smectic-cholesteric (SC) phase transition (T_{SC}=79.7^{o}C) for cholesteryl myristate.

3.1.3.2 Analysis of the Specific Heat of Cholesteryl Myristate in the Supercooled Solid Phase of Liquid Crystals

The specific heat was analyzed close to the smectic-solid transition and, in the rapidly and slowly cooled regions for CM according to a power-law formula using the experimental data [56] taken from the literature, which is given in Tables 3.16 and 3.17. Close to the smectic-solid (T_{SS}=73.6^{o}C) transition, the temperature dependence of the C_p was analyzed using the power-law expression (Eq. 2.3) in the logarithmic form for the two temperature intervals, with the values of α and A, as given in Table 3.15. The temperature range was divided into the two for our analysis to get a linear variation of C_p with the temperature in the log-log scale according to Eq. 2.4. In Figs. 3.27 and 3.28 we give our plots of the C_p as a function of the reduced temperature ε (in the log-log scale) for the temperature intervals indicated. In this study, we were particularly interested in the stability limit for the rapidly cooled and slowly cooled solid phases of CM [60]. So, the experimental data for the C_p [56] was analyzed using the power-law formula for the stability limit [47]. In the power-law formula T_c was taken as T_s, which is the stability temperature. α=1/2 is the critical exponent and A is the amplitude, as before. From our analysis, we determined the stability temperature as T_s=-19.6^{o}C from the C_p data for the rapidly cooled solid [56] according to the Eq. 2.39. Table 3.18 gives the fitted parameters (Eq. 2.39) in the temperature interval indicated for the rapidly cooled CM. A plot of logC_p against log(T-T_s) is given in Fig. 3.28, according to 2.40.

Table 3.16: Experimental data for the specific heat C_p as a function of temperature in the smectic A-solid phase transition and rapidly cooled solid phase in Cholesteryl Myristate [56].

Smectic A-Solid Phase Transition		Rapidly Cooled Solid Phase	
T (^{o}C)	C_p (cal/g.deg)	T (^{o}C)	C_p (cal/g.deg)
108.121	0.012	19.967	66.015
107.646	0.026	19.976	61.136
105.924	0.040	19.996	56.282
105.628	0.065	20.024	51.036
104.737	0.096	20.037	46.373
103.313	0.163	20.069	41.338
102.364	0.233	20.092	36.285
102.126	0.233	20.128	31.464
101.355	0.303	–	–
101.057	0.303	–	–

Table 3.17: Experimental values for the specific heat C_p as a function of temperature in the rapidly and slowly cooled solid phase in Cholesteryl Myristate [56].

Rapidly Cooled Solid Phase		Slowly Cooled Solid Phase			
T (^{o}C)	C_p (cal/g.deg)	T (^{o}C)	C_p (cal/g.deg)	T (^{o}C)	C_p (cal/g.deg)
125.59	0.545	99.07	0.688	127.54	0.544
119.42	0.566	101.35	0.791	125.55	0.566
105.61	0.590	104.77	0.854	125.49	0.591
89.49	0.620	114.26	1.077	115.77	0.620
83.14	0.650	–	–	103.95	0.652
69.50	0.689	–	–	–	–
61.50	0.735	–	–	–	–
50.73	0.789	–	–	–	–

Table 3.18: Values of the critical exponent α and the amplitude A for the rapidly cooled, supercooled and solid phases of CM and PAA in the stability limit according to a power-law formula Eq. 2.40

Phase	Stability Temperature T_s (^{o}C)	α	A (cal/g.^{o}C)	Temperature interval (^{o}C)
Rapidly cooled solid (CM)	-19.6	0.50±0.02	2.98	11.9<T<46.4
Supercooled (PAA)		-0.020±0.004	0.43	101.8<T<116.3
Solid (PAA)	90	0.0030±0.0004	0.345	90.2<T<95.38

.

We have also plotted C_p as a function of $(1\text{-}T/T_s)^{-1/2}$ for the rapidly cooled solid (CM) in Fig. 3.28. Furthermore, we analyzed the experimental C_p [56] for the slowly cooled solid (CM) according to Eq. 2.39 with the α=1/2 and we used the stability temperature as T_s=-19.6^{o}C. For the two different temperature regions, we plot C_p as a function of $(1\text{-}T/T_s)^{-1/2}$ in Fig. 3.29 for the slowly cooled solid. In these figures, the solid lines represent the curves fitted to the experimental data [56].

For the rapidly cooled solid, C_p varies linearly with the $(1\text{-}T/Ts)^{-1/2}$ in the temperature interval given. For slowly cooled solid, because of the kink that occurs around 25 ^{o}C in the experimental C_p [56], almost linear variation of C_p with the $(1\text{-}T/Ts)^{-1/2}$ changes towards a nonlinear behaviour at higher temperatures. The C_p curves increasing in the solid phase and decreasing in the slowly cooled solid phase with decreasing temperature, construct a kink at

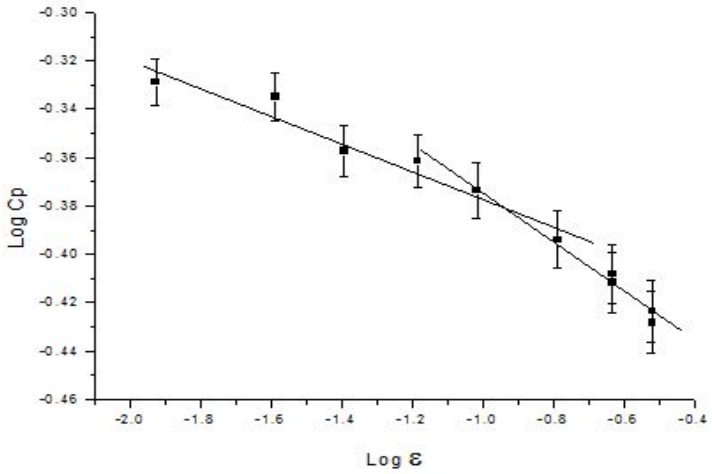

Figure 3.27: The specific heat C_p as a function of the reduced temperature (ε=|T_c-T|/T_c) in a log-log scale close to the smectic A-solid transition (T_{SS}=73.6^{o}C) for the cholesteryl myristate (CM) using the experimental data [56] analyzed according to Eq.2.39 (see Table 3.15).

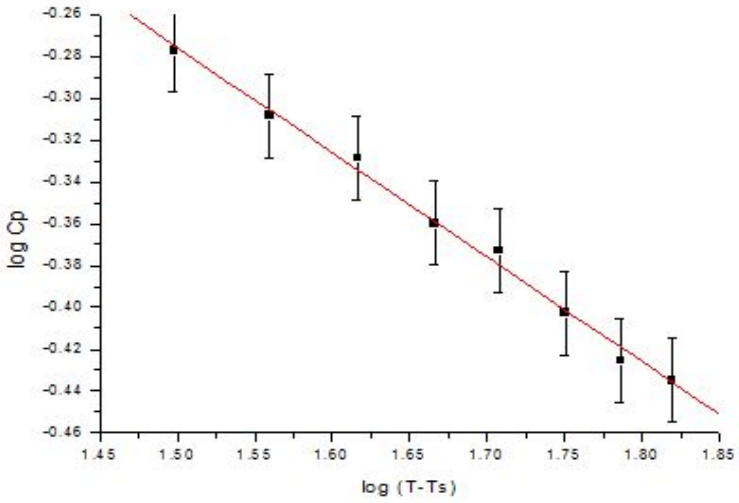

Figure 3.28: The specific heat C_p in a log-log scale as a function of the temperature with respect to the stability temperature T_s for the rapidly cooled solid phase of cholesteryl myristate (CM) using the experimental data [56] analyzed according to Eq.2.39 (see Table 3.18).

around 25 ^{o}C. This can be due to the fact that long-range ordering of the molecules is not completed in the solid phase or to some extent the molecules are still disordered (increasing

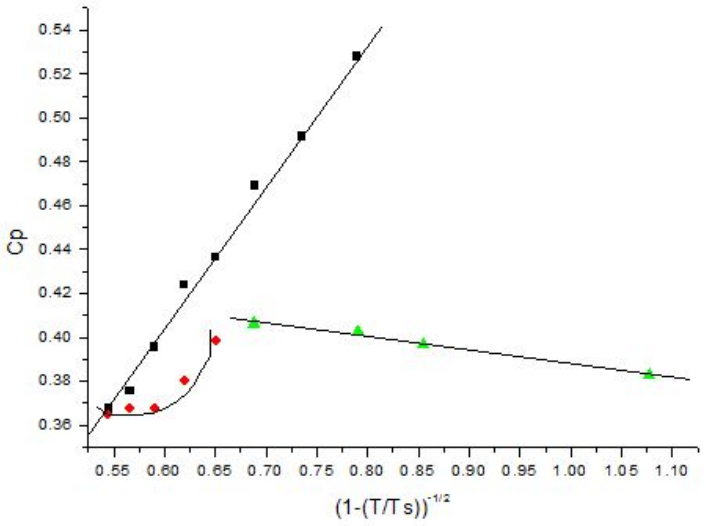

Figure 3.29: The specific heat C_p as a function of the reduced temperature with respect to the stability temperature T_s for the rapidly cooled solid phase (■ and •) and for the slowly cooled solid phase (▲) of CM. The solid lines represent the best fit to the experimental data [56] analyzed according to Eq. 2.39 (see Table 3.18).

C_p), whereas in the slowly cooled solid phase the molecules are more ordered (decreasing C_p), as the temperature decreases. Thus, the occurrence of the kink in C_p indicates a kind of transition from the solid phase with some disorder to the slowly cooled solid phase with the molecules oriented orderly.

3.2 Analysis of Some Ferroelectric Liquid Crystals

3.2.1 4-(3-methyl-2-chlorobutanoyloxy)-4′-heptyloxybiphenyl (A7)

3.2.1.1 Temperature Dependence of the Polarization and Tilt Angle Under an Electric Field Close to the Smectic AC* Phase Transition in a Ferroelectric Liquid Crystal

While calculating the temperature dependence of the tilt angle θ and the polarization P for the AC^* phase transition of the ferroelectric liquid crystal 4-(3-methyl-2-chlorobutanoyloxy)-4′-heptyloxybiphenyl (A7) under the fixed electric fields [51], we used the polarization data at zero electric field according to Eq. 2.52. In a previous study [18], expression for the

temperature-dependent θ derived from the mean field model was fitted to the experimental data [16] for the tilt angle θ of the compound A7 in the case of zero electric field for the AC* phase transition, and the values of the coefficients a, b, c, D and e were determined [18], as also tabulated in Table 3.20. Then, the temperature dependence of the polarization P was calculated for this liquid crystalline material [18]. The experimental data taken from the literature and analyzed in this study is given in Fig. 3.30 and Table 3.19.

Table 3.19: Experimental values of the tilt angle and the polarization as a function of temperature for the smectic A-smectic C* phase transition of A7 [21].

T (^{o}C)	Tilt Angle θ (rad)	Polarization P x 10^{-4} (C/m^2)
71.81	0.443	14.85
72.01	0.432	14.43
72.11	0.428	14.26
72.21	0.419	13.96
72.40	0.411	13.63
72.59	0.398	13.16
72.69	0.390	12.85
72.89	0.374	12.23
73.20	0.341	11.01
73.30	0.329	10.54
73.40	0.314	9.93
73.50	0.290	9.01

Table 3.20: Values of the parameters given in Eq. 2.41, which were obtained from an earlier study [18] at zero electric field for 4-(3-methyl-2-chlorobutanoyloxy)-4′-heptyloxybiphenyl (A7) for the AC* transition.

a	2.65x10^7 J/(m^3.K.rad^2)
b	-1.67x10^8 J/(m^3.rad^4)
c	2.09x10^9 J/(m^3.rad^6)
D	7.45x10^{11} J.m/(C^2.rad^2)
e	1.20x10^{17} J.m^5/C^4

In this study, we first calculated the polarization P, by using in Eq. 2.45 the θ values at E=0 as a function of temperature. θ and P are plotted as a function of temperature for the zero electric field in Figs. 3.31 and 3.32, respectively for the AC* phase transition of A7 [51].

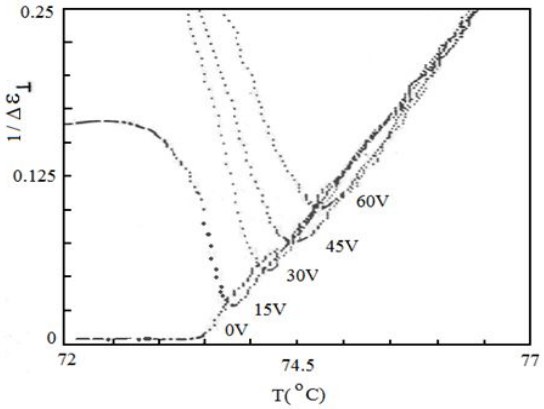

Figure 3.30: Plot of $1/\Delta\varepsilon_\perp$ versus temperature at different dc voltages for the ferroelectric liquid crystal of A7 [21].

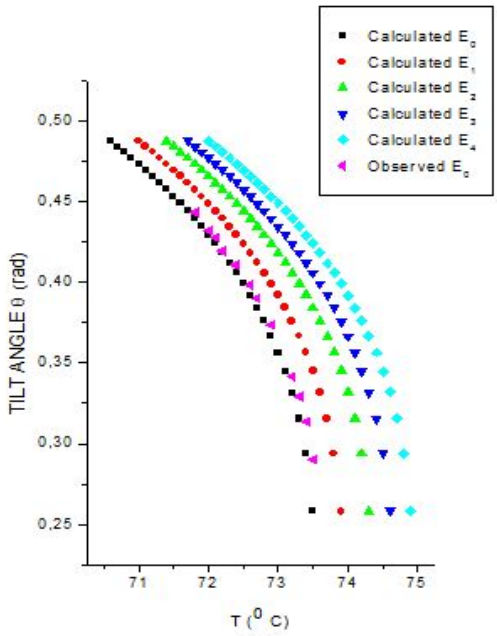

Figure 3.31: The temperature dependence of the tilt angle calculated for constant electric fields E_0=0, E_1=150/9, E_2=100/3, E_3=50, E_4=200/3 kV/cm for the AC* phase transition in 4-(3-methyl-2-chlorobutanoyloxy)-4′-heptyloxybiphenyl. Our calculated θ values for zero electric field are taken from a previous study [18]. The observed θ values for zero electric field are also shown here.

In accordance with the experimental measurements of the dielectric constant ε for the AC* transition of this ferroelectric liquid crystal with high spontaneous polarization [21], we per-

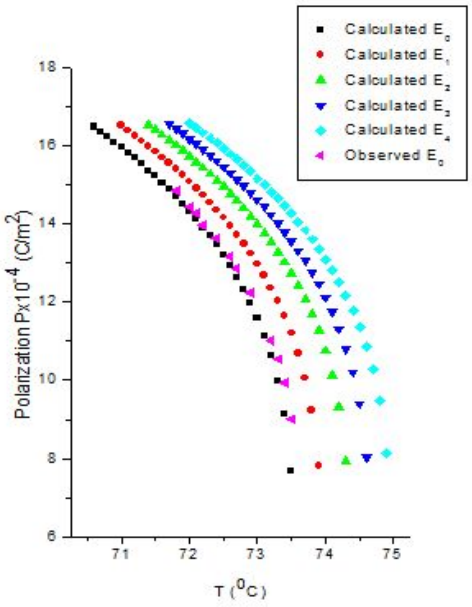

Figure 3.32: The temperature dependence of the polarization calculated for constant electric fields E_0=0, E_1=150/9, E_2=100/3, E_3=50, E_4=200/3 kV/cm for the AC* phase transition in 4-(3-methyl-2-chlorobutanoyloxy)-4′-heptyloxybiphenyl. Our calculated P values for zero electric field are taken from a previous study [18]. The observed P values for zero electric field are also shown here.

formed here our calculations of the tilt angle θ and the polarization P for constant electric fields (at dc voltages of 0, 15, 30, 45 and 60V). Table 3.23 gives the transition temperatures for the dc voltages and correspondingly the applied electric fields for a sample of thickness 9 μm [21] of the ferroelectric compound for its AC* phase transition [51].

The polarization at different electric fields was calculated as a function of temperature by Eq. 2.52 using the polarization values at zero electric field [18]. Also, the tilt angle θ was calculated at different electric fields by Eq. 2.44 where the polarization values (Eq. 2.52) were used as a function of temperature for A7. As indicated in the experimental study [21], this material is pure optically active for the AC* phase transition. Fig. 3.31 gives our plots of the tilt angle θ calculated using Eq. 2.44 as a function of temperature for constant electric fields studied (Table 3.23). Also, in Fig. 3.32 we plot our calculated polarization P (Eq. 2.52) as a function of temperature for the compound studied for various electric fields (Table 3.23) [51].

Figs.3.31 and 3.32 show that as the electric field increases, the value of the tilt angle and/or

polarization correspond to a higher value of temperature. Increasing of the electric field causes an increasing the value of the tilt angle and/or the polarization.

3.2.1.2 Calculation of the Dielectric Constant as a Function of Temperature Near the Smectic AC* Phase Transition in Ferroelectric Liquid Crystals

We calculated the temperature dependence of the dielectric constant for the AC* phase transition in A7 under constant electric fields [52]. The dielectric constant ε was calculated from the dielectric susceptibility χ using the values of the polarization P(E=0) and P(E) at various temperatures for the fixed dc voltages of 15, 30, 45 and 60V in accordance with the experimental measurements of ε for this compound, which are taken from the literature [21]. This data was analyzed here, as given in Tables 3.21 and 3.22.

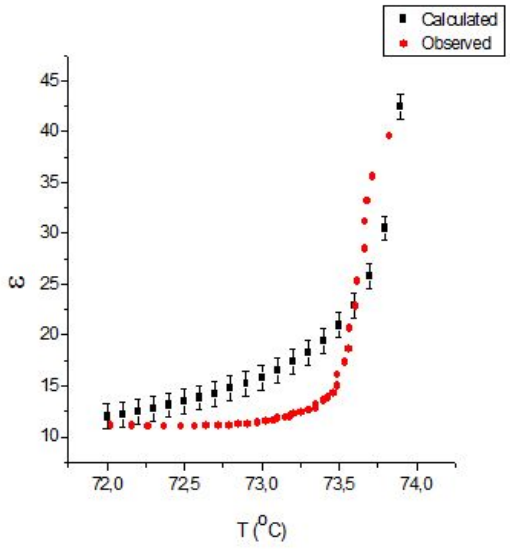

Figure 3.33: The constant ε calculated from Eq. 2.50 as a function of temperature for a constant electric field of E_1=50/3 kV/cm for the smectic C* phase close to the AC* phase transition (T_c=73.9^{o}C) in 4-(3-methyl-2-chlorobutanoyloxy)-4′-heptyloxybiphenyl. Observed data [21] are also shown here.

The values of the polarization P(E) were calculated at constant electric fields as a function of temperature according to Eq. 2.52 for this liquid crystal. For those values of the polarization calculated (Eq. 2.52) at different electric fields, the polarization values at zero electric field

Table 3.21: Experimental values of dielectric constant ε as a function of temperature for the electric field values of 50/3 kV/cm and 100/3 kV/cm for A7 [21].

E=50/3 kV/cm		E=100/3 kV/cm	
T (^{o}C)	ε	T (^{o}C)	ε
72.025	11.106	73.351	9.072
72.163	11.066	73.351	9.155
72.266	11.026	73.369	9.251
72.369	11.007	73.395	9.351
72.481	11.007	73.421	9.457
72.567	11.026	73.438	9.578
72.644	11.046	73.49	9.683
72.721	11.086	73.49	9.818
72.79	11.127	73.508	9.961
72.849	11.21	73.517	10.113
72.909	11.253	73.56	10.273
72.977	11.361	73.586	10.445
73.028	11.52	73.612	10.645
73.079	11.59	73.664	10.879
73.104	11.76	73.664	11.154
73.155	11.887	73.69	11.434
73.181	12.019	73.716	11.691
73.206	12.212	73.733	12.023
73.256	12.417	73.734	12.451
73.307	12.634	73.786	12.863
73.349	12.795	73.812	13.401
73.349	13	73.829	13.887
73.348	13.216	73.829	14.437
73.399	13.521	73.855	15.223
73.432	13.85	73.882	15.887
73.465	14.3	73.908	16.571
73.49	14.956	73.934	17.430
73.488	16.103	73.96	18.233
73.537	17.295	73.985	18.827
73.561	18.672	74.003	19.830
73.568	20.658	74.055	20.709
73.61	22.786	74.193	23.166
73.617	25.355	–	–
73.667	28.487	–	–
73.666	31.171	–	–
73.683	33.185	–	–
73.716	35.533	–	–
73.827	39.566	–	–

Table 3.22: Experimental values of the dielectric constant ε as a function of temperature for the electric field values of 50 kV/cm and 200/3 kV/cm for A7 [21].

E=50 kV/cm		E=200/3 kV/cm	
T (^{o}C)	ε	T (^{o}C)	ε
73.472	9.017	73.739	9.067
73.489	9.098	73.79	9.140
73.515	9.172	73.834	9.24
73.541	9.268	73.877	9.304
73.567	9.359	73.86	9.376
73.584	9.465	73.877	9.471
73.61	9.576	73.903	9.560
73.636	9.680	73.903	9.652
73.662	9.815	73.929	9.773
73.688	9.931	73.981	9.860
73.714	10.052	74.024	9.978
73.74	10.180	74.05	10.102
73.758	10.346	74.05	10.248
73.81	10.505	74.076	10.386
73.836	10.692	74.102	10.531
73.827	10.893	74.128	10.667
73.853	11.068	74.128	10.829
73.879	11.317	74.146	11.000
73.879	11.542	74.198	11.180
73.931	11.733	74.198	11.351
73.949	11.988	74.249	11.554
73.957	12.293	74.25	11.746
74.001	12.593	74.276	11.923
74.001	12.921	74.327	12.109
74.053	13.275	74.345	12.336
74.079	13.583	74.371	12.515
74.122	14.001	74.397	12.735
74.122	14.369	74.448	12.933
74.174	14.764	74.474	13.179
74.174	15.198	74.518	13.599
74.2	15.608	74.595	14.106
74.2	15.989	74.621	14.529
74.252	16.464	–	–
74.278	16.908	–	–
74.347	17.551	–	–
74.381	17.899	–	–

[18] were used for this material. For this calculation, we fitted Eq. 2.50 to the experimental data for the dielectric constant ε [21], our calculated values of the polarization at electric field,

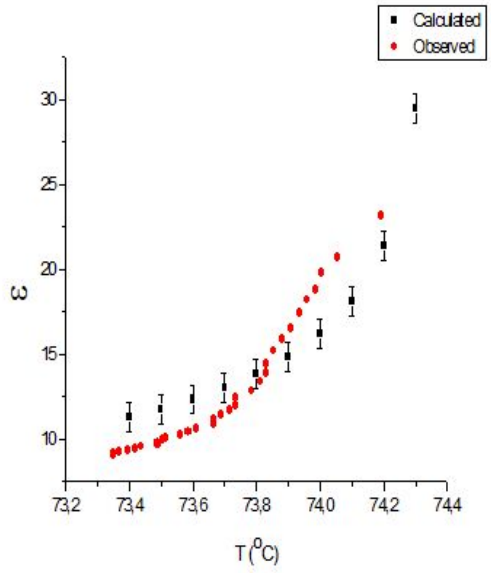

Figure 3.34: The constant ε calculated from Eq. 2.50 as a function of temperature for a constant electric field of E_2=100/3 kV/cm for the smectic C* phase close to the AC* phase transition (T_c=74.3^{o}C) in 4-(3-methyl-2-chlorobutanoyloxy)-4′-heptyloxybiphenyl. Observed data [21] are also shown here.

P(E=0) [18] and the electric field dependence of the polarization, P(E), which we calculated according to Eq. 2.52. This fitting was performed for the observed ε [21] and, the calculated P(E=0) and P(E) at various temperatures for constant electric fields (15, 30, 45, 60V) in the smectic C* phase of A7 close to its AC* phase transition. For each constant electric field, we determined the value of the coefficient e subject to the shifts in the transition temperature T_c (Eq. 2.53). Table 3.23 gives the transition temperatures T_c and the values of the fitting parameter e for constant electric fields (dc voltages) for the liquid crystalline material studied here. For the e values we obtained, we first fitted the dielectric constant ε against P(E=0)P(E) according to Eq. 2.50 we plot the dielectric constant as a function of temperature for constant electric fields considered here [52].

Figs. (3.33-3.36) give our calculated dielectric constant ε as a function of temperature for constant electric fields or the dc voltages of, respectively, 15, 30, 45 and 60V for A7 in the smectic C* phase close to its AC* phase transition [52]. We also plot here the observed $\varepsilon_\perp$ values [21]. At the electric field of E1=150/9 kV/cm, calculated dielectric constant ε increases smoothly whereas the observed ε gets sharper, as the temperature increases from the smectic C* phase toward the transition temperature. Also, for the electric field of E2=100/3 kV/cm,

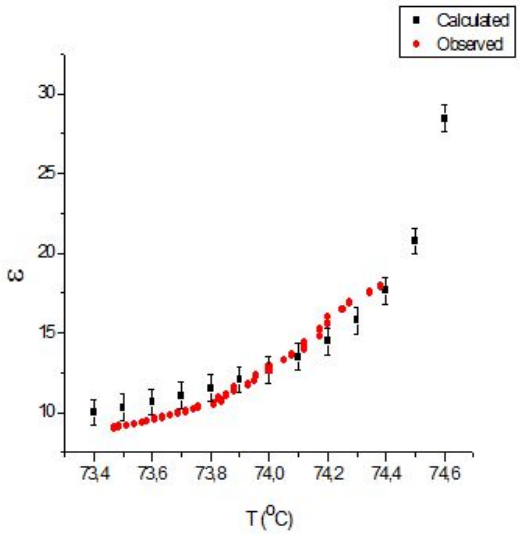

Figure 3.35: The constant ε calculated from Eq. 2.50 as a function of temperature for a constant electric field of E_3=50 kV/cm for the smectic C* phase close to the AC* phase transition (T_c=74.6^{o}C) in 4-(3-methyl-2-chlorobutanoyloxy)-4′-heptyloxybiphenyl. Observed data [21] are also shown here.

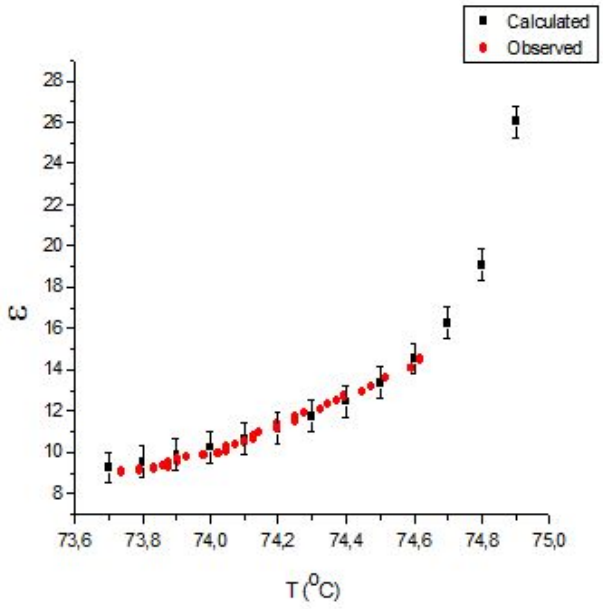

Figure 3.36: The constant ε calculated from Eq. 2.50 as a function of temperature for a constant electric field of E_4=200/3 kV/cm for the smectic C* phase close to the AC* phase transition (T_c=74.9^{o}C) in 4-(3-methyl-2-chlorobutanoyloxy)-4′-heptyloxybiphenyl. Observed data [21] are also shown here.

Table 3.23: Transition temperatures and the values of the fitting parameter e (Eq. 2.50) for constant electric fields indicated close to the AC* phase transition in 4-(3-methyl-2-chlorobutanoyloxy)-4′-heptyloxybiphenyl.

dc voltage (V)	E (kV/cm)	T_c (^oC)	e x 10^4 ($V.m^5/C^3$)
0	0	73.5	–
15	50/3	73.9	2.01±0.04
30	100/3	74.3	2.88±0.06
45	50	74.6	2.95±0.06
60	200/3	74.9	3.19±0.06

our calculated and the observed dielectric constant ε both increase smoothly, as the temperature increases in the smectic C* phase from about 73.4 ^{0}C to the transition temperature. Agreement is better when the electric field gets larger.

When the electric field increases, values of the tilt angle and polarization increase. Since in this analysis we used the Landau free energy with the $P^2\theta^2$ coupling, as the electric field increases, the influence of $P^2\theta^2$ coupling increases. At the same time, interaction of the molecules in small distances increases. Because of these reasons, the agreement of the calculated and the observed values of dielectric constant is better when the electric field is higher.

Also, the validity of the approximate relation for the polarization at higher electric fields starting from the zero electric field and the expression for the dielectric susceptibility χ or the dielectric constant ε which was essentially derived at zero electric field from our mean field model can be argued when we compare our calculated values with the experimental data.

3.2.1.3 Calculation of the Dielectric Constant of a Ferroelectric Liquid Crystal from a Mean Field Model

The temperature dependence of the orientational order parameter θ (Eq. 2.76) and the inverse susceptibility χ^{-1} (Eq. 2.75) were calculated for pure optically active compound of A7 (T_c=81.6^{o}C). Fig. 3.38 gives a plot of θ calculated (Eq. 2.76) as a function of temperature ($T<T_c$) for this compound. The calculated values of θ as a function of temperature were then used in Eq.2.75. Eq.2.75 was fitted to the experimental data which is taken from the literature, as given in Fig. 3.37 and Table 3.24. For $\varepsilon_\perp$ [21] below the transition temperature (T_c=81.6^{o}C) where the order parameter θ is nonzero, the coefficients were then determined

[61]. By using the definition of α' (Eq. 2.73) with the temperature-dependent coefficient α in Eq.2.75, the reciprocal susceptibility χ^{-1} can be rewritten as

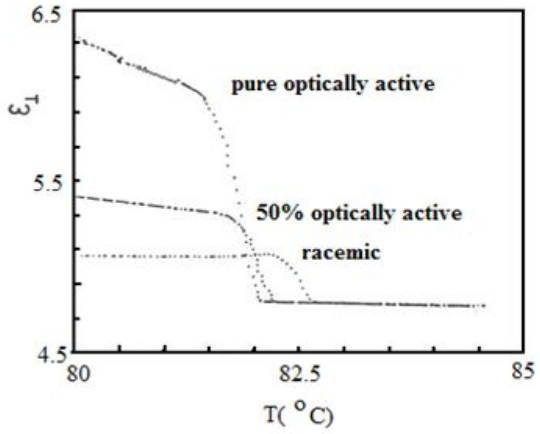

Figure 3.37: Temperature dependence of $\varepsilon_\perp$ of the pure optically active compound, the 50% optically active mixture and the racemate at the smectic A-isotropic transition [21].

$$\chi^{-1} = a(T - T_o) + \frac{2D}{e\chi_o\varepsilon_o} + a_1\theta^2 + a_2\theta^4 \tag{3.8}$$

where a_1=3b′ and a_2=5c′ . At the transition temperature (T=T_o) the order parameter θ is zero (Fig.3.38), which gives a constant value for χ^{-1} (Eq. 3.8) as $\chi^{-1}\Big|_{T=T_o} = \frac{2D}{e\chi_o\varepsilon_o}$. Using the experimental values of $\varepsilon_\perp$ or χ^{-1} at T=81.57^{o}C [21], and also using the calculated θ values as a function of temperature (Eq. 2.76), Eq.3.8 was fitted to the experimental data [21] for $\varepsilon_\perp$ (or χ^{-1}), and the coefficients a, a_1 and a_2 were determined, which are tabulated in Table 3.25. We plot our calculated values of the dielectric constant $\varepsilon_\perp$ as a function of temperature in the smectic A phase (T<Tc) in Fig.3.39. The observed $\varepsilon_\perp$ data is also given in this plot for the SmA-I transition of A7. Using the values of the coefficients a, a_1, a_2 and χ^{-1} (T_c=81.57^{o}C) (Table 3.25), the transition temperature was calculated as T_o=84.3^{o}C from Eq. 2.74 where the experimental value of T_c=81.6^{o}C [21] was used [61], as also given in Table 3.25.

Since there is no discontinuous change in $\varepsilon_\perp$, the SmA-I transition tends to be a nearly second order type. A first order condition for the SmA-I transition was also tested here using the values of the coefficients α', b' and c'. This gave us the values of 0.96 and 0.51 at the transition temperature (T_c=81.6^o C) and at T_c=80.03^o C, as the upper and lower limits of the SmA

Table 3.24: Experimental values of the temperature dependence of the dielectric constant $\varepsilon_\perp$ of the pure optically active compound at the smectic A-isotropic transition[21].

T (^{o}C)	$\varepsilon_\perp$
80.032	6.35
80.282	6.281
80.475	6.228
80.677	6.179
80.823	6.155
80.944	6.115
81.065	6.09
81.137	6.074
81.25	6.062
81.436	5.997
81.468	5.977
81.565	5.888
81.717	5.648
81.821	5.449
81.869	5.298
81.917	5.14
81.949	5.002
82.021	4.888
82.045	4.823

Table 3.25: Values of the coefficients a, a_1 and a_2 determined by fitting the experimental data [21] for the dielectric constant $\varepsilon_\perp$ of A7 according to Eq.(3.8). The experimental $\varepsilon_\perp$ and χ^{-1} values at T_c=81.57^{o}C are given here. We also give the observed T_c and calculated T_o (Eq. 2.74) values for this pure optically active compound at the smectic A-isotropic liquid (SmA-I) transition.

T_c	a (^{o}C^{-1})	a_1	a_2	$\varepsilon_\perp$	χ^{-1}	T_o(^{o}C)
81.6	0.061	1.160	3.496	5.89	0.205	84.3

phase, respectively. Compared to the value 3/16=0.1875, the above values are much higher for a first order SmA-I transition of A7. The value of the ratio $\alpha' c' / b'^2$ even increases to 1.73 if one uses T_o=84.3 ^{o}C for α'. This deviates largely from the expected value of 3/16 for a first order transition. On the other hand, we found the temperature difference $\Delta T = T_c - T_o = 2.7^o$C using the coefficients. This temperature difference between the experimental T_c and the calculated T_o values, is relatively large. This, however, indicates that the first order features are still significant for the SmA-I transition so that this transition can be considered

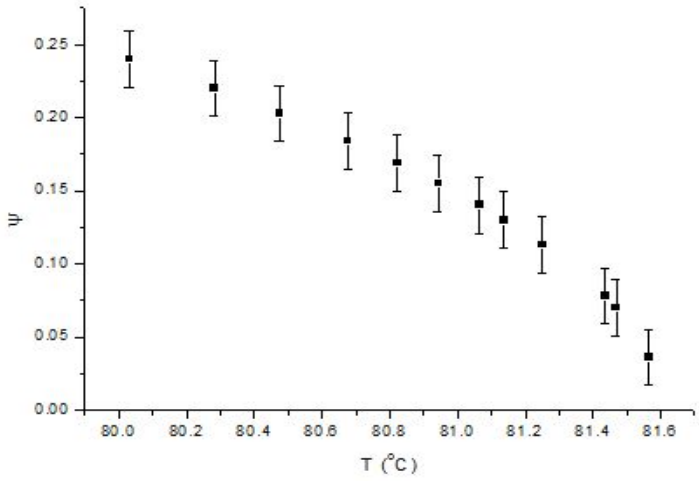

Figure 3.38: The temperature dependence of the orientational order parameter θ calculated from the mean field theory (Eq. 2.76) close to the smectic A-isotropic liquid (SmA-I) transition (T_c=81.6^{o}C) for A7.

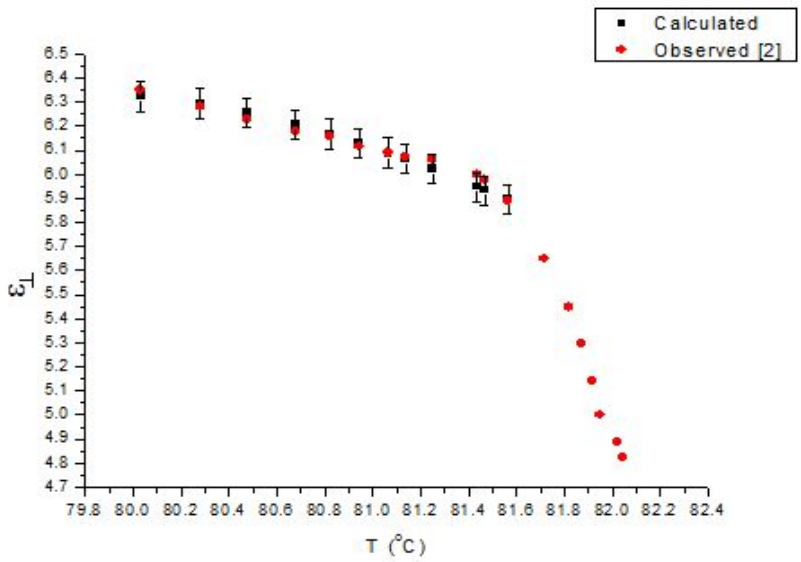

Figure 3.39: The temperature dependence of the dielectric constant $\varepsilon_\perp$ calculated from the mean field theory (Eq. 3.8) below the smectic A-isotropic liquid (SmA-I) transition (T_c=81.6^{o}C) for A7. The experimental data [21] for $\varepsilon_\perp$ is also shown here.

as a weak first order or close to a second order in pure optically active compound of A7.

3.2.1.4 Critical Behaviour of the Dielectric Susceptibility for the Ferroelectric Liquid A7

In order to investigate the critical behaviour of the dielectric susceptibility of A7, we analyzed the experimental data [21] for the temperature dependence of the dielectric constant $\varepsilon_\perp$ of the pure optically active A7 and its 50% mixture near the smectic A- isotropic liquid phase transition which is taken from the literature and is given in Fig. 3.40 and Table 3.26. We performed our analysis according to a power-law formula for the dielectric susceptibility given in Eq. 2.5. Since the dielectric constant ε is directly related to the dielectric susceptibility χ according to $\varepsilon=\chi+1$, using the experimental data for the dielectric constant $\varepsilon_\perp$, we deduced the values of the critical exponent γ for the pure optically active A7 and its 50 % mixture. Table 3.27 gives our values of the critical exponent γ and the amplitude A above and below the transition temperature within the reduced temperature for the 50% mixture and pure optically active A7 [40]. We plot the dielectric susceptibility χ as a function of $|T-T_c|$ above and below T_c in a log-log scale according to a linear relation given in Eq. 2.6.

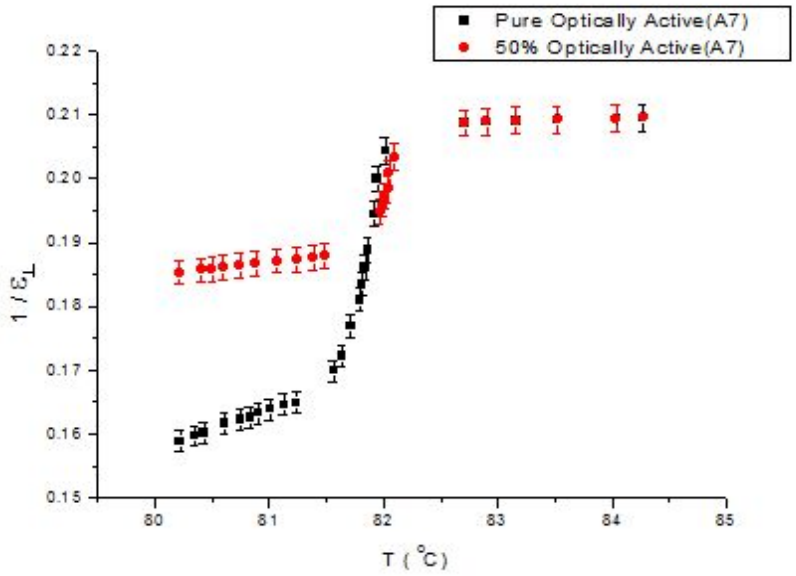

Figure 3.40: Experimental data for the reciprocal of the dielectric constant $\varepsilon_\perp$ [21] as a function of temperature for the pure optically active compound and the 50 % optically active mixture at the smectic A -isotropic liquid transition.

Table 3.26: Temperature dependence of the dielectric constant $\varepsilon_\perp$ of the pure optically active compound and the 50% optically active mixture of A7 at the smectic A-isotropic transition [21].

T (^{o}C)	$1/\varepsilon_\perp$ (Pure)	T (^{o}C)	$1/\varepsilon_\perp$ (50 %)
80.217	0.1589	80.213	0.1853
80.345	0.1597	80.406	0.1857
80.426	0.1601	80.503	0.1859
80.611	0.1617	80.599	0.1861
80.747	0.1622	80.744	0.1864
80.828	0.1626	80.881	0.1867
80.908	0.1633	81.066	0.1871
81.005	0.1639	81.243	0.1874
81.126	0.1646	81.388	0.1877
81.238	0.1649	81.485	0.1880
81.56	0.1699	81.967	0.1949
81.64	0.1722	81.991	0.1960
81.712	0.1770	82.015	0.1973
81.792	0.1810	82.039	0.1984
81.815	0.1835	82.047	0.2010
81.839	0.1861	82.095	0.2034
81.863	0.1888	82.706	0.2088
81.919	0.1945	82.9	0.2089
81.942	0.2000	83.157	0.2091
82.014	0.2045	83.52	0.2093
82.706	0.2088	84.035	0.2094
82.9	0.2089	84.268	0.2096
83.157	0.2091	–	–
83.52	0.2093	–	–
84.035	0.2094	–	–
84.268	0.2096	–	–

Figs. 3.41 and 3.42 give lnχ against ln|T-T_c| above and below the transition temperature (T_c=81.9^{o}C), respectively, for 50% optically active mixture of A7. We plot in Figs. 3.43 and 3.44, lnχ against ln|T-T_c| above and below T_c for the pure optically active A7 (T_c=81.6^{o}C). We give here Figs. 3.43 and 3.44 as representative plots within the temperature intervals indicated (Table 3.27) for the pure optically active A7 [40].

We also analyzed the experimental data for the dielectric constant $\varepsilon_\perp$ [21] using the renormalization group relation from the scaling theory [58] according to

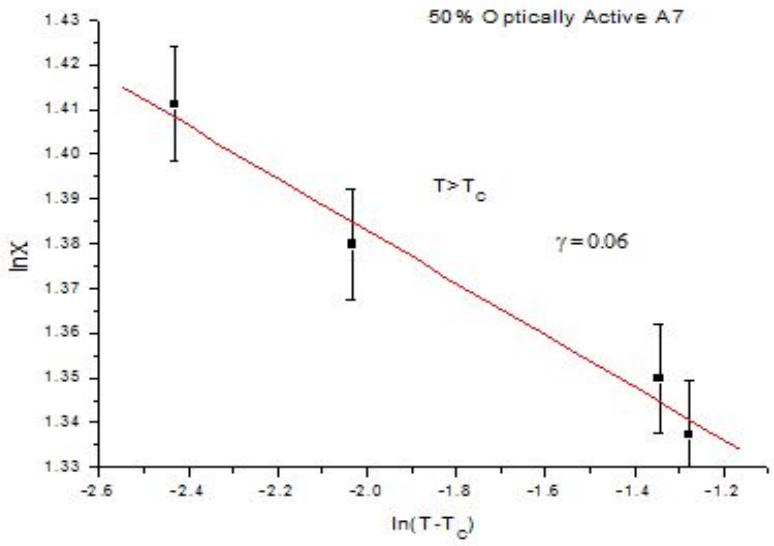

Figure 3.41: Dielectric susceptibility χ as a function of T-T_c in a log-log scale for the smectic A-isotropic liquid transition (T_c= 81.9^{o}C) according to Eq. 2.6 for the 50 % optically active A7 (T>T_c).

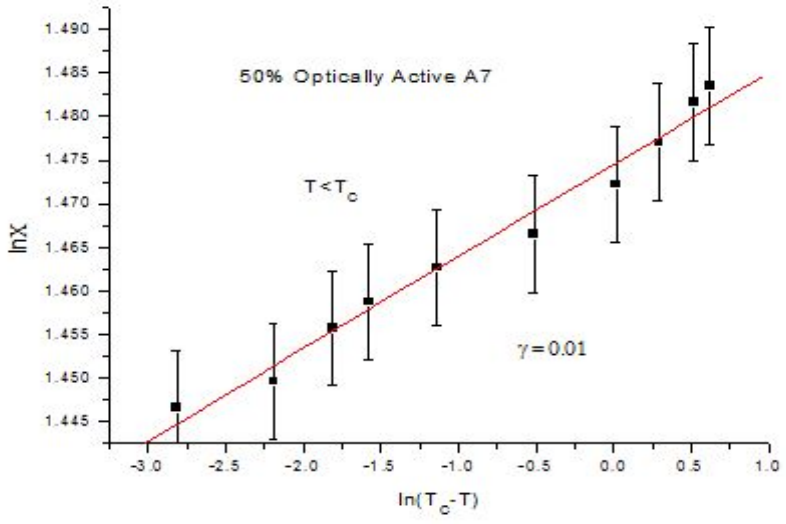

Figure 3.42: Dielectric susceptibility χ as a function of T_c-T in a log-log scale for the smectic A-isotropic liquid transition (T_c= 81.9^{o}C) according to Eq. 2.6 for the 50 % optically active A7 (T<T_c).

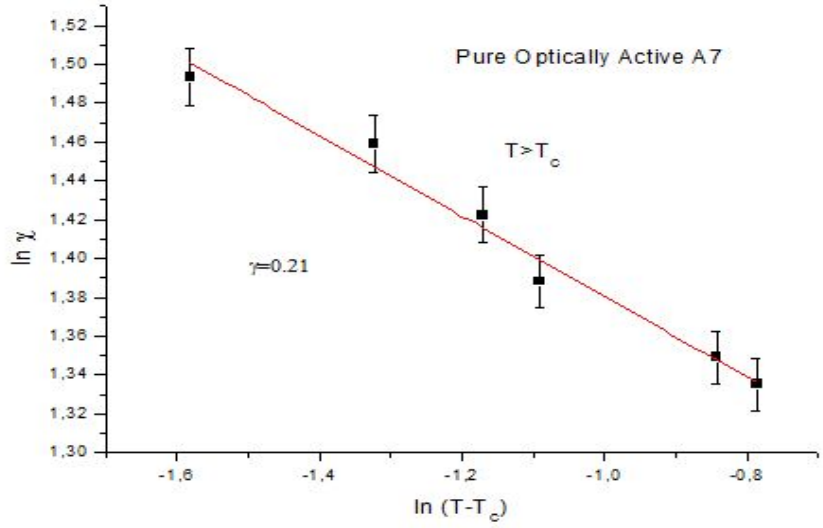

Figure 3.43: Dielectric susceptibility χ as a function of T-T_c in a log-log scale for the smectic A-isotropic liquid transition (T_c= 81.6^{o}C) according to Eq. 2.6 for the pure optically active A7 (T>T_c).

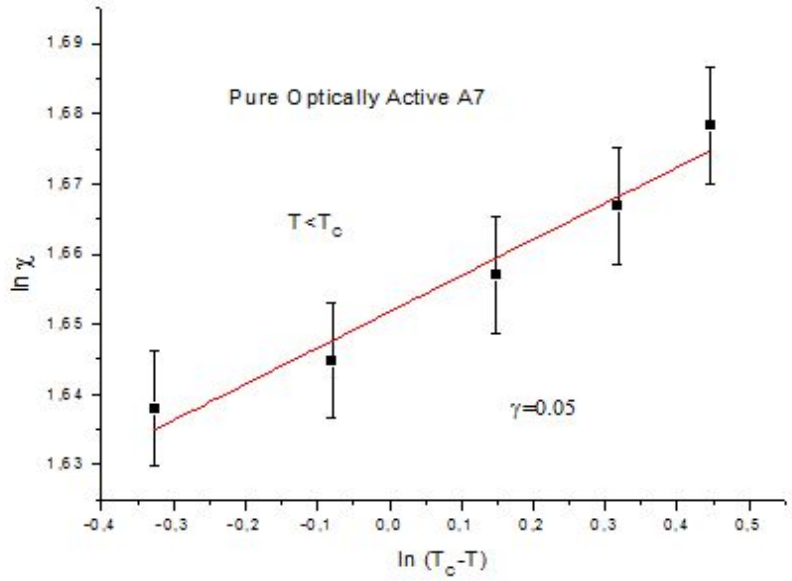

Figure 3.44: Dielectric susceptibility χ as a function of T_c-T in a log-log scale for the smectic A-isotropic liquid transition (T_c= 81.6^{o}C) according to Eq. 2.6 for the pure optically active A7 (T<T_c).

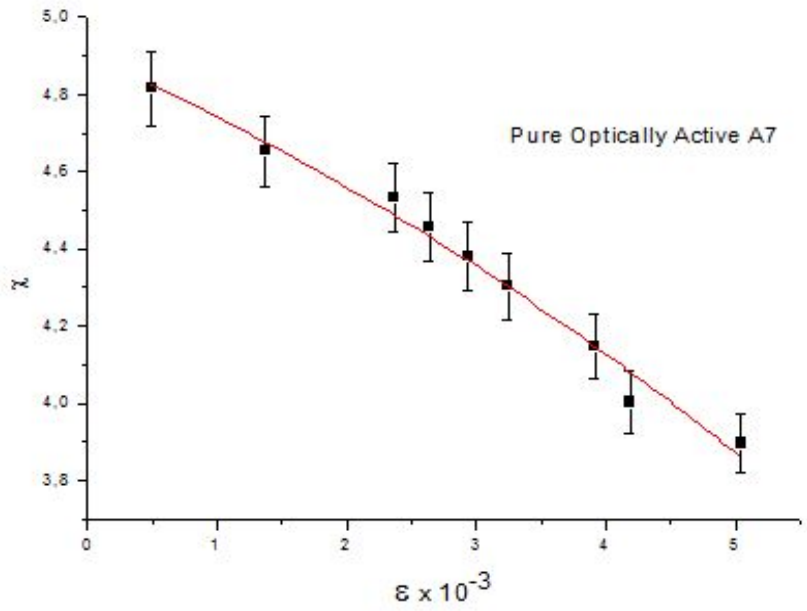

Figure 3.45: Dielectric susceptibility χ as a function of the reduced temperature, close to the smectic A- isotropic liquid transition for the pure optically active A7. Eq. 3.9 was fitted to the experimental data for the dielectric constant $\varepsilon_\perp$ [21] with the fitted parameters given in Table 3.28.

$$\chi = k_o \varepsilon^{-\gamma}(1 + k_1\varepsilon^{\Delta} + k_2\varepsilon^{2\Delta} + ...) \tag{3.9}$$

In this equation ε^{Δ} and $\varepsilon^{2\Delta}$ are corrections-to-scaling terms with Δ=0.5, k_o, k_1 and k_2 are constants. Eq. 3.9 reduces to Eq. 2.5 when the correction terms are not considered [40].

For our first analysis of the $\varepsilon_\perp$ experimental data [21] by Eq.2.5 as plotted in Figs. (3.41-3.44) with the values given in Table 3.27 in different temperature intervals, it can be argued whether a non-linear behaviour of lnχ versus ln|T-T_c| occurs. In the case of a non-linear variation of lnχ with ln|T-T_c|, correction terms are needed as given in Eq. 3.9 by which the $\varepsilon_\perp$ data [21] was reanalyzed here. Table 3.28 gives the values of the fitted parameters according to Eq. 3.9 for the pure and 50 % optically active A7 in the temperature intervals indicated. Uncertainties in the parameters k_o, k_1 and k_2 are given. Since the uncertainties in the critical exponent γ are very small, they are not indicated. Figs. 3.45 and 3.46 give our fits of the dielectric susceptibility χ (Eq. 3.9) to the experimental data [21] for the dielectric constant $\varepsilon_\perp$ as a function of reduced temperature, for pure and 50% optically active A7, respectively [40].

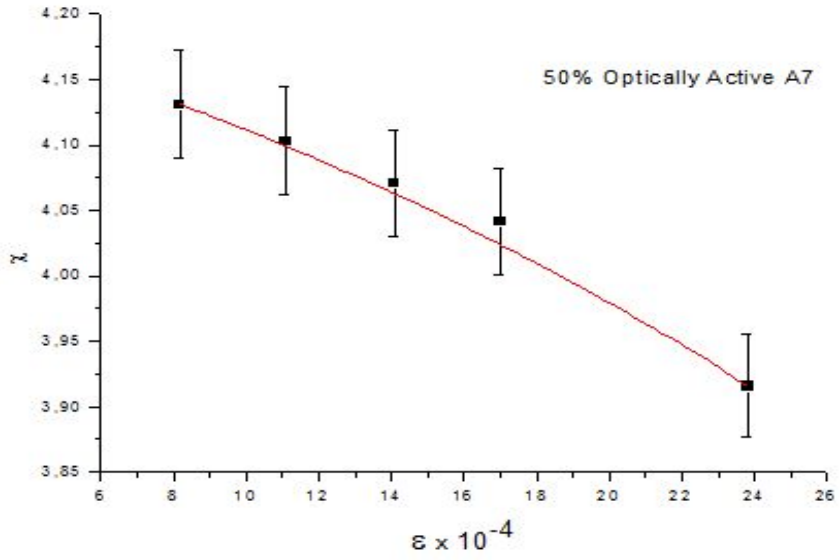

Figure 3.46: Dielectric susceptibility χ as a function of the reduced temperature, close to the smectic A- isotropic liquid transition for the 50 % optically active A7. Eq. 3.9 was fitted to the experimental data for the dielectric constant $\varepsilon_\perp$ [21] with the fitted parameters given in Table 3.28

We also determined the slopes of the $1/\varepsilon_\perp$ versus temperature T (Fig. 3.40) in the smectic A and the isotropic liquid for both pure and 50% optically active mixture of A7. The slope values determined in both phases of smectic A and the isotropic liquid according to a linear variation of $1/\varepsilon_\perp$ with the temperature,

$$1/\varepsilon_\perp = a + bT \tag{3.10}$$

where a and b are constants. Eq. 3.10 was used for both the pure and the 50% optically active A7. Since the experimental data [21] gives the same variation of $1/\varepsilon_\perp$ with T in the isotropic liquid (Fig. 3.40), the coefficients a and b (slope) should be the same in the same temperature interval, as given in Table 3.29. The slope values were also determined in the smectic A (SmA) phase for the pure and 50% optically active A7. The coefficients are determined in the temperature interval studied, as given in Table 3.30. We then constructed the ratio of the slope of the SmA phase to that of the isotropic liquid (I), as given in Table 3.31.

Our values for the critical exponent γ which vary from 0.01 to 0.21 (Tables 3.27 and 3.28)

Table 3.27: Values of the critical exponent γ and the amplitude A for the dielectric susceptibility χ within the reduced temperature ε close to the smectic A-isotropic liquid transition according to Eq. 2.5 for the 50 % and pure optically active A7.

A7	T(^{o}C)	T_c(^{o}C)	γ	A($^o C^{\gamma}$)	ε=|T-T_c|/T_c
50% Optically Active	T>T_c	81.9	0.06±0.01	3.5463	$1.1x10^{-3}<\varepsilon<3.4x10^{-3}$
	T<T_c		0.010±0.001	4.3689	$7.3x10^{-4}<\varepsilon<2.3x10^{-2}$
Pure Optically Active	T>T_c	81.6	0.05±0.01	4.0915	$3.9x10^{-4}<\varepsilon<3.3x10^{-3}$
			0.21±0.01	3.2381	$2.5x10^{-3}<\varepsilon<5.6x10^{-3}$
Pure Optically Active	T<T_c	81.6	0.05±0.01	5.2158	$8.9x10^{-3}<\varepsilon<1.9x10^{-2}$
			0.020±0.001	5.1588	$1.1x10^{-3}<\varepsilon<5.8x10^{-3}$

Table 3.28: Values of the critical exponent γ for the dielectric susceptibility χ and the amplitudes k_o, k_1 and k_2 according to the scaling relation (Eq. 3.9) within the reduced temperature ε in the smectic A phase close to the SmA-I transition for pure and 50 % optically active A7. Transition temperatures of pure and 50 % optically active A7 are 81.6 ^{o}C and 81.9 ^{o}C, respectively.

A7	γ	k_o	k_1	-k_2	ε=(T_c-T)/T_c
Pure optically active	0.30	0.14±0.02	133.06±9.28	954.75±43.57	$4.9x10^{-4}<\varepsilon<5.1x10^{-3}$
50% optically active	0.20	0.44±0.03	59.37±0.38	511.73±18.62	$8.1x10^{-4}<\varepsilon<2.4x10^{-3}$

Table 3.29: Values of the coefficients a and b for a linear variation of the reciprocal dielectric constant ($1/\varepsilon_{\perp}$) with the temperature interval indicated for the isotropic liquid of both pure and 50% optically active A7 from the experimental data [21], as shown in Fig. 3.40. $\triangle$T represents the temperature difference given here.

A7	a	b$x10^{-4}$(^{o}C)	Temperature interval(^{o}C)	$\triangle$T(^{o}C)
Isotropic Liquid	0.17	4.9	82.7<T<83.5	0.8

are too small compared to the theoretical models such as the mean field theory (γ=1), the 3-d Ising model (γ=1.2390.003), Heisenberg model (γ=1.380.02) and helium analogy or XY model (γ=1.32). So, these models are unable to describe the critical behaviour of the dielectric susceptibility for the pure and 50 % optically active. Since these models are designed essentially for a second order transition, our values of the critical exponent for the dielectric

Table 3.30: Values of the coefficients a and b for a linear variation of the reciprocal dielectric constant ($1/\varepsilon_{\perp}$) with the temperature (Eq. 3.10) in the temperature interval indicated for the Smectic A (SmA) phase of A7 from the both pure and 50% optically active A7 from the experimental data [21], as shown in Fig. 3.40. $\triangle$T represents the temperature difference given here.

A7 (SmA)	a	bx10^{-3}(^{o}C)	Temperature interval(^{o}C)	$\triangle$T(^{o}C)
Pure optically active	-0.33	6.1	80.2<T<81.3	1.1
50% optically active	0.02	2.1	80.2<T<81.5	1.3

Table 3.31: Ratio of the slopes b (Eq. 3.10) deduced for the SmA (Table 3.28) and the isotropic liquid (Table 3.29) for the pure and 50% optically active A7 in the temperature difference indicated (Tables 3.29 and 3.30).

SmA/I	Slope ratio	Temperature range, $\triangle$T(^{o}C)
Pure optically active	12:1	0.8-1.1
50% optically active	4:1	0.8-1.3

susceptibility indicate that smectic A-isotropic liquid transition of the pure and 50 % optically active A7 is of a nearly second order or weakly first order in character.

3.2.2 4-(3-methyl-2-chloropenta- noyloxy)-4′-heptyloxybiphenyl (C7)

3.2.2.1 Critical Behaviour of the Polarization, Tilt Angle, Electric Susceptibility and the Specific Heat Close to the SmA- Ferroelectric SmC (SmC*) Phase Transitions

We analyzed here the temperature dependence of the polarization jump ΔP_{θ} according to Eq. 2.67. we used the temperature dependence of the polarization jump and the susceptibility for the AC* phase transition of C7, which were obtained experimentally, as given in the literature [31] (Figs. 3.47 and 3.49 and Tables 3.32 and 3.33), and analyzed in this study. The values of β and A [62] were determined as given in Table 3.36. We plot in a log-log scale the polarization jump ΔP_{θ} as a function of temperature for C7 (T_c= 55.925^{o}C) in Fig. 3.50.

The electric susceptibility χ_{θ} was analyzed at various temperatures using the experimental data for C7 [31] close to the AC* phase transition in this liquid crystalline system. This

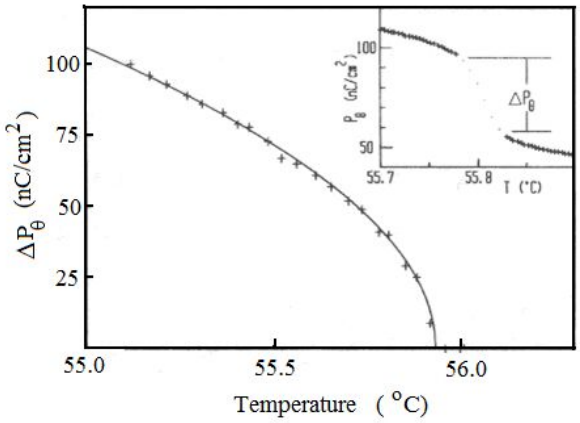

Figure 3.47: Temperature dependence of the polarization jump values for the C7 [31].

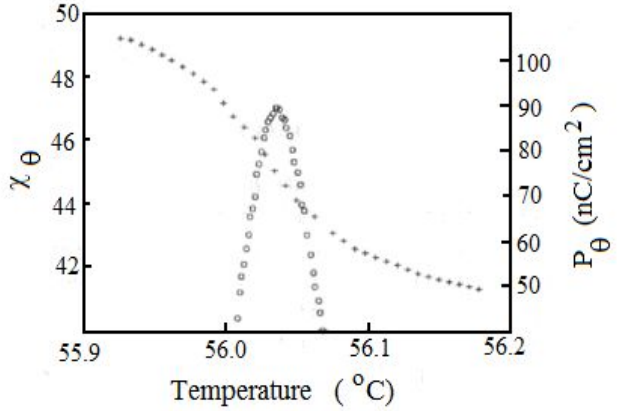

Figure 3.48: Experimental values of susceptibility and polarization as a function of temperature for C7 [31].

analysis was performed both below ($T<T_c$) and above ($T>T_c$) the transition temperature (T_c=55.925^{o}C) by means of Eq. 2.68. From our analysis the values of γ and A which were extracted, are given in Table 3.36. Log-log plots of $(\chi_\theta^{-2} - \chi_{\theta C}^{-2})^{1/2}$ as a function of temperature are presented in Fig. 3.51 ($T<T_c$) and Fig. 3.52 ($T>T_c$) for C7 [62].

Our final analysis for C7 close to its AC* phase transition was the electric field dependence of the polarization, according to Eq. 2.69. For this analysis, we used the experimental measurements for C7 with the values of E_c=50.1kV/cm, $P_{\theta C}$=72 nC/cm^2 and T_c=55.56^{o}C [31]. Table 3.37 gives the values of the critical isotherm δ and the amplitude A. We plot in Figs. 3.53 and

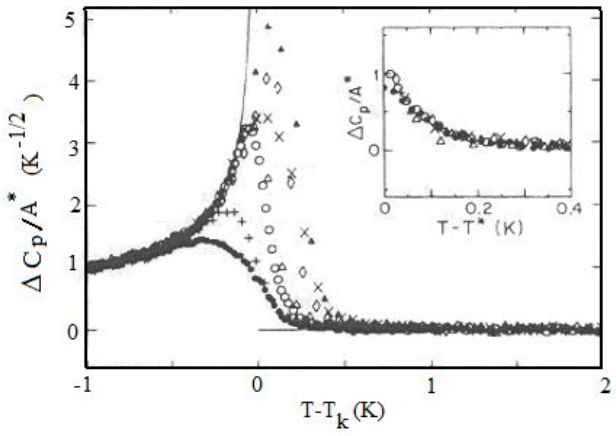

Figure 3.49: Experimental data of the excess heat capacity $\triangle C_p$ as a function of the temperature for the binary mixture of 2f+3f [32].

Table 3.32: Temperature dependence of the polarization jump values for the C7 [31].

-ln(T_c-T) x 10^{-1}	ln(ΔP_θ) x 10^{-1}(nC/cm^2)
39.12	21.97
28.13	32.19
24.08	34.34
21.20	36.64
18.33	36.89
16.09	39.12
14.27	39.51
12.73	40.60
10.22	41.90
9.17	42.20
8.21	42.91
7.13	43.57
6.54	43.70
5.80	44.19
4.94	44.54
4.31	44.89
3.43	45.33
2.74	45.64
0.94	46.05

3.54 the electric field E as a function of the polarization P with respect to their critical values in a log-log plot below and above E_c, respectively [62].

Table 3.33: Experimental values of the thermal susceptibility χ as a function of temperature for C7 [31].

-ln(T_c-T) x 10^{-1}	-ln($\chi_\theta{}^{-1}$-$\chi_{\theta C}{}^{-1}$)$^{1/2}$ x 10^{-1}	-ln(T_c-T) x 10^{-1}	-ln($\chi_\theta{}^{-1}$-$\chi_{\theta C}{}^{-1}$)$^{1/2}$ x 10^{-1}
40.17	61.10	40.17	61.10
30.79	53.37	35.76	55.04
24.89	49.06	30.58	54.17
21.20	46.05	23.75	50.69
18.52	42.90	21.12	46.83
16.40	40.51	17.37	45.38
14.27	39.32	15.47	43.51
13.17	38.26	13.86	41.93
11.58	37.13	12.14	40.75
10.47	36.27	10.97	39.74
8.99	35.34	9.82	38.97
7.92	34.97	9.19	38.26
–	–	8.10	37.42
–	–	7.11	37.94
–	–	6.03	36.12
–	–	5.53	35.47
–	–	3.64	33.81

Table 3.34: Experimental values of the polarization as a function of the electric field for C7 [31].

ln(P_θ-$P_{\theta C}$) x 10^{-1} (nC/cm^2)	ln(E_C-E) (kV/cm)	ln(P_θ-$P_{\theta C}$) x 10^{-1} (nC/cm^2)	ln(E_C-E) (kV/cm)
39.02	3.03	19.10	-2.21
35.77	2.67	25.65	0.59
33.84	1.90	29.58	1.13
32.39	1.52	30.80	1.65
30.91	0.90	33.32	1.75
38.23	2.50	34.18	2.29
24.85	0.46	34.58	2.49
15.04	-1.14	35.70	2.82

We also analyzed in this study the temperature dependence of the specific heat C_p for a mixture of 2f+3f liquid crystal using the experimental data from the literature [32], as given in Fig. 3.49 and Table 3.35 close to its AC* phase transition. By using Eq. 2.70, our analysis was done for the mole % 2f of X_{2f}=38.72 in a mixture of 2f+3f close to its AC* phase transition (T_k=393.845 K) [32]. Values of the critical exponent α and the amplitude A, which we

Table 3.35: Experimental data of the excess heat capacity ΔCp as a function of the temperature for the binary mixture of 2f+3f [32].

-ln(T_k-T) x 10^{-1} (K)	ln($\Delta C_p/A^*$) x 10^{-1} ($K^{-1/2}$)
-20.83	-8.21
-17.10	-5.98
-12.73	-4.16
-6.73	-1.28
-0.68	0
3.43	4.38
6.35	9.36

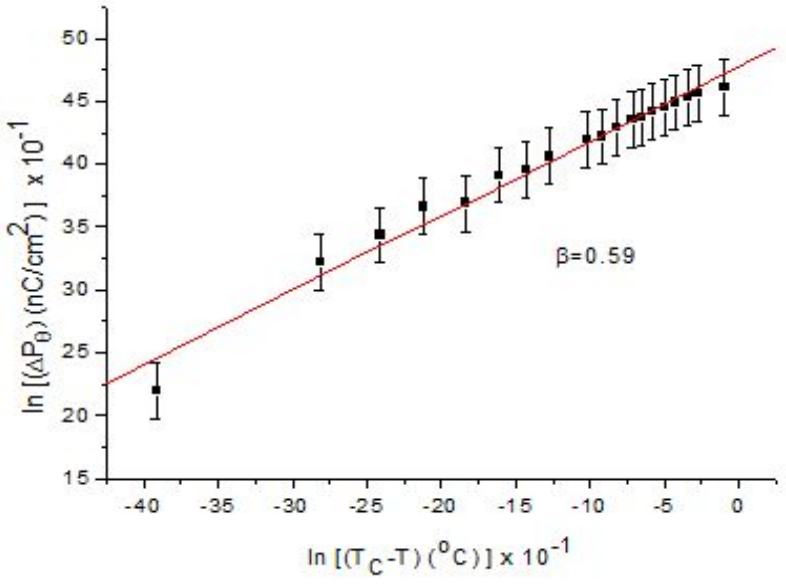

Figure 3.50: The polarization jump $\triangle P_\theta$ as a function of temperature in a log-log scale for C7 (T_c=55.925^{o}C). β is the critical exponent for the order parameter according to Eq. 2.67 [31].

extracted from our analysis are given in Table 3.38. Fig. 3.55 represents in a log-log scale $\Delta C_p/A^*$ plotted as a function of temperature for the AC* phase transition in a mixture of 2f+3f with the X_{2f} and T_k values given above [62].

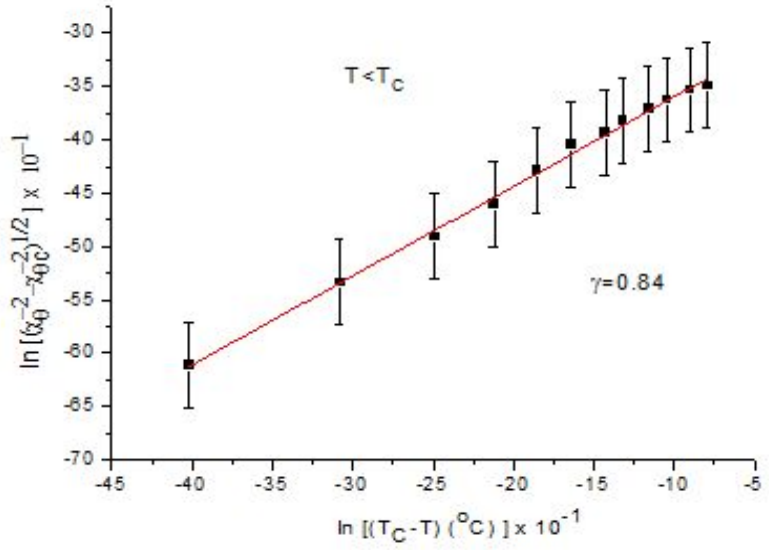

Figure 3.51: The electric susceptibility χ_θ as a function of temperature in a log-log scale for C7 below the transition temperature (T_c=55.925^{o}C). γ is the critical exponent for χ_θ according to Eq. 2.68 where $\chi_{\theta C}$ is the critical value of the electric susceptibility [31].

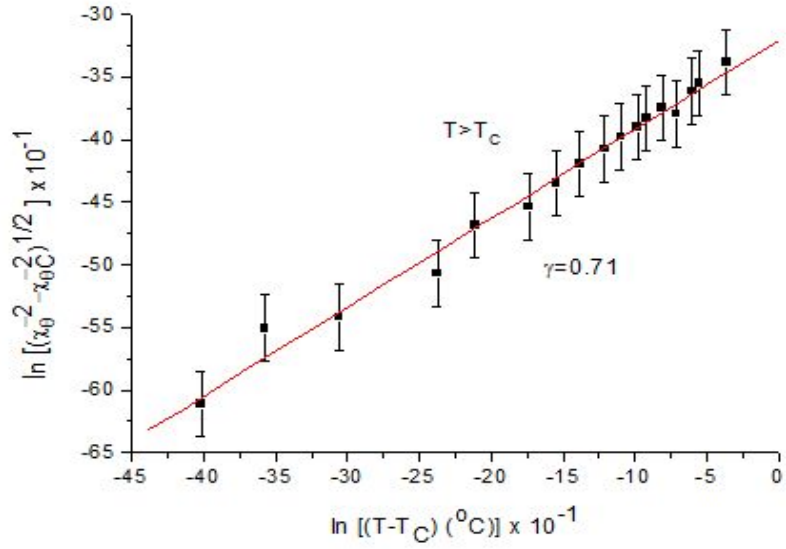

Figure 3.52: The electric susceptibility χ_θ as a function of temperature in a log-log scale for C7 above the transition temperature (T_c=55.925^{o}C). γ is the critical exponent for χ_θ according to Eq. 2.68 where $\chi_{\theta C}$ is the critical value of the electric susceptibility [31].

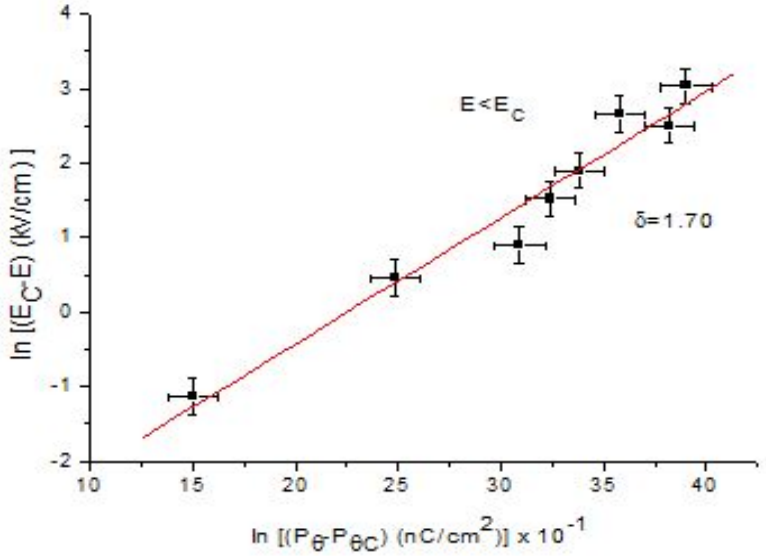

Figure 3.53: Electric field as a function of polarization in a log-log scale for C7 below the critical field ($E<E_c$), δ is the critical isotherm according to Eq. 2.69 where the critical values of the electric field and the polarization are E_c=50.1 kV/cm and $P_{\theta C}$=72 nC/cm^2, respectively [31].

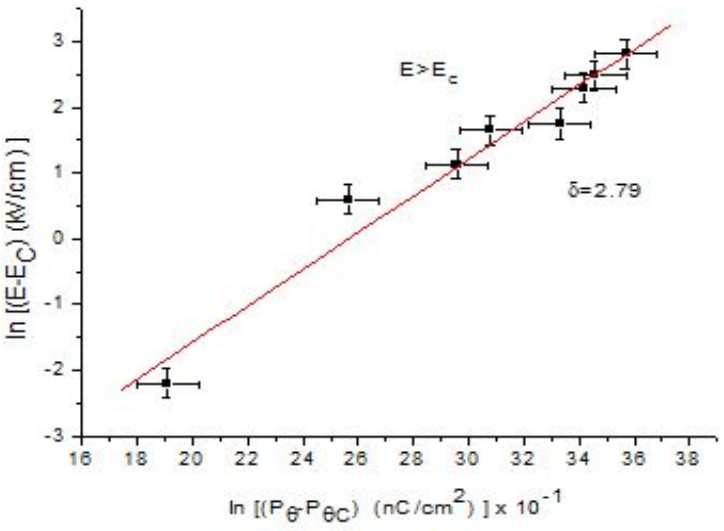

Figure 3.54: Electric field as a function of polarization in a log-log scale for C7 above the critical field ($E>E_c$), δ is the critical isotherm according to Eq. 2.69 where the critical values of the electric field and the polarization are E_c=50.1 kV/cm and $P_{\theta C}$=72 nC/cm^2, respectively [31].

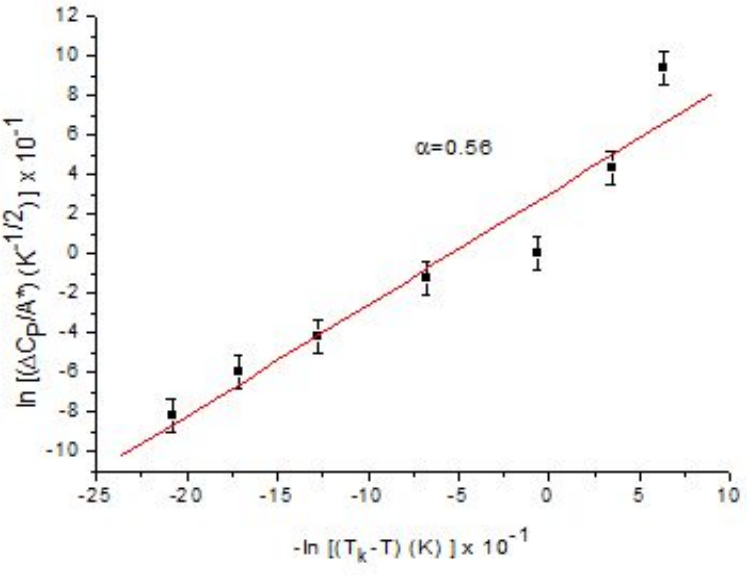

Figure 3.55: The excess heat capacity ΔC_p scaled with the amplitude A* as a function of temperature in a log-log scale for 2f+3f (X_{2f}= 38.72). α is the critical exponent for the specific heat according to Eq. 2.70 where T_k=393.845 K [32].

Table 3.36: Values of the critical exponent β for the polarization jump ΔP_θ and the amplitude A (Eq. 2.67), and the values of the critical exponent γ for the electric susceptibility χ and the amplitude A (Eq. 2.68) for C7 below and above the transition temperature for the AC* transition (T_c=55.925^{o}C). Our predicted values of the critical exponent α for the specific heat C_p of C7, are also given here.

C7	Eq.(2.67)	Eq.(2.67)	Eq.(2.68)	Eq.(2.68)	Predicted
	A (nC/cm^2.^{o}C)	β	A (nC/kV.cm)	γ	α
T<T_c	118.07±2.36	0.59±0.01	0.063±0.001	0.84±0.02	0.32±0.01
T>T_c	—	—	0.041±0.001	0.71±0.01	0.58±0.01

Using the values of β=0.59 and γ=0.84 (T<T_c) from our analysis, through the relation $P^2 \propto \chi^{-1} \approx (T_c\text{-}T)^\gamma$, we find $2\beta=\gamma$=0.84, which gives β=0.42. This is lower than the value of β=0.59 but both of them are closer to the mean field value of 0.5. For the analysis of the electric susceptibility χ_θ of C7, we used a power-law formula which can also be interpreted similarly in the sense that $\chi^{-1} \propto P^2 \approx (T_c\text{-}T)^{2\beta}$. Using the value of β=0.59 from our analysis, we find that γ=1.18 which is higher than the value of 0.84 (T<T_c). We also find that γ=0.71 for the electric susceptibility. Both values of γ=0.84 (T<T_c) and γ=0.71 (T>T_c), can be

Table 3.37: Values of the critical isotherm δ and the amplitude A below and above the electric field applied for C7, according to Eq. 2.69 where E_c=50.1kV/cm, $P_{\theta C}$=72nC/cm^2 and T_c=55.56^{o}C [31].

C7	Eq.(2.69)	Eq.(2.69)
	A(kV.cm/nC)	δ
E<E_c	0.0219±0.0004	1.70±0.03
E>E_c	0.00077±0.00002	2.79±0.06

Table 3.38: Values of the critical exponent α for the excess specific heat scaled with the A*, ΔC_p/A* and the amplitude A for a mixture of 2f+3f with the mole fraction X_{2f}=38.72, according to Eq. 2.70 where T_k=393.845K [32] for its AC* phase transition. Our predicted values of the critical exponents γ and β for the susceptibility and the order parameter, respectively, are also given here.

2f+3f	Eq.(2.70) A($K^{1/2}$)	Eq.(2.70) α	Predicted γ	Predicted β
T<T_c	1.36±0.03	0.56±0.01	0.72±0.01	0.36±0.01

compared with the mean field value of γ=1. Also, our analysis for the AC* transition of C7 gave the values for the critical isotherm as δ=1.70 (E<E_c) and δ=2.79 (E>E_c). This value of 2.79 is closer to the value of δ=3, as expected from the mean field model. From the power-law expression, $C_p \approx |T\text{-}T_c|^{-(2-2\gamma)}$ or $C_p \approx |T\text{-}T_c|^{-\alpha}$, we have α=2-2γ. Using the γ=0.84 (T<T_c) and γ=0.71 (T>T_c), our predicted values are α=0.32 (T<T_c) and α=0.58 (T>T_c). Using the scaling relation $\alpha+2\beta+\gamma=2$ and the values of β=0.59 and γ=0.84 (T<T_c), the value of $\alpha \approx 0$ is predicted. This is in accordance with the mean field value, together with the mean field values of β=1/2 and γ=1 in the scaling relation.

We also analyzed a mixture of 2f+3f close to its AC* phase transition using a power-law. We obtained α=0.56 (T<T_c) for 2f+3f, which then predicts γ=0.72 (T<T_c) according to γ=(2-α)/2. By means of the scaling relation $\alpha+2\beta+\gamma=2$, we also predicted the value of the critical exponent for the order parameter as β=0.36 for the AC* phase transition in a mixture of 2f+3f liquid crystalline system

CHAPTER 4

DISCUSSION

By analyzing the experimental data for the thermal expansivity α_p as a function of pressure for the N-I and C-N transitions in PAA [45], we obtained a linear variation of the specific heat C_p with the α_p, and also a linear variation of α_p with the isothermal compressibility κ_T for the N-I and C-N phase transitions in PAA. The values of the critical exponent γ and the amplitude A_1 were determined and we were able to calculate the pressure dependence of those thermodynamic quantities. Then, we compared our calculated values of the thermal expansivity α_p with those calculated on the basis of the Maier-Saupe model [54]. We also compared our calculated specific heat C_p for the NI transition in PAA with the experimental data [56]. For both comparisons, we find that there occurs a discrepancy between the calculated and the experimental values which are taken from the literature for the thermal expansivity and the specific heat. Around the melting point in PAA,it was obtained that the orientational disorder increases [56, 63]. Adjacent to the melting line, this indicates a second order transition prior to melting accompanied with the orientational disorder in PAA.

For PAA, AAD and the CM the values of the critical exponent α were extracted and analyzed. When we compare the results of these analyses, we saw that PAA and AAD have the same characteric properties at their transition points, since their chemical and physical features are very close to each other. Also, the CM has similar properties. Both PAA and AAD can be analyzed on the basis of the three-dimensional Ising model, helium analogy and the inverted XY model for liquid crystals and also the mean-field-tricritical model. For the CM, tricritical mean field theory is valid to analyze the characterization of its phase transition.

The C_p data [56] was also analyzed for the rapidly cooled and slowly cooled solid of CM. Close to the SmA-solid transition, the value of the critical exponent,$\alpha \cong 0.1$, indicates that this

transition is of a second order. It is not a mean-field like (α=0), but it is rather of a λ-type transition, for the CI and SC transitions [56]. For the rapidly and slowly cooled samples of CM, the exponent value becomes 1/2 and the stability limit was reached at the stability temperature of T_s=-19.6^{o}C for the CM. Similar analysis was performed for the supercooled solid phase of PAA. Differently from the rapidly and slowly cooled solid phase of CM, supercooled solid phase of PAA has a negative critical exponent (α=-0.02). For the solid phase, α is positive. The power-law formula for the stability limit was appropriate for rapidly and slowly cooled solid of CM. But, it was obtained that it was not satisfactory for the supercooled solid phase of PAA.In general, this power-law formula can also be applied to some other systems which exhibit superheating and supercooling phases.

In this thesis work, the temperature dependence of the enthalpy and the entropy in the nematic phase were also calculated from the specific heat C_p. Both the difference in enthalpy ΔH and in the entropy ΔS, increase with increasing temperature. As a part of this work, we analyzed the observed specific heat C_p data for CM [56] and we obtained the values of the critical exponent α.

In another part of this thesis work, by analyzing the experimental data for the ferroelectric liquid crystal of A7, we calculated the tilt angle θ and the polarization P as a function of temperature for some constant electric fields (Table 3.23). This was based on calculated values of θ and P for zero electric field [18] for A7 at its AC* phase transition by using the quadratic $P^2\theta^2$ coupling in the free energy for the mean field model studied here. Our calculated θ and P values at zero electric field are in very good agreement with the observed data [16], as also given previously [18]. This is due to the fact that the $P^2\theta^2$ coupling which describes a quadrupolar interaction, is the dominant mechanism for the AC* phase transition in A7 [18]. This compares with the calculated θ and P values using the Pθ coupling in the free energy expansion for the mean field model of this liquid crystal, which is not in agreement with the experimental data [16] for the AC* phase transition at zero electric field.

The calculated values of the polarization were then used to calculate the temperature dependence of the dielectric constant at zero and nonzero electric fields. When compared with the experimental data for the dielectric constant ε [21], our calculated values agree better, as the electric field increases.

Since we started with the approximate relation for the polarization which was derived from

our mean field model [18], calculation of the dielectric constant ε should be examined. From our fitting of Eq.(10) to the experimental data for the ε [21] and, the calculated values of the polarization, P(E=0) and P(E), plots of ε against P(E=0)P(E) were not very satisfactory for the electric field of E_1=150/9 kV/cm. For a constant electric field of E_2=100/3 kV/cm, ε against P(E=0)P(E) graph was better, which improved agreement between our calculated and the observed ε as a function of temperature. This was still better when plotted the dielectric constant ε against P(E=0).P(E) for a constant electric field of E_3= 50 kV/cm, which provided that the calculated and observed dielectric constant agreed much better at various temperatures. A very good fit was obtained for ε against P(E=0).P(E) for a constant electric field of E_4=200/3 kV/cm, which gave us a perfect agreement between calculated and the observed ε.

Calculation of $\varepsilon_\perp$ was conducted in the SmA phase on the basis of the temperature dependence of the nonzero values of θ. Above T_c in the isotropic liquid, since θ=0, we were unable to calculate the dielectric constant in this phase using our mean field model. The observed data for $\varepsilon_\perp$ [21] decreases continuously as the temperature increases from SmA to I for A7. Finally, regarding the calculated dielectric constant $\varepsilon_\perp$ below T_c using our mean field model with the biquadratic $P^2\theta^2$ coupling, the observed behaviour of $\varepsilon_\perp$ was described satisfactorily. This indicates that the quadrupolar interaction between P and θ is the dominant mechanism for the SmA-I transition in A7 with high spontaneous polarization. Also, the dielectric susceptibility χ was analyzed using the experimental data for the dielectric constant $\varepsilon_\perp$ of A7 [21] according to a power-law formula and the values of the critical exponent γ were deduced. In our analysis for the pure optically active A7, the values of the critical exponent varied from γ=0.05 to 0.02 below T_c. Above T_c, variation of γ was considerably large, which was between 0.2 and 0.05, as the transition temperature T_c is approached. For the 50% optically active mixture of A7, our exponent value of γ=0.06 above the transition temperature is close to the value extracted for the pure optically active A7. Below the transition temperature, our exponent value for 50% optically active mixture is very close to that for the pure optically active A7 close to the smectic A-isotropic liquid transition. This indicates that both pure and 50% optically active A7 exhibit similar critical behaviour of the dielectric susceptibility close to the smectic A- isotropic liquid transition. For the temperature intervals not very close to the transition temperature T_c, the dielectric susceptibility does not exhibit similar critical behaviour for pure and 50% optically active A7.

Using the free energy, we derived the tilt angle θ related to the electric susceptibility χ and also

the polarizability P related to χ as a function of temperature for C7. The observed data was analyzed by using a power-law formula for ΔP_θ and for the electric susceptibility χ_θ. From this analysis, values of the critical exponents β and γ were extracted for ΔP_θ and χ_θ, respectively. Those values of the critical exponents are closer to the mean field values. Considering the value of β=0.42 which we predicted from the electric susceptibility χ, corresponds to the value of the critical exponent for the tilt angle θ, where $\theta^2 \propto \chi^{-1} \approx (T_c\text{-}T)^\gamma$, which is the same as the polarization P.

For the analysis of the electric susceptibility χ_θ of C7, we used a power-law formula which can also be interpreted similar to the $\chi^{-1} \propto P^2 \approx (T_c\text{-}T)^{2\beta}$ since the temperature dependence of the polarization is dominant here. This value of δ is closer to the value of δ=3, as expected from the mean field model.

Using the temperature dependence of the electric susceptibility $\chi \approx |T\text{-}T_c|^{-\gamma}$, the second derivative of the free energy with respect to the temperature, gives $C_p \approx |T\text{-}T_c|^{-(2-2\gamma)}$ or using a power-law, $C_p \approx |T\text{-}T_c|^{-\alpha}$, we then obtain α=2-2γ. The value of the critical exponent α is also in accordance with the mean field value.

CHAPTER 5

CONCLUSIONS

The experimental C_p data from the literature was analyzed in this thesis work according to a power-law formula (in terms of the critical exponent γ) and the observed λ-type behaviour of C_p was explained for the thermotropic liquid crystals of p-azoxyanisole (PAA), anisaldazine (AAD) and cholesteryl myristate (CM). From this analysis, values of the critical exponent for the specific heat C_p, were extracted for the transition between nematic and isotropic liquid, and also in the supercooled region just above the solid-nematic transition for AAD. They were compared with the expected values from the theoretical models. For PAA, our exponent values for T<TNI and T<T_{SN} can be described by a three-dimensional Ising model. For T>T_{NI} our exponent value is much larger than that predicted by theoretical models. For T>T_{SN} the negative exponent value is close to the expected value of the helium analogy or XY model of liquid crystal. The negative value of the critical exponent for liquid crystals may be due to the existence of supercooled region where there is a jump discontinuity in PAA [54]. For the CM, the values of the critical exponent indicate that above CI and below SC, the phase transition can be of a second order type. Thus, our exponent values indicate that below CI and above SC, the transition tends to change toward a first order in CM. The specific heat C_p was also analyzed for the rapidly cooled and slowly cooled solid phases of CM and for the solid and supercooled solid phases of PAA. It was found that a power-law formula in the stability limit with the critical exponent 1/2 was satisfactory for the CM, but it was inadequate for PAA. With some accurate measurements of the specific heat C_p for the supercooled solid phase of PAA, our method of analysis can be reexamined. From our findings, we suggest that our method of analysis can be applied to some other liquid crystals exhibiting supercooling and superheating phases.

From the analysis of the experimental data and also from our calculations of the thermodynamic quantities, we were able to apply the Pippard relations to PAA, AAD and CM. This was based on the assumption that these thermodynamic quantities have the same critical exponent since they exhibit similar divergence behaviour as the critical point is approached.

Our calculations for the temperature dependence of the α_p and κ_T can be compared with the experimental data when available in the literature.

In this thesis work, the tilt angle θ, polarization P and the dielectric constant ε were also studied as a function of temperature at constant electric fields for the pure and 50% optically active A7 near the smectic A-isotropic liquid transition using our mean field model with the quadratic $P^2\theta^2$ coupling.

Our calculated θ and P values at various temperatures for the fixed electric fields show similar critical behaviour of A7, and the calculated ε values agree with the observed data. This agreement is even better as the electric field increases. This indicates that the quadrupolar interaction is the dominant mechanism for the SmA-I transition in A7 with high spontaneous polarization. Our exponent values indicate that for pure and 50% optically active A7, the SmA-I transition is of a nearly second order or weakly first order.

Another part of this thesis work was to analyze the experimental data for the temperature dependence of the order parameters (polarization P and tilt angleθ) and the electric susceptibility χ of C7 and also the temperature dependence of the specific heat C_p for a binary mixture of 2f+3f. The values of the critical exponents α for the specific heat, γ for the susceptibility and β for the order parameter for C7 and a mixture of 2f+3f, were extracted using the scaling relation close to their AC* phase transition. The observed behaviour of C7 and 2f+3f were then described satisfactorily close to their AC* phase transitions by using this analysis.

Since the mean field model studied here describes adequately the observed behaviour of A7 and C7, the expressions for the temperature dependence of the polarization, tilt angle and the dielectric constant which we derive, can also be applied to some other ferroelectric liquid crystals to explain their observed behaviour.

The predictions and the calculations given in this thesis work show that this method of analysis is adequate to describe the observed critical behaviour of the thermodynamic quantities for the thermotropic and ferroelectric liquid crystals studied. A similar analysis can be used and

also applied to some other thermodynamic and ferroelectric liquid crystals.

REFERENCES

[1] Modell, Michael; Robert C. Reid (1974). Thermodynamics and Its Applications. Englewood Cliffs, NJ: Prentice-Hall.

[2] Wikipedia, http://en.wikipedia.org/wiki/Phase_transition, Last visited in 15 November 2010.

[3] Stanley,H.E., Introduction to Phase Transitions and Critical Phenomena, Clarendon Press, Oxford 1971

[4] P. G. de Gennes and J. Prost, The Physics of Liquid Crystals, Claredon Press, 1993.

[5] Liquid Crystals, http://nobelprize.org/educational/physics/liquid_crystals/history/index.html, Last visited on 01 January 2011.

[6] Sven T. Lagerwall, Ferroelectric and Antiferroelectric Liquid crystals" Wiley-VHC, 1998.

[7] P. Papon, J. Leblond and P.H.E., Meijer The physics of phase transitions: concepts and applications; foreword by P. G. de Gennes ; translated by S.L. Schnur. Publication Info. Berlin : London : Springer-Verlag, 2002.

[8] Pollmann P, Schulte K, The Influence of Helical Orientation on the Tricritical Behavior of the Liquid-Crystal Phase-Transition Cholesteric Smectic-A - Thermodynamic and Optical Measurements on Cholesteryl Myristate and Its Binary-Mixtures with Para-Pentylphenyl-2-Chloro-4-(Para-Pentylbenzoyloxy)Benzoate or Cholesteryl Benzoate up to 2 Kbar And 120-Degrees-T, Berichte Der Bunsen-Gesellschaft-Physical Chemistry Chemical Physics, 89(7) 780-786 (1985)

[9] Peter J. Collings,"Liquid Crystals, Nature's Delicate Phase of Matter", Princeton University Press, 2002.

[10] J. D. McNutt, W. W. Kinnison and M. D. Searces, Physical Review B, 5 (3) 826-830 1972

[11] Joseph A. Castellano Liquid Gold: The story of Liquid Crystal Displays and the Creation of an Industry.

[12] T. Svedberg, Arkiv. Kem. Min. Geol. 4(39), 1-5 (1913)

[13] J.L. Galigne and J. Falgueirettes, "Structure Cristalline de l'Anisaldehyde-azine" B24 1523-1529 (1968)

[14] Bryan M. Craven and George T. DeTitta, J.Chem. Soc., Perkin Trans. 2, 814 - 822, 1976

[15] I. Musevic, R. Blinc and B. Zeks, The physics of ferroelectric and antiferroelectric liquid crystals, World Scientific, 2000.

[16] Bahr Ch, Heppke G, and Sabaschus B, Ferroelectrics 84, 103-118, (1988).

[17] Blinc R: Models for phase transitions in ferroelectric liquid crystals: Theory and experimental results. In: Martellucci S, Chester AN, eds. Phase Transitions in Liquid Crystals. New York: Plenum Press; 1992:343

[18] Salihoğlu S, Yurtseven H, Giz A, Kayşoğlu D and Konu A, Phase Trans. 66, 259-270, (1998).

[19] Salihoglu S, Yurtseven H and Bumin B, Int J. Mod. Phys.B12, 2083, (1998)

[20] Garoff S and Meyer RB, Phys. Rev. A19, 338 (1979)

[21] Bahr Ch, Heppke G and Sharma NK, Ferroelectrics 76, 151-157, (1987).

[22] Lien SC, Huang CC and, Goodby J, Phys. Rev. A29, 1371 (1984)

[23] Huang CC and Lien SC, Phys. Rev. A31, 2621 (1985)

[24] Huang CC and Dumrongrattana S, Phys. Rev. A34, 5020 (1986)

[25] Bahr Ch. and Heppke G, Mol. Cryst. Liq. Cryst. Lett. 4, 31 (1986)

[26] Bahr Ch. and Heppke G, Mol. Cryst. Liq. Cryst. 150b, 313 (1987)

[27] Ranta BR, Shashidhar R, Nair GG, Prasad SK, Bahr Ch. And Heppke G, Phys. Rev. A37, 1824 (1988)

[28] Shashidhar R, Ranta BR, Nair GG, Prasad SK, Bahr Ch.and Heppke G, Phys. Rev. Lett. 61 547 (1988)

[29] H. Y. Liu, C. C. Huang, Ch. Bahr, and G. Heppke, Phys. Rev. Lett. 61, 345 (1988).

[30] Sakurai T, Mikami N, Higuchi R, Honma M, Ozaki M and Yoshino K, J. Chem. Soc.-Chem. Commun. 12, 978 (1986)

[31] Bahr, Ch., and Heppke, G., Phys. Rev. A 44, 3669, (1991).

[32] Goates, J. B., Garland, C. W., and Shashidhar, R., Phys. Rev. A 41, 3192, (1990).

[33] Bahr C, Fliegner D, Physical Review A Volume: 46 Issue: 12 Pages: 7657-7663 (1992)

[34] Blundell, Stephen J. Katherine M. Blundell, Concepts in Thermal Physics. Oxford University Press, (2008).

[35] Pippard A.B., The Elements of Classical Thermodynamics for Advanced Students of Physics, Cambridge [Eng.] University Press, 1957.

[36] Binney J.J. et. al, The Theory of Critical Phenomena, (1992).

[37] Kilit E. and Yurtseven H., Journal of Molecular Liquids, 140, 84-86, (2008).

[38] Yurtseven H. and Kilit E., Journal of Optoelectronics and Advanced Materials Symposia, Vol.1 No3, 597-599, (2009).

[39] Kilit, E. and Yurtseven, H., 48(4), 450-460, (2010).

[40] Yurtseven H., Kilit E., Journal of Phase Equilibria and Diffusion, (in press) 2011.

[41] Wikipedia, http://en.wikipedia.org/wiki/Mean_field_theory, Last visited in 15 November 2010.

[42] Wikipedia, http://en.wikipedia.org/wiki/Ising_model, Last visited in 15 November 2010.

[43] Huang K., Statistical Mechanics, John Wiley and Sons., (1963).

[44] Wikipedia, http://en.wikipedia.org/wiki/Spherical_model, Last visited in 15 November 2010.

[45] Pruzan, Ph., Liebenberg, D.H., and Mills, R.L., J. Phys. Chem. Solids 47, 949-961, (1986).

[46] Kilit, E. and Yurtseven, H., Stare Jablonki 2005 Poland, Conference Proceedings, 327-334 (2007).

[47] Speedy, R.J., J. Phys. Chem 86, 3002, (1982).

[48] Hareng M. and Leblond J., J. Chem. Phys., 72, 622, (1980).

[49] Speedy R. J., and Angell C. A., J. Chem. Phys., 65, 851, (1976).

[50] Voronel A. V., JETP Lett. (Engl. Transl.), 14, 174, (1971).

[51] Yurtseven H. and Kilit E., Ferroelectrics, 365, 122-129, (2008).

[52] Kilit E. and Yurtseven H., Ferroelectrics, 365, 130-138, (2008).

[53] Matsushita, M., J. Chem. Phys. 65, 23-29.(1976).

[54] Maier, V.W., and Saupe, A., Z. Naturforsch, 15a, 287- 292, (1960).

[55] Yurtseven H. and Kilit E., Journal of Molecular Liquids, 138, 84-87, (2008).

[56] Barrall, E.M., Porter, R.S., and Johnson, J. F., J. Phys. Chem. 71, 895,(1967).

[57] Kapustin, A.P., and Bykova, N. T., Sov. Phys. Crystallog 11, 297, (1966).

[58] Wegner, F. J., Phys. Rev. B5, 4529, (1972).

[59] Lushington, K. J., and Garland, C. W., J. Chem. Phys. 72, 5752, (1980).

[60] Kilit, E. and Yurtseven, H., International Liquid Crystal Conference, Krakow, (2010).

[61] Kilit E., Yurtseven H., ISAF, Scotland, (2010).

[62] Yurtseven H., Bellici S., and Kilit E., Phase Transitions, Ferroelectrics, 344, 83-92, (2006).

[63] R. Pynn and T. Riste, in Anharmonic Lattices Structural Transitions and Melting (Edited by T. Riste) p.363, Noordhoff Leiden (1974)

[64] H. Yurtseven, Phase Trans. 53 (1995) 75.

[65] Liu HY, Huang CC, Min T, Wand MD, Walba DM, Clark NA, Bahr Ch, and Heppke G,. Phys. Rev. A40 6759 (1989)

[66] Zeks B, Mol. Cryst. Liq. Cryst.114, 259 (1984)

[67] Dumrongrattana S and Huang CC, Phys. Rev. Lett. 56, 464 (1986)

[68] Wikipedia, http://en.wikipedia.org/wiki/XY_model, Last visited in 15 November 2010.

CURRICULUM VITAE

PERSONAL INFORMATION

Surname, Name: Kilit, Emel
Nationality: Turkish (TC)
Date and Place of Birth: 9 April 1978, Eskişehir
Phone: +90 312 210 50 96
email: ekilit@metu.edu.tr

EDUCATION

High School: Eskişehir Kılıçoğlu Anadolu Lisesi, 1996.
B.S.: Ankara University, The Faculty of Engineering, Department of Physics Engineering, June 2001.
M.Sc: Ankara University, The Graduate School of Natural and Applied Sciences, Physics Engineering, 2004.
Fall 2003- Present Ph.D. Program, Middle East Technical University (METU), Ankara

PUBLICATIONS

1. Hamit Yurtseven, Sumru Bellici and Emel Kilit, "Critical Behaviour of the Polarization, Tilt Angle, Electric Susceptibility and the Specific Heat Close to the SmA-Ferroelectric SmC (SmC*) Phase Transitions" Ferroelectrics. **344** 83-92, 2006.

2. Hamit Yurtseven, Selami Salihoğlu, Özlem Tarı, Emel Kilit, Beril Akkök, Filiz Akın and Sinem Durmaz, " λ- Phase Transitions in Ice Ih Near The Melting Point" Chemical Engineering Communications. **194** 913-923, 2007.

3. Hamit Yurtseven and Emel Kilit , ”Temperature Dependence of The Polarization and Tilt Angle Under an Electric Field Close to The Smectic AC* Phase Transition in a Ferroelectric Liquid Crystal” Ferroelectrics. **365** 122-129, 2008.

4. Emel Kilit and Hamit Yurtseven, ”Calculation of the Dielectric Constant as a Function of Temperature Near the Smectic AC* Phase Transition in Ferroelectric Liquid Crystals” Ferroelectrics. **365** 130-138, 2008.

5. Hamit Yurtseven and Emel Kilit, ”Temperature Dependence of the Thermal Expansivity and The Specific Heat Near The Nematic-Isotropic (NI) Phase Transition In PAA” Journal of Molecular Liquids. **138** 84-87, 2008.

6. Emel Kilit and Hamit Yurtseven, ”Temperature Dependence of the Specific Heat of Anisaldazine Close to Phase Transitions” Journal of Molecular Liquids. **140** 84-86, 2008.

7. Hamit Yurtseven and Emel Kilit, ”Calculation of the Compressibility and Heat Capacity of Ice I in the Pre-Melting Region” Physics and Chemistry of Liquids. **47(5)** 495-504, 2009.

8. Hamit Yurtseven and Emel Kilit, ”Temperature Dependence of the Specific Heat of Cholesteryl Myristate Close to Phase Transitions” Journal of Optoelectronics and Advanced Materials Symposia. **1(3)** 597-599, 2009.

9. Emel Kilit and Hamit Yurtseven, ”Analysis of the specific heat of p-azoxyanisole (PAA) near the phase transitions” Physics and Chemistry of Liquids. **48(4)** 450-460, 2010.

10. Emel Kilit and Hamit Yurtseven, ”Calculation of Volume As Functions of Temperature And Pressure In Ice I Close To The Melting Point” International Journal of Molecular Physics B. **24(19)** 3749-3758, 2010.

11. Hamit Yurtseven and Emel Kilit, ”Critical Behaviour of The Dielectric Susceptibility For The Ferroelectric Liquid A7” Journal of phase equilibria and diffusion (in press), 2011.

12. Hamit Yurtseven, Bahri Raşitoğlu and Emel Kilit, ”Vibrational Frequencies Studied as a Function of Pressure in Phase II of Solid Benzene” Journal of Molecular Structure, (in press), 2011.

CONFERENCES ATTENDED

1. 16th Conference on Liquid Crystals, 18-21 September 2005, Stare Jablonki, POLAND.
2. 11th International Conference on Ferroelectric Liquid Crystals, 3-8 September 2007, Sapporo, JAPAN.
3. 13th Meeting on Condence Matter Physics,3 November 2006, Middle East Technical University, Ankara, TURKEY.
4. 14th Meeting on Condence Matter Physics, 2 November 2007, Hacettepe University, Ankara, TURKEY.
5. Condensed Matter Physics Conference of Balkan Countries, 26 - 28 May 2008, Mugla University, Mugla, TURKEY
6. International Symposium on Molecular Materials, MOLMAT2008, 8-11 July 2008 , University Paul Sabatier, Toulouse, FRANCE.
7. 23rdInternational Liquid crystal Conference , ILCC 2010, 11-16 July 2010, Krakow, POLAND
8. 19th International Symposium on the Applications of Ferroelectrics (10th European Conference on the Applications of Polar Dielectrics), ISAF-ECAPD 2010, 9th - 12th August 2010, Edinburgh, UNITED KINGDOM.
9. 17th Meeting on Condence Matter Physics, 5 November 2010, Ankara University, Ankara, TURKEY.

PROCEEDINGS

1. Emel Kilit and Hamit Yurtseven, ”Pippard Relations For The C-N and N-I Phase Transitions in PAA”.16th Conference on Liquid Crystals. 18-21 September, 2005 Stare Jablonki, Poland. SPIE, Conference Proceedings, 327-334 (2007).

CONFERENCE ABSTRACTS

1. 9th European Conference on Liquid Crystals, July 2- 6, 2007 Lisbon, Portugal "Analysis of the Specific Heat Close to the Solid-Nematic (SN) and Nematic-Isotropic Liquid (NI) Phase Transitions in Anisaldazine" E. Kilit and H. Yurtseven.

2. 13th Meeting on Condence Matter Physics, Ankara, November 3, 2006 "Calculation of the Specific Heat and the Thermal Expansivity For the Nematic- Isotropic (NI) Phase Transition in PAA."E. Kilit and H. Yurtseven.

3. 14th Meeting on Condence Matter Physics, Ankara, 2 November, 2007 "Critical Behaviour of Specific Heat for Anisaldazine Close to the Isotropic Liquid-Nematics-Solid Transitions" by E. Kilit and H. Yurtseven.

4. International Symposium on Molecular Materials, Toulouse- France, 8-11 July 2008 "Analysis of the Dielectric Constant as a Function of Temperature Close to the Smectic A - Isotropic Liquid Phase Transition in DOBAMBC" by H. Yurtseven and E. Kilit.

RESEARCH EXPERIENCES

- 2003 - Present, Research Assistant, Project, METU, Ankara.

- 2008 - 2009, Researcher, Simulations and Modeling on Phase Transitions on Liquid Crystal, Universita Degli Studi Di Bologna, Dipertimento Di Chimica Fisica Ed Inorganica, Bologna, Italy.

- 2000 Trainee, Ankara Nuclear Research and Education Center, Ankara.